Dissertation zur Erlangung des Doktorgrades

der Fakultät für Chemie und Pharmazie

der Ludwig-Maximilians-Universität München

Influence of Arabidopsis PIP2s on PIP1s and their regulation at the protein level

Jessica Martina Lehnert, geborene Lutterbach

aus

München, Deutschland

2022

Erklärung

Diese Dissertation wurde im Sinne von § 7 der Promotionsordnung vom 28. November 2011 von PD Dr. Anton Schäffner betreut.

Eidesstattliche Versicherung

Diese Dissertation wurde eigenständig und ohne unerlaubte Hilfe erarbeitet.

Oberschweinbach, am 14.10.2022

(Jessica Lehnert)

Dissertation eingereicht am: 19.05.2022

1. Gutachter: PD Dr. Anton Schäffner

2. Gutachter: Prof. Dr. Jörg Durner

Mündliche Prüfung am: 22.07.2022

Table of content

Table of content 2

Summary 6

Abbreviations 7

List of figures and tables 10

Tables 10

Figures 11

1 Introduction 12

1.1 Importance of aquaporins 12

1.2 Structure and selectivity of aquaporins 12

1.3 Aquaporins in plants 14

1.4 Classification 15

1.4.1 Expression and localization of PIPs in *Arabidopsis* 16

1.4.2 Trafficking and interaction of PIPs 17

1.4.3 Regulation of aquaporins and therefore water permeability of membranes 18

1.4.4 PIP2-dependent PIP1 regulation 19

1.5 Protein degradation pathways 20

1.5.1 ER-associated degradation (ERAD) 20

1.5.2 Autophagy related degradation 22

1.6 Aims of this work 23

2 Results 24

2.1 Where does the interaction between PIPs take place? 24

2.2 Is the interaction with PIP2s sufficient to protect PIP1s from degradation? 26

2.2.1 Expression and localization of BFP-PIP2 EGFP-PIP1 26

2.2.2 Influence of the mutated PIP2 diacidic motif on the localization of PIP1s and PIP2s and PIP1 protein stability 27

2.3 Can PIP2;3 or PIP2;7 prevent degradation of PIP1s in the absence of PIP2;1 and PIP2;2? 33

2.3.1 PIP2;3 33

2.3.2 PIP2;7 35

2.4 Which degradation pathway is involved in PIP1 degradation in the absence of PIP2s? 36

2.4.1 Influence of the proteasome inhibitor syringolin A on PIP protein level 36

2.4.2 PIP1 protein degradation in the presence of proteasome inhibitor (MG132) and/or protein biosynthesis inhibitor (CHX) 38

2.4.3 PIP1 protein level in different degradation mutant backgrounds 40

2.5 When does the degradation take place? 41

2.5.1 Expression and localization of newly generated mEosFP-PIP1 lines 42

2.5.2 Photoconversion capability of mEosFP-PIP1 43

2.5.3 Recovery of green mEosFP-PIP1 signal 1h after photoconversion 46

3 Discussion 48

3.1 The role of interaction in PIP1 and PIP2 co-regulation 48

3.2 Regulation of PIP1s relies on PIP2s' amino acid sequence 50

3.3 Degradation of PIP1s in the absence of PIP2s 51

3.3.1 Progress in determining the degradation pathway 51

3.3.2 Time point of degradation (exocytosis rate) 54

3.4 Potential physiological role of co-regulation 55

4 Outlook 57

5 Material and Methods 58

5.1 Material 58

5.1.1 Plant material 58

5.1.2 Bacteria 60
5.1.3 Kits 61
5.1.4 Media 61
5.1.5 Buffer 62
5.1.6 Chemicals 63
5.1.7 Antibiotics 64
5.1.8 Enzymes 64
5.1.9 Antibodies 65
5.1.10 Primer 65
5.1.11 Vectors and plasmids 67
5.1.12 Instruments 69
5.1.13 Internet tools and software 70
5.2 Methods 71
5.2.1 Plant methods 71
5.2.1.1 Cultivation on soil 71
5.2.1.2 Cultivation on plates 71
5.2.1.3 Generation of multiple mutants and backcrossing of single mutants 72
5.2.1.4 Generation and characterization of transgenic lines 72
5.2.2 Molecular methods 73
5.2.2.1 Isolation of genomic DNA (CTAB method) 73
5.2.2.2 Polymerase chain reaction 73
5.2.2.3 Agarose gel electrophoresis 74
5.2.2.4 Extraction of DNA from agarose gels 74
5.2.2.5 Gibson Assembly 74
5.2.2.6 BP reaction (Gateway) 74
5.2.2.7 LR reaction (Gateway) 75

5.2.2.8 Preparation of chemically competent E. coli DH5α cells 75
5.2.2.9 Transformation of chemically competent E. coli DH5α cells 75
5.2.2.10 Preparation of electro competent A. tumefaciens GV3101 pMP90 76
5.2.2.11 Transformation of electro competent A. tumefaciens GV3101 pMP90 76
5.2.2.12 Plasmid isolation 76
5.2.2.13 Restriction digestion 76
5.2.2.14 DNA sequencing 77
5.2.2.15 PCR-based mutagenesis 77
5.2.2.16 Agrobacterium tumefaciens mediated plant transformation 78
5.2.2.17 Protoplast isolation 78
5.2.2.18 PEG-mediated transient protein expression 79
5.2.3 Biochemical methods 79
5.2.3.1 Microsomal fraction isolation 79
5.2.3.2 Determination of protein concentration with Bradford 80
5.2.3.3 ELISA 80
5.2.3.4 Degradation assay (CHX and MG132) 81
5.2.4 Microscopy 82
5.2.4.1 Ratiometric bimolecular fluorescence complementation (rBiFC) 82
5.2.4.2 Fluorescence recovery after photobleaching (FRAP) 83
5.2.4.3 Corrected fluorescence recovery after photoconversion (cFRAPc) 84
6 Appendix 85
7 References 94
8 Acknowledgements 105

Summary

Aquaporins are channel proteins that facilitate water flow across membranes and can be found in all three domains of life. In plants they play an important role in adapting to different environmental stimuli. A subgroup of aquaporins, localized to the plasma membrane, is called plasma membrane intrinsic proteins (PIP). The genome of *Arabidopsis thaliana* includes thirteen PIPs divided into PIP1s (5 isoforms) and PIP2s (8 isoforms) and it has been shown that they can be regulated for example by post-translational modifications such as phosphorylation and removal from the plasma membrane. Previous studies in our laboratory revealed a role of PIP2;1 and PIP2;2 on the post-translational regulation of PIP1s, where the absence of these two PIP2 isoforms led to a reduction in the PIP1 protein level. However, the mechanism behind the co-regulation was still unclear as in when this degradation is taking place and which pathway is involved.

Interaction between PIP1;1 and PIP2;1/PIP2;2 takes place as early as at the endoplasmic reticulum as was shown by bimolecular fluorescence complementation studies. Therefore, regulation of the PIP1s could already happen before routing to the plasma membrane. Moreover, the specificity of the co-regulation was assessed by complementing the *pip2;1 pip2;2* mutant with different PIP2 hybrid constructs demonstrating a dependency on the amino acid sequence rather than the expression pattern.

In addition, some preliminary studies were performed to determine the time point of degradation in the absence of PIP2;1/PIP2;2. For this purpose corrected fluorescence recovery after photoconversion (cFRAPc) was optimized for analyzing the PIP proteins. However, first tests over the time course of one hour revealed no measurable exocytosis of PIP1;2, showing that a longer observation period will be necessary in future investigations. To prevent the roots from drying the implementation of additional methods is required.

Evidence for the involvement of the proteasomal degradation in the down-regulation in the presence and even more pronounced in the absence of PIP2;1/PIP2;2 could be gathered by performing inhibitor (MG132) studies on protoplasts. On the other hand, no change in the PIP1 protein level could be detected in mutants deficient in autophagy or ERAD, leading to the assumption that compensation by other degradation pathways was taking place in the degradation mutants.

Abbreviations

ABTS	2,2'-azino-bis(3-ethylbenzothiazoline-6-sulphonic acid)
AHA1	activator of 90 kDa heat shock protein ATPase homolog 1
Ala	alanine
ar/R	aromatic/arginine
Asn	Asparagine
Asp	aspartic acid
ATG	autophagy-related protein
BFP	blue fluorescence protein
BHT	butylated hydroxytoluene
BiFC	bimolecular fluorescence complementation
BSA	bovine serum albumin
BT toxin	*Bacillus thuringiensis* toxin
cDNA	complementary DNA
cFRAPc	corrected fluorescence recovery after photoconversion
CHX	cycloheximide
CNX	calnexin
COFRADIC	combined fractional diagonal chromatography
CRT	calreticulin
CTAB	cetyltrimethylammoniumbromid
C-terminus	carboxyl-termiuns
ddH_2O	double distilled water
DM	*pip2;1 pip2;2* double mutant
DMSO	dimethyl sulfoxide
DNA	deoxyribonuclei acid
Doa10	degradation of alpha factor
DTT	dithiothreitol
E. coli	*Escherichia coli*
EDTA	ethylene diamine tetra-acetic acid
EGFP	enhanced green fluorescence protein
ELISA	enzyme-linked immunosorbent assay
ER	endoplasmic reticulum
ERAD	ER-associated degradation pathway
EtOH	ethanol

EYFP	enhanced yellow fluorescence protein
Gent	gentamicin
GIP	GlpF-like intrinsic proteins
Glu	glutamic acid
GUS	β-glucoronidase
h	hour
HIP	hybrid intrinsic protein
His	histidine
Hrd	HMG-CoA reductase degradation
Htm1	homologous to mannosidase 1
Hyg	hygromycin
LB	lysogeny broth
Leu	leucine
mEosFP	monomeric Eos fluorescence protein
MES	2-(N-morpholino)-ethanesulfonic acid
MF	microsomal fraction
min	minute
MIP	membrane intrinsic protein
mRFP	monomeric red fluorescence protein
MS	Murashige and Skoog
NBR	nonbleached region
NIP	NOD26-like intrinsic protein
NPA	asparagine-proline-alanine
N-terminus	amino-termius
OD	optical density
PAS	preautophagosomal structure
PBS	phosphate-buffered saline
PCR	polymerase chain reaction
PE	phosphatidylethanolamine
PIP	plasma membrane intrinsic protein
PM	plasma membrane
PMSF	phenylmethane sulfonyl fluoride
PMT	photomultiplier
Pro	proline
qRT-PCR	quantitative real-time PCR
RB	rich broth, Luria-Bertani
Rif	rifampicin

ROI	region of interest
ROS	reactive oxygen species
rpm	revolutions per minute
RT	room temperature
sec	second
Ser	serine
SIP	small basic intrinsic protein
SNARE	soluble N-ethylmaleimide sensitive factor attachment protein receptors
Spec	spectinomycin
TIP	tonoplast intrinsic protein
TSPO	translocator protein
UPR	unfolded protein response
UV	ultraviolet
v/v	volume per volume
Val	valine
w/v	weight per volume
WT	wild type
XIP	uncategorized X intrinsic protein
Yos9	osteosarcoma 9

List of figures and tables

Tables

Table 1: PIP1 – PIP2 combinations 27
Table 2: Influence of syringolin A on PIP1 protein levels 37
Table 3: Plant lines used in this work, which were ordered or already present in the lab 58
Table 4: Plant lines generated in this work 59
Table 5: Bactria strain 60
Table 6: Applied kits 61
Table 7: Media used for growing bacteria or plants 61
Table 8: Prepared buffers 62
Table 9: Chemicals 63
Table 10: Antibiotics 64
Table 11: Enzymes 64
Table 12: Antibodies 65
Table 13: Genotyping primer for the WT allele 65
Table 14: Genotyping primer for insertion 65
Table 15: Primer used for mutagenesis 66
Table 16: Primer used for cloning 66
Table 17: Vectors 67
Table 18: Plasmids 68
Table 19: Instruments 69
Table 20: Internet tools and software 70
Table 21: growth conditions on plates 72
Table 22: PCR program used for mutagenesis 77
Table 23: Inhibitors used for the degradation assay 81
Table 24: Microscope settings for rBiFC 82
Table 25: Microscope settings for FRAP 83
Table 26: Microscope settings for cFRAPc 84

Figures

Figure 1: **Structure of aquaporins**. 13
Figure 2: **The three different water routes through plant tissues.** 14
Figure 3: **Phylogenetic tree of the 35 Arabidopsis thaliana MIPs**. 15
Figure 4: **Reduction of the PIP1 protein level in pip2 mutants.**. 20
Figure 5: **Putative degradation pathways for PIP1s.** 21
Figure 6: **Interaction of PIP1;1 and localization of different PIP combinations in protoplasts.** 25
Figure 7: **Diacidic mutant of BFP-PIP2;1 in the EGFP-PIP1;1 line.** 28
Figure 8: **Diacidic mutant of BFP-PIP2;1 in the EGFP-PIP1;2 line.** 29
Figure 9: **FRAP experiments to estimate the intracellular labelling of BFP-PIP2;1.**. 30
Figure 10: **FRAP experiments to estimate the intracellular labelling of BFP-PIP2;1.** 31
Figure 11: **Complementation of the pip2;2 mutant with PIP2;3.** 34
Figure 12: **Complementation of the pip2;2 mutant with PIP2;7.** 35
Figure 13: **Influence of proteasomal degradation on the PIP1;1 protein.** 39
Figure 14: **PIP1 protein level in degradation mutants.** 41
Figure 15: **mEosFP tagged PIP1;1 and PIP1;2 lines.** 42
Figure 16: **cFRAPc imaging of mEos-PIP1;1.** 44
Figure 17: **cFRAPc imaging of mEos-PIP1;2.** 45
Figure 18: **Determination of necessary scan number for efficient conversion.** 45
Figure 19: **Determination of newly synthesized mEos-PIP1;2 within one hour.** 47
Figure 20: **Influence of mutation of PIP2s' diacidic motif on the stability of PIP1s.**. 49
Figure 21: **Scheme for putative the role PIP2-PIP1 co-regulation.** 56
Figure 22: **Vector map of the rBiFC system.** 82

1 Introduction

1.1 Importance of aquaporins

Major intrinsic proteins (MIPs) also called aquaporins are water channels that can facilitate the passive movement of water across membranes. They are present in all three domains of life (eukarya, bacteria, archaea) underlining their importance for all living beings. The first hint for water channels was detected at the human red blood cell membrane by Benga *et al*. in 1985, later called aquaporins (Benga and Popescu, 1986). Moreover, it was discovered that aquaporins are present in all fluid-related structures in humans (Laloux *et al.*, 2018) such as kidneys (reviewed by Noda and Sasaki, 2006), sweat glands (reviewed by Nejsum *et al.*, 2002), lacrimal glands (reviewed by Schey *et al.*, 2014), salivary glands and pancreatic cells (reviewed by Delporte, 2014). Humans possess 18 aquaporins, a quite high number compared to the 13 – 15 paralogs usually present in mammals, but still low in comparison to the large quantity of different MIPs in plants.

In contrast to mammals, plants are sessile life forms that have to adjust their water uptake and transport depending on the surrounding environment and occurring biotic and abiotic stresses. To achieve such a tight regulation, plants have developed a wide array of different aquaporins with various functions and localizations within the plant cell.

1.2 Structure and selectivity of aquaporins

Aquaporins are small membrane proteins (23 – 31 kDa) and consist of six transmembrane α-helices (H1-H6) connected by 5 loops (LA-LE) protruding into the cytoplasm or the extracellular space, while both the N-terminus and the C-terminus are facing the cytosolic space (**Figure 1 A**). Loop B and E are partially integrated into the membrane from opposite directions, forming an additional pseudo transmembrane helix. A conserved Asn-Pro-Ala (NPA) motif is present in both loops close to the center of the pore, constituting a filter by hydrogen bond formation for proper positioning of entering molecules (De Groot and Grubmüller, 2001). The protruding asparagines from the NPA motifs form hydrogen bonds with oxygen of the water molecule resulting in a bipolar orientation of the neighboring molecules and preventing proton entry (Sui *et al.*, 2001; Tajkhorshid *et al.*, 2002). The narrowest part of the pore with a diameter of

only about 3 Å presents another layer of selectivity by size exclusion, being just big enough to let a water molecule (2.8 Å) pass (Murata *et al.*, 2000). The ar/R (aromatic/arginine) filter at the extracellular portion of the channel plays a crucial role in selectivity determination (Wallace *et al.*, 2006; Kosinska Eriksson *et al.*, 2013).

Four aquaporin channels interact with each other and thereby form a tetramer, where each monomer retains its water transport function (compare **Figure 1 B**; Daniels *et al.,* 1999). A tetramer can consist of single aquaporin isoforms (homotetramer) or a combination of different isoforms (heterotetramer). The composition can affect the regulation, trafficking and function of the channels in the tetramer (Fetter *et al*., 2004; Yaneff *et al.*, 2014; Jozefkowicz *et al.*, 2016). A side effect of the assembly of four monomers is the formation of a central pore which might be involved in solute transport (Bertl and Kaldenhoff, 2007; Frick *et al.*, 2013; Zwiazek *et al.*, 2017).

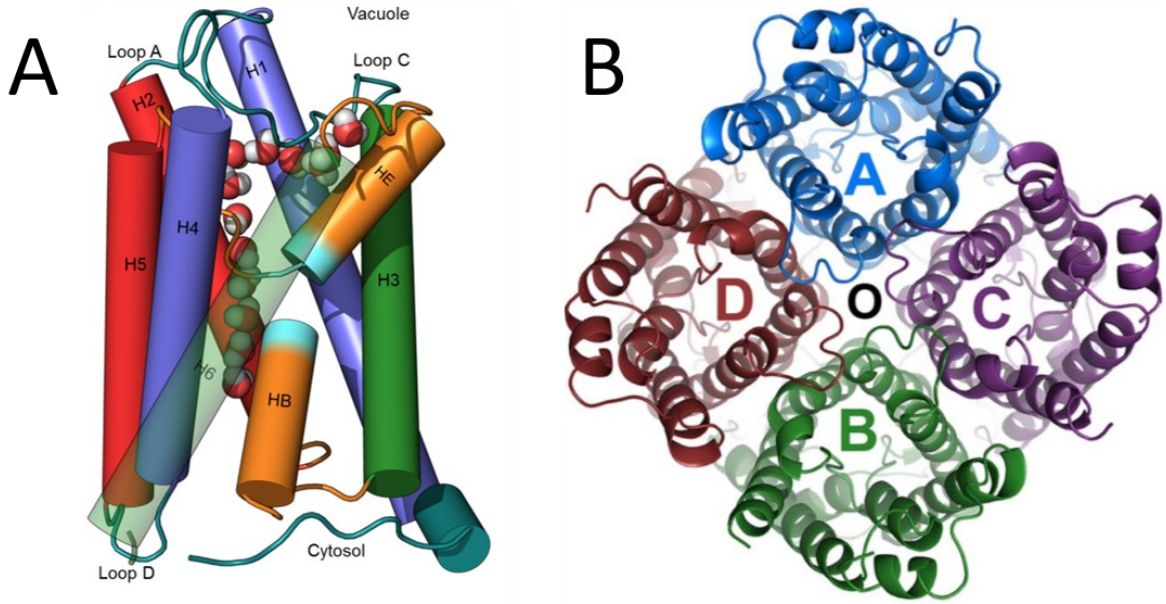

Figure 1: ***Structure of aquaporins****. (A) Representation of the folding of aquaporins with their six transmembrane helices, the connecting loops and the two pore helices (HB and HE). (B) The top view of a tetramer shows the water channel in each monomer (depicted in blue, green, purple and red) is labeled with A – D and the putative central pore is marked with an O. From Kirscht* et al.*, 2016 (© 2016 Kirscht et al.) and Horsefield* et al.*, 2008 (© 2008 by The National Academy of Sciences of the USA).*

The name aquaporin already implies the role in water permeability, but not only water can permeate through those channels. Over the last years several studies concerning the specificity of MIPs have been performed, revealing a broad spectrum of possible substrates. Small molecules like boric acid (Takano *et al.*, 2006; Tanaka *et al.*, 2008; Ampah-Korsah *et al.*,

2016; Mosa *et al.*, 2016), urea (Liu *et al.*, 2003; Gu *et al.*, 2011; Yang *et al.*, 2015), hydrogen peroxide (Bienert *et al.*, 2006; Tian *et al.*, 2016; Rodrigues *et al.*, 2017), silicic acid (Fauteux *et al.*, 2006; Jian *et al.*, 2006; Mitani *et al.*, 2008; Chiba *et al.*, 2009) and glycerol (Biela *et al.*, 1999; Dean *et al.*, 1999) have been reported to pass membranes through aquaporins. They even have been associated with the permeability of the plasma membrane of gases like ammonia (Holm *et al.*, 2005; Bertl and Kaldenhoff, 2007; Kirscht *et al.*, 2016), O_2 (Zwiazek *et al.*, 2017) and CO_2 (Heckwolf *et al.*, 2011; L. Li *et al.*, 2015; Wang *et al.*, 2016) and ions (Byrt *et al.*, 2017). Substrates can differ between aquaporin isoforms and at the same time one isoform can have several substrates (Perez Di Giorgio *et al.*, 2016).

1.3 Aquaporins in plants

Water is an essential resource for plants needed for processes such as photosynthesis, stability (turgor) or as a solvent for nutrients taken up from soil and to transport them among the different parts of the plant. There are three water routes through plant tissues (compare **Figure 2**; Steudle and Peterson, 1998): apoplastic path (around protoplasts, **A**), symplastic path (mediated by plasmodesmata forming a cytoplasmic continuum, **B**) and transcellular path (across membranes, **C**). Since aquaporins facilitate water movement across membranes, they play an important role in the transcellular path.

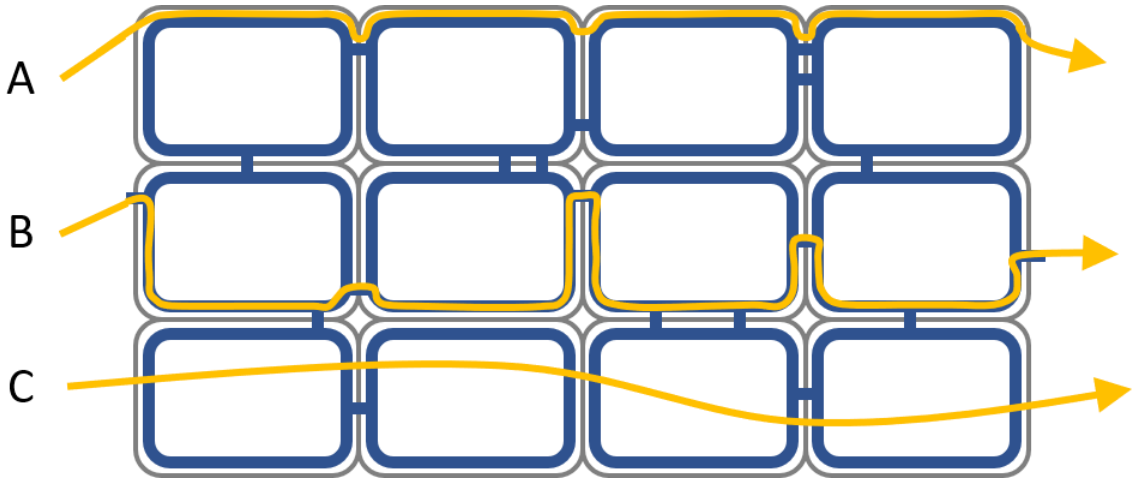

Figure 2: ***The three different water routes through plant tissues.*** *(A) The apoplastic path describes the water flow around the protoplasts. (B) The symplastic path allows water to travel through plasmodesmata, which connect the cytoplasm of neighboring cells. (C) The transcellular path leads the water across membranes (cell walls: grey; cytoplasmic continuum: blue).*

1.4 Classification

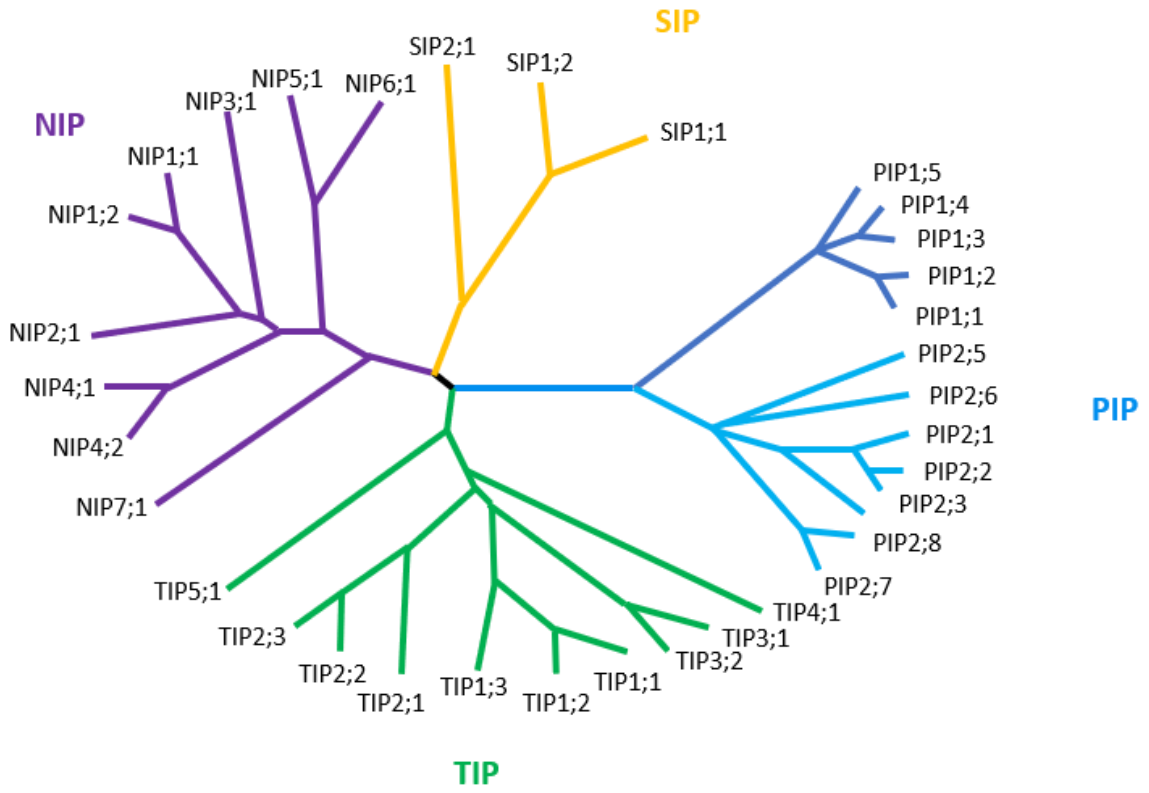

Figure 3: ***Phylogenetic tree of the 35*** **Arabidopsis thaliana** ***MIPs****.* A. thaliana *aquaporins can be divided into 4 subgroups: PIPs, TIPs, NIPs and SIPs.*

Arabidopsis thaliana has 35 MIP isoforms that can be divided into four subfamilies: plasma membrane intrinsic proteins (PIPs), tonoplast intrinsic proteins (TIPs), NOD26-like intrinsic proteins (NIPs) and the small basic intrinsic proteins (SIPs) (see **Figure 3**; Johanson *et al.*, 2001; Quigley *et al.*, 2002). PIPs are located to the plasma membrane (PM) and can be further divided into PIP1s (five isoforms) and PIP2s (eight isoforms). Together with TIPs (ten isoforms in five subgroups) that are targeted to the tonoplast, they represent the most abundant aquaporins in *Arabidopsis.* The third subfamily are the NIPs, named for their high similarity to nodulin 26, a water channel from soybean connected to osmoregulation in symbiosome membranes (Wallace *et al*., 2006). It consists of nine isoforms separated into seven groups and a putative localization to the endoplasmic reticulum (ER) and plasma membrane has been shown (Mizutani *et al.*, 2006; Takano *et al*., 2006). The final and smallest group is the SIP family with only three isoforms in two groups localized to the ER membrane (Johanson and Gustavsson, 2002; Ishikawa *et al.*, 2005).

In addition, three other subfamilies have been detected: hybrid intrinsic protein (HIPs), GlpF-like intrinsic proteins (GIPs) and the uncategorized X intrinsic protein (XIPs), but they were lost during evolution in some plant lineages such as *A. thaliana* (Gustavsson *et al.*, 2005; Danielson and Johanson, 2008; Gupta and Sankararamakrishnan, 2009; Bienert *et al.*, 2011; Lopez *et al.*, 2012).

1.4.1 Expression and localization of PIPs in *Arabidopsis*

Studies concerning the expression of PIPs revealed diverse patterns regarding different tissues, developmental stages and stress responses. In seeds only *PIP1;2* transcripts were detected, whereas *PIP1;1*, *PIP1;2*, *PIP1;4*, *PIP2;1*, *PIP2;2*, *PIP2;6* and *PIP2;7* were present in two-day-old seedlings (Vander Willigen *et al.*, 2006). The dominant *PIP* transcripts in two-week-old seedlings both in roots and leaves were *PIP1;1, PIP1;2* and *PIP2;7* (Jang *et al.*, 2004). Older plants (4 – 6 weeks) showed a high expression of *PIP1;2*, *PIP2;1* and *PIP2;6* in leaves and *PIP1;1*, *PIP2;2* and *PIP2;7* in roots (Alexandersson *et al.*, 2005; Boursiac *et al.*, 2005). Mass spectrometry and targeted proteomics show mainly the same tendencies on the protein level, PIP2;6 being the exception with high transcription and low protein levels (Santoni *et al.*, 2003; Monneuse *et al.*, 2011). The other PIP transcripts and proteins could be detected, but at relatively low amounts (Jang *et al.*, 2004; Alexandersson *et al.*, 2005; Monneuse *et al.*, 2011). Stresses like drought, high salinity and cold lead to a down regulation of most of the PIPs and in contrast to that, an upregulation of some isoforms, hinting at different functions among the aquaporins (Jang *et al.*, 2004; Alexandersson *et al.*, 2005; Monneuse *et al.*, 2011).

The expression patterns of *PIPs* were observed utilizing *PIP* promoter-β-glucuronidase gene fusions. GUS staining could be observed in vascular tissue and bundle sheath cells in the leaves and in the endodermal cells and the stele in the roots under the control of the PIP2;1 promoter. *PIP2;2* showed a similar localization pattern in the roots, but in addition it is spread to the surrounding mesophyll in leaves (Javot *et al.*, 2003; Da Ines *et al.*, 2010). All leaf tissues were stained for *PIP1;2*, but the expression in roots was confined to the epidermis and the stele as well (Postaire *et al.*, 2010). *PIP2;6* is exclusively localized to the veins, whereas *PIP2;7* shows a more patchy expression in mesophyll cells (Prado *et al.*, 2013). Moreover, it was shown that PIPs are involved in lateral root development (Péret *et al.*, 2012; Zhao, 2013). Most *PIP* transcripts are reduced in response to the rising auxin levels and *PIP2;1* and *PIP2;2* were

excluded from the lateral root tip. In contrast to that, *PIP1;2* and *PIP2;7* were present in the lateral root primordium from the early stages on and were only absent in the regions of highest auxin levels.

The differences in the substrate selectivity, expression, localization and stress responses show the diversity among the aquaporins and their possible role in various physiological processes.

1.4.2 Trafficking and interaction of PIPs

The final destination of PIPs is the plasma membrane and to reach it they follow the secretory pathway. They are synthesized and cotranslationally inserted into the ER and there are two ER export signals known that allow leaving the ER: a diacidic motif (DXE) in the N-terminus and an LxxxA motif in the transmembrane helix 3 (Zelazny *et al.*, 2009; Sorieul *et al.*, 2011; Chevalier *et al*., 2014). After reaching the Golgi apparatus, BEX5/RabA1b, a regulator of protein trafficking, is required for traveling to the PM (Feraru *et al.*, 2012). Moreover, it has been shown that reaching the PM is dependent on SNAREs (soluble N-ethylmaleimide sensitive factor attachment protein receptors), proteins that are involved in vesicle trafficking, fusion and secretion (Zhang *et al.*, 2011; Besserer *et al.*, 2012; Hachez, *et al.*, 2014). After reaching the PM, PIPs show extremely low lateral diffusion, but undergo constant cycling processes mediated by clathrin and membrane raft pathways (Li *et al.*, 2011).

The tetramer formation of the aquaporins occurs even before trafficking to the PM. The first step is the formation of disulfide bridges between two monomers to form a dimer (Bienert *et al.*, 2012; Jozefkowicz *et al.*, 2013). The assembly into tetramers is dependent on amino acid residues in the transmembrane domains (Berny *et al.*, 2016; Yoo *et al.*, 2016). The tetramer formation is very important, because composition of different monomers does not only affect the function, but additionally the trafficking. There is evidence from several different plant species, that a homotetramer of PIP1s is retained at the ER and that heteromerization with PIP2s converts the ability to reach the plasma membrane, suggesting a co-regulation of the two PIP subfamilies (Zelazny *et al.*, 2007; Mut *et al.*, 2008; Matsumoto *et al.*, 2009; Sorieul *et al.*, 2011; Bienert *et al.*, 2018).

1.4.3 Regulation of aquaporins and therefore water permeability of membranes

The regulation of aquaporins can take place at different levels. First of all, numerous post-translational modifications of aquaporins have been reported, which are linked to their regulation. Among these modifications are methylation (Santoni *et al.*, 2006), protonation (Törnroth-Horsefield *et al.*, 2006), disulfide bond formation (Bienert *et al.*, 2012), S-acylation (Hemsley *et al.*, 2013), deamination (di Pietro *et al.*, 2013), ubiquitination (Lee *et al.*, 2009) and phosphorylation (Johansson *et al.*, 1998; Nuhse, 2004; Daniels and Yeager, 2005; Boursiac, *et al.*, 2008). Several kinases and phosphatases modifying aquaporins have been identified (Johnson and Chrispeels, 1992; Azad *et al.*, 2004; Sjövall-Larsen *et al.*, 2006; Li *et al.*, 2015) and the role on gating was elucidated (Johansson *et al.*, 1998; Guenther *et al.*, 2003).

Moreover, gating itself represents another layer of regulation. The high-resolution structure of spinach SoPIP2;1 in an open and closed conformation was used to propose the gating mechanism of aquaporins (Törnroth-Horsefield *et al.*, 2006; Nyblom *et al.*, 2009). The cytosolic loop D folds under the opening of the channel and a conserved leucin (position 197) enters a cavity close to the entrance. By interaction with His 99, Val 104 and Leu 108, a hydrophobic barrier is created, blocking water from entering the pore. Stabilization of the closed conformation is achieved by a network of hydrogen and ionic bonds connecting the loop D with loop B (Ser 115) and a divalent cation binding site in the N-terminus (Asp 28 and Glu 31). Phosphorylation of Ser 115 in loop B and Ser 274 in the C-terminus leads to a displacement of loop D and helix 5 is turned slightly, resulting in an open conformation.

A third mode of regulation is to prevent water transport activity of aquaporins by removing them from the membrane. Studies revealed an internalization of aquaporins in response to high salinity, reducing their content in the membrane and therefore hydraulic conductivity (Boursiac *et al.*, 2005; Luu *et al.*, 2012). Moreover, accumulation of H_2O_2, a reactive oxygen species (ROS) involved in stress signaling, lead to an increased recycling of PIPs (Boursiac, Boudet, *et al.*, 2008). The phosphorylation state of Ser 283 of PIP2;1 regulates the trafficking, where dephosphorylation results in internalization (Prak *et al.*, 2008). The two known pathways involved in endocytosing aquaporins are the membrane raft-associated pathway and the clathrin-dependent pathway (Dhonukshe *et al.*, 2007; Li *et al.*, 2011; Martinière *et al.*, 2012). Taken together this data suggests that stress induced H_2O_2 and dephosphorylation internalize PIPs to regulate membrane water permeability.

Degradation of aquaporins prevents them from transporting water across membranes and thus can be considered as fourth mode of regulation. The hints about MIP degradation in plants in the literature is scarce, but some suggestions are made for the degradation pathways of AtPIP2;1 and AtPIP2;7. PIP2;1 has been shown to be polyubiquitinated and degraded by the proteasome after overexpression of Rma1, an E3 ubiquitin ligase induced by abiotic stresses (Lee *et al.*, 2009). On the other hand, a lytic vacuole-dependent degradation after dark treatment and PIP2;1 trafficking from the PM to the vacuolar lumen was reported (Kleine-Vehn *et al.*, 2008; Ueda *et al*., 2016). Recently, Hachez *et al.* (2014) discovered the interaction between TSPO, a multi-stress regulator, and PIP2;7 at the ER and Golgi membranes. They could show that elevated TSPO protein levels resulted in degradation of PIP2;7 by the autophagic pathway. Even though there is limited knowledge about the degradation of aquaporins, there is evidence for the involvement of several degradation pathways for varying environmental conditions and different PIP isoforms.

1.4.4 PIP2-dependent PIP1 regulation

The dependence of PIP1s on PIP2s to reach the plasma membrane and the increased osmotic water permeability in heterotetramers suggest a co-regulation among these two subfamilies (Fetter *et al*., 2004). Previous studies in our lab (Liu, 2015) revealed a down-regulation of PIP1 proteins in the absence of PIP2;1 in leaves or PIP2;2 in roots (compare **Figure 4**). Quantitative mass spectrometry revealed a down-regulation of all five PIP1 isoforms in the *pip2;1 pip2;2* double mutant (DM) (Zhao, 2013). This observation was further underlined by quantitative ELISA for HA tagged PIP1;1 and PIP1;2 and mean fluorescence measurement for EGFP tagged PIP1s (Liu, 2015). To determine when this down-regulation occurs, qRT-PCR was performed, but no decrease in the *PIP1* transcript levels could be detected in the DM compared to the wild type (Liu, 2015). A His-FLAG tagged ribosomal protein expressed under the control of the *PIP2;2* promotor was introduced into the wild type and DM background to study, weather less *PIP1* mRNAs are bound to the ribosome in the DM in comparison to the wild type. No decrease in ribosome-bound *PIP1* could be detected in the *pip2;1 pip2;2* background compared to the wild type, suggesting that the down-regulation is post-transcriptional and potentially even at the post-translational level (Liu, 2015). PIP2;1 and PIP2;2 might play a role in PIP1 stabilization and their absence leads to ribosome stalls or to degradation of the PIP1 proteins. Since PIP1s might be retained at the ER in the DM, the ER-associated degradation pathway (ERAD) could

be involved. On the other hand, it has been shown that persistent ER stress like protein accumulation leads to the induction of the autophagy and there have been hints for autophagy related degradation of PIP2;7, presenting an alternative pathway for regulation at the protein level (Hachez *et al.*, 2014; Srivastava *et al.*, 2018). Identification of the degradation pathway involved might lead to a better understanding of the PIP2-dependent PIP1 regulation.

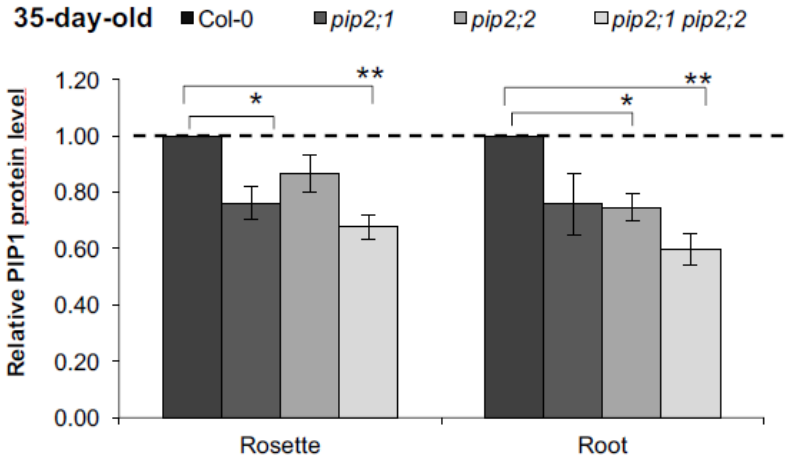

Figure 4: ***Reduction of the PIP1 protein level in* pip2 *mutants.*** *The microsomal fraction of 35-day-old plants was isolated and the PIP1 protein level was determined by an ELISA assay using an anti-PIP1 antibody (detecting all five PIP1 isoforms). Three biological replicates were performed and the standard deviation and significant differences between the lines are shown. Significance was determined by a two-tailed one-sample Student's t-test (p≤0.05: *, p≤0.01: **;* Liu, 2015*).*

1.5 Protein degradation pathways

The fate of PIP1s in the absence of PIP2;1 and PIP2;2 is yet unknown. In the following two putative degradation pathways will be described that could be involved in the PIP2-dependent PIP1 protein down-regulation (compare **Figure 5**).

1.5.1 ER-associated degradation (ERAD)

Secretory and membrane proteins enter the secretory pathway at the ER, where glycosylation and folding cycles involving ER chaperon-like CNX (calnexin)/CRT (calreticulin) take place (Hammond *et al.*, 1994; Aebi, 2013). Folding sensors detect unfolded or misfolded proteins and retain them at the ER (Buck *et al.*, 2007; D'Alessio *et al*., 2010). Htm1 (homologous to mannosidase 1) modifies glycans and thereby stops the folding cycle and marks the misfolded protein for degradation (Clerc *et al.*, 2009).

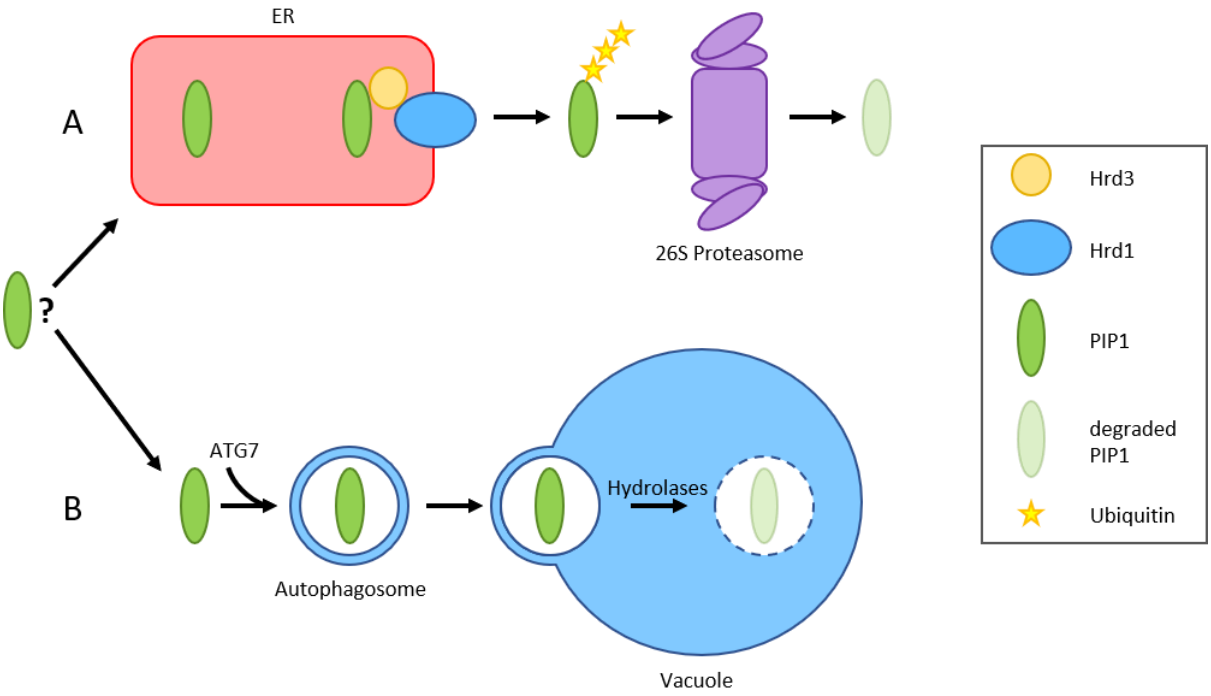

Figure 5: ***Putative degradation pathways for PIP1s.*** *(A) An accumulation of proteins at the ER leads to stress and therefore the activation of the ER associated degradation pathway. The target protein is recruited by Hrd3 and delivered to Hrd1, which is responsible of translocation into the cytosol and ubiquitination. The ubiquitinated protein is then targeted by the 26S proteasome and degraded. (B) Autophagy is a process to recycle cytosolic cell components and is activated by ATG7, an E1-like enzyme. An autophagosome is developed around the cargo, which then fuses with the vacuole for degradation.*

The recognition of ERAD targets involves two proteins: (1) Hrd3 (HMG-CoA reductase degradation 3), which binds to exposed hydrophobic amino acid residues and (2) Yos9 (osteosarcoma 9), decoding the N-glycan ERAD signal (Hirsch *et al.*, 2009). In addition, they transport the ERAD substrates to the membrane-anchored ERAD complex, including a membrane protein with a RING finger-type ubiquitin ligase (E3) activity. Target proteins can be divided into three types, depending on the location of the folding lesion (Vashist and Ng, 2004; Carvalho *et al.*, 2010). The Hrd1 (HMG-CoA reductase degradation 1) complex ubiquitinates proteins with lesions in the ER luminal area ($ERAD_L$) and the transmembrane segment ($ERAD_M$), whereas Doa10 (Degradation of alpha 2) is responsible for substrates with lesions in the cytosolic domain ($ERAD_C$). The catalytic domains of the E3s are on the cytosolic surface of the ER membrane and therefore a retrotranslocation of the client is needed for ubiquitination. Several proteins have been suggested as putative retrotranslocons and the E3 ligase Hrd1 itself was among them (Pilon *et al.*, 1997; Ye *et al.*, 2004; Carvalho *et al.*, 2010; Schoebel *et al.*, 2017). The ubiquitinated targets are subsequently extracted from the ER

lumen and delivered to the cytosolic 26S proteasome for degradation (Wolf and Stolz, 2012). A schematic of this degradation pathway can be seen in **Figure 5 A**.

Most of the proteins involved in ERAD have already been identified in *Arabidopsis thaliana* (Rancour *et al.*, 2002; Jin *et al.*, 2007, 2009; Liu *et al.*, 2011; Hüttner *et al.*, 2012). It has been shown that the degradation of known ERAD substrates was inhibited in *hrd3a* mutants (Liu *et al.*, 2011; Su *et al.*, 2011). Therefore, an *HRD3A* insertion line can be used to study the involvement of ERAD in the PIP2-dependent degradation of PIP1s.

1.5.2 Autophagy related degradation

Autophagy is a degradation process in which cytoplasmic cell contents are recycled and different types have been described: microautophagy, macroautophagy, chaperone-mediated autophagy and organelle-specific autophagy. The molecular mechanisms of macroautophagy (from now on only called autophagy) are summarized below (compare **Figure 5 B**).

During autophagy, an autophagosome forms around the cargo, which is then transported to the vacuole for degradation. Two ubiquitin-like conjugation systems are required for autophagy, involving two ubiquitin-like proteins: ATG8 (autophagy-related protein 8) and ATG12. Both are activated by ATG7, an E1-like enzyme (Mizushima *et al.*, 1998; Ichimura *et al.*, 2000) and localized to the PAS (preautophagosomal structure) during autophagosome formation, driving membrane expansion and vesicle completion. ATG9 is proposed to deliver the lipids required for this process (Suzuki *et al.*, 2001).

In contrast to the yeast system with only one isoform for each ATG, there are often whole families known in *A. thaliana*, for example ATG8 with nine isoforms (Hanaoka, 2002; Sláviková *et al.*, 2005; Chung, Phillips and Vierstra, 2010; Shin *et al*., 2014). ATG7 is involved in both conjugation systems and there is only one gene for it in the *A. th*. genome. Mutation of the *ATG7* gene results in autophagy deficiency, supplying an ideal tool to study this degradation pathway (Doelling *et al.*, 2002).

1.6 Aims of this work

The goal of this work was to get a deeper insight into the PIP2-dependent down-regulation of PIP1 by answering the following questions: (1) When is the interaction taking place? (2) When is the degradation of PIP1 in the absence of PIP2s happening? (3) Which pathway is involved in the degradation of PIP1s?

First of all, Bimolecular fluorescence complementation (BiFC) was used to determine when interaction between different PIP isoforms, especially PIP1s with PIP2s takes place. This approach has the advantage to monitor the cellular localization and the interaction of the proteins of interest at the same time.

In the second part of this thesis the putative stabilizing effect of PIP2 on PIP1 isoforms was analyzed. Mutation of PIP2s' diacidic motif should retain them at the ER and thus make them available for interaction with PIP1s, but not for aiding in trafficking. Therefore, it would be possible to determine whether the interaction as such is sufficient to protect PIP1s from degradation.

A third line of investigation was the specificity of this co-regulation. PIP2;3 and PIP2;7 were expressed under the regulatory elements of *PIP2;2* in the *pip2;1 pip2;2* mutant to analyze whether they can prevent the down-regulation of PIP1s. It can be distinguished, if the specificity depends on the amino acid sequence or the expression pattern.

The fourth topic concerned the degradation mechanism and therefore three approaches were used: (1) previously published and available proteomics data were checked for the influence of degradation inhibitors on PIP protein levels, (2) protoplasts were treated with a proteasome inhibitor and the PIP1;1 level was monitored, and (3) mutants of two different degradation pathways were crossed with *pip2;1 pip2;2* to study the influence on the PIP1 protein level.

The final experiment addressed the question of when the degradation is taking place. PIP1s were tagged with a photoconvertible tag and introduced into the wild type and DM background. Corrected fluorescence recovery after photoconversion (cFRAPc) allows the calculation of the exocytosis rate of the tagged protein and therefore enables to determine, if PIP1s are first traveling to the PM and then degraded or removed before they even reach the plasma membrane.

2 Results

2.1 Where does the interaction between PIPs take place?

It has been shown that some PIP1s need the presence of PIP2s to efficiently reach the plasma membrane which gave rise to the idea that interaction might play a role in the aided trafficking (Zelazny *et al.*, 2007; Sorieul *et al.*, 2011). The transient expression vector pBiFC-2in1-NN generated by Grefen and Blatt (2012) links two proteins of interest with one half of a split enhanced yellow fluorescence protein (EYFP) each. If interaction between the proteins takes place, the EYFP halves will be in close proximity and the fluorescence ability is regained. Moreover, a soluble monomeric red fluorescence protein (mRFP1) is included as a transformation control, to distinguish between unsuccessful transformation and lack of interaction in the absence of a YFP signal. This approach was used to uncover new AtPIP interaction pairs and to determine whether the interaction between the PIPs takes place at the ER or the PM. To prevent interference of endogenous PIPs the *pip1;1 pip1;2 pip2;1 pip2;2* quadruple mutant was used for protoplast isolation and transient transformation.

PIP1;1 was chosen to perform localization and interaction studies with other PIP members. PIP1;2 can interact with PIP1;1 when co-expressed in protoplasts (**Figure 6A**), but they are mainly present at the ER and cannot reach the PM. In contrast to that, combination of PIP1;1 with PIP2;1 and PIP2;2 (**Figure 6B** and **C**, respectively) leads to correct trafficking and a clear signal at the plasma membrane. In addition to that, weak interaction can be detected within the cell, most likely the ER, showing that heteromerization can also take place before routing to the PM. AHA1 is a H^+-ATPase localized to the plasma membrane and was used as a negative control in this experimental setup. As expected, the combination of PIP1;1 and AHA1 (**Figure 6D**) leads to no interaction at the PM. A weak signal can be detected in other regions of the protoplast. This can be explained by the high abundance of the transiently expressed proteins which can lead to random collisions triggering the YFP signal without true physical interaction (Kodama and Hu, 2012). Taken together, this experiment presents new AtPIP interaction pairs which have not been shown in the literature so far. Additionally, the signal at the ER supports the notion that PIP2s guide PIP1s to the plasma membrane by physical interaction.

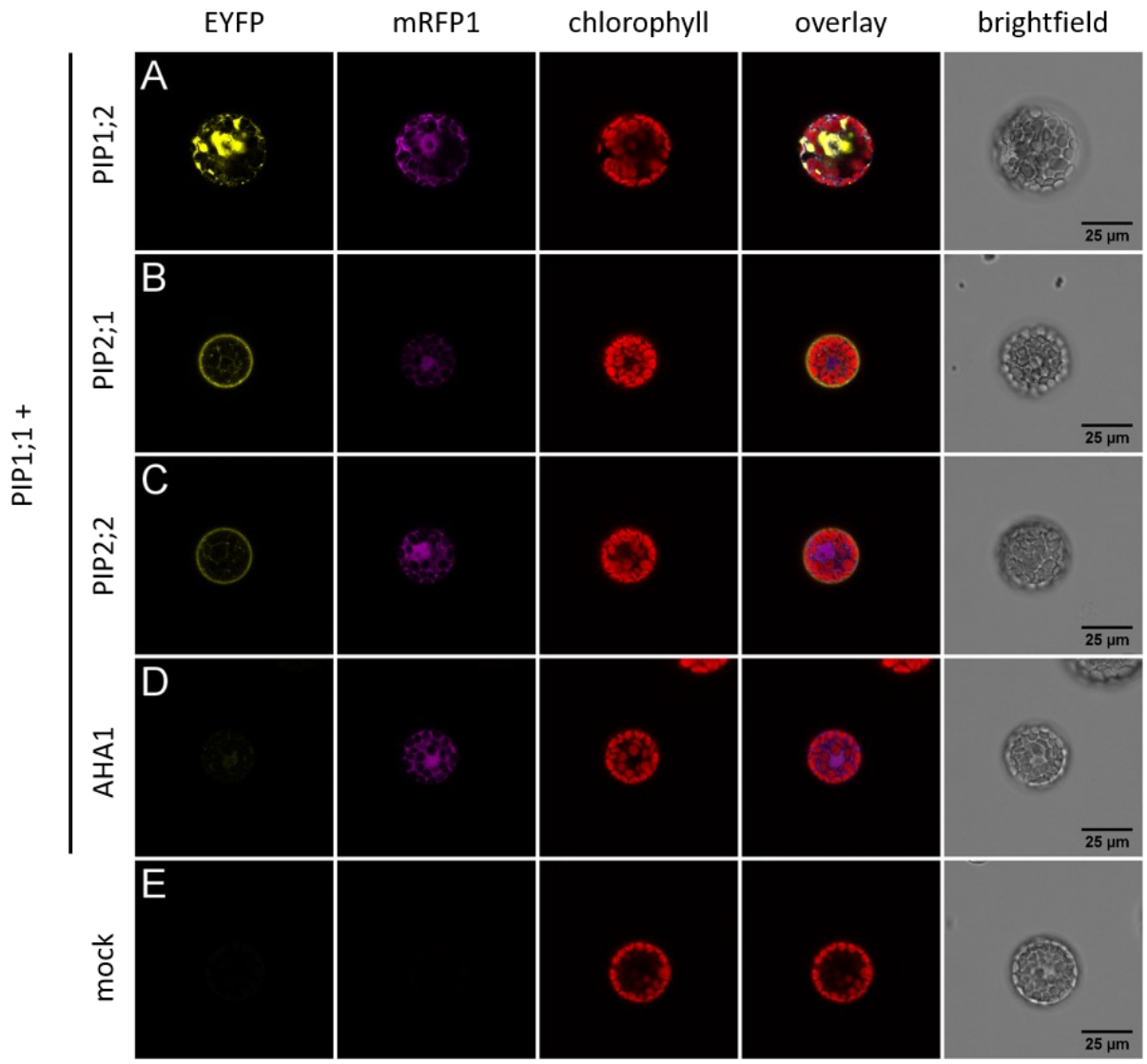

Figure 6: ***Interaction of PIP1;1 and localization of different PIP combinations in protoplasts.*** *Representative confocal images of pBiFC-2in1-NN destination vectors (Grefen and Blatt, 2012) transiently expressed in* A. thaliana *mesophyll protoplasts of the* pip1;1 pip1;2 pip2;1 pip2;2 *quadruple mutant harboring the indicated combination of PIP or control coding sequences. The vector combines the split-EYFP system (tagging both proteins of interest with one half of EYFP) with a monomeric soluble red fluorescence protein (mRFP1) as a transformation control. A Leica SP8 microscope was used for imaging with the following settings for excitation and detection wavelength: 524 nm/520-550 nm (YFP), 590 nm/600-630 nm (RFP) and 514 nm/650-750 nm (detection of autofluorescence of chlorophyll). EYFP^{n}-PIP1;1 was combined with (A) EYFP^{c}-PIP1;2, (B) EYFP^{c}-PIP2;1, (C) EYFP^{c}-PIP2;2 and (D) EYFP^{c}-AHA1. (E) Protoplasts transformed with a mock solution (buffer without DNA) were used as a negative control. Four biological replicates were performed.*

2.2 Is the interaction with PIP2s sufficient to protect PIP1s from degradation?

It has been shown in previous studies (Da Ines, 2008; Zhao, 2013; Liu, 2015; Jhala, personal communication, 2020) that the absence of PIP2;1 and PIP2;2 leads to a reduction in the total PIP1 protein level, suggesting a co - regulation of these proteins (compare **Supplemental Figure 1**). Since neither the transcription nor the translation of PIP1s was affected, the regulation had to take place at the post-translational level.

Chapter 2.1 revealed a role of physical interaction between PIP1s and PIP2s to ensure correct trafficking to the plasma membrane, whereas the absence of PIP2s leads to a retention of PIP1s at the ER (**Chapter 2.1**; Zelazny *et al.*, 2007; Sorieul *et al.*, 2011). The aim of the next experiment was concerning the question, if interaction with PIP2s is sufficient to protect PIP1s from degradation or if trafficking to the PM is needed in addition. Zelazny *et al.* (2009) revealed that a diacidic motif (DVE) at the N-terminus of ZmPIP2;1 is responsible for PIP2's ability to exit the ER. A mutation of this motif (D4A/E6A) leads to a partial retention at the ER, providing a tool to study the dependence of PIP1 protection on trafficking.

2.2.1 Expression and localization of BFP-PIP2 EGFP-PIP1

A diacidic motif as described by Zelazny *et a*l. can be found at the N-terminus of AtPIP2;1, AtPIP2;2 and AtPIP2;3 in *Arabidopsis thaliana*. Since PIP2;3 is expressed at low levels, only PIP2;1 and PIP2;2 were used to study the effect of a mutated diacidic motif of PIP2s on PIP1 proteins. The mutation should lead to a partial retention of PIP2 proteins at the ER, preventing them from guiding PIP1 proteins to the PM, but still being available for interaction. In this experiment the question is addressed, if heteromerization between PIP1s and PIP2s at the ER is sufficient to prevent PIP1 degradation. Visualization of the proteins of interest was achieved by N-terminally tagging them with different fluorescence tags (mTagBFP for PIP2 and EGFP for PIP1). To exclude the influence of endogenous PIP isoforms, multiple mutant lines were used for transformation: *pip1;1 pip2;1 pip2;2 (EGFP-PIP1;1)* and *pip1;2 pip2;1 pip2;2* (EGFP-PIP1;2) to analyze the influence on PIP1;1 and PIP1;2, respectively. Either PIP2;1 or PIP2;2 were added in the mutated (D4A/E6A) or wild-type (WT) modification, resulting in eight different combinations with two independent lines each (compare **Table 1** and EGFP/BFP lines in **Table 4**).

Table 1: PIP1 – PIP2 combinations

PIP2	PIP1	resulting line
PIP2;1	PIP1;1	*pip1;1 pip2;1 pip2;2 (EGFP-PIP1;1, BFP-PIP2;1)*
PIP2;1	PIP1;2	*pip1;2 pip2;1 pip2;2 (EGFP-PIP1;2, BFP-PIP2;1)*
PIP2;1 D4A/E6A	PIP1;1	*pip1;1 pip2;1 pip2;2 (EGFP-PIP1;1, BFP-PIP2;1 D4A/E6A)*
PIP2;1 D4A/E6A	PIP1;2	*pip1;2 pip2;1 pip2;2 (EGFP-PIP1;2, BFP-PIP2;1 D4A/E6A)*
PIP2;2	PIP1;1	*pip1;1 pip2;1 pip2;2 (EGFP-PIP1;1, BFP-PIP2;2)*
PIP2;2	PIP1;2	*pip1;2 pip2;1 pip2;2 (EGFP-PIP1;2, BFP-PIP2;2)*
PIP2;2 D4A/E6A	PIP1;1	*pip1;1 pip2;1 pip2;2 (EGFP-PIP1;1, BFP-PIP2;2 D4A/E6A)*
PIP2;2 D4A/E6A	PIP1;2	*pip1;2 pip2;1 pip2;2 (EGFP-PIP1;2, BFP-PIP2;2 D4A/E6A)*

Five-day-old roots were examined at the beginning of the root hair zone with the PIP1;1 – PIP2;1 and PIP1;2 – PIP2;1 combinations. PIP2;1 is higher expressed in the endodermis and the pericycle, whereas both PIP1 isoforms are evenly distributed among all root layers (compare **Figure 7 A** and **Figure 8 A**). The subcellular localization of the PIP proteins is in the periphery of the cells, consistent with their expected position at the PM (compare **Figure 7 B** and **Figure 8 B**). Mutation of PIP2;1's diacidic motif should result in a partial retention at the ER. No difference in the localization between the wild-type (WT) and the mutated versions (D4A/E6A) of PIP2;1 can be detected, leading to the assumption that the mutation of the diacidic motif does not play a role in trafficking to the PM. The same is true for the PIP1,1 – PIP2;2 and PIP1;2 – PIP2;2 combinations (**Supplemental Figure 2** and **Supplemental Figure 3**).

2.2.2 Influence of the mutated PIP2 diacidic motif on the localization of PIP1s and PIP2s and PIP1 protein stability

Distinguishing the plasma membrane from the ER can be difficult in plant cells, because the vacuole takes up most of the space within the cell. Sorieul *et al.* (2011) applied a method to distinguish between PM and intracellular localized PIPs by using FRAP. This tool was used in the following experiment to determine localization differences between WT and mutant lines.

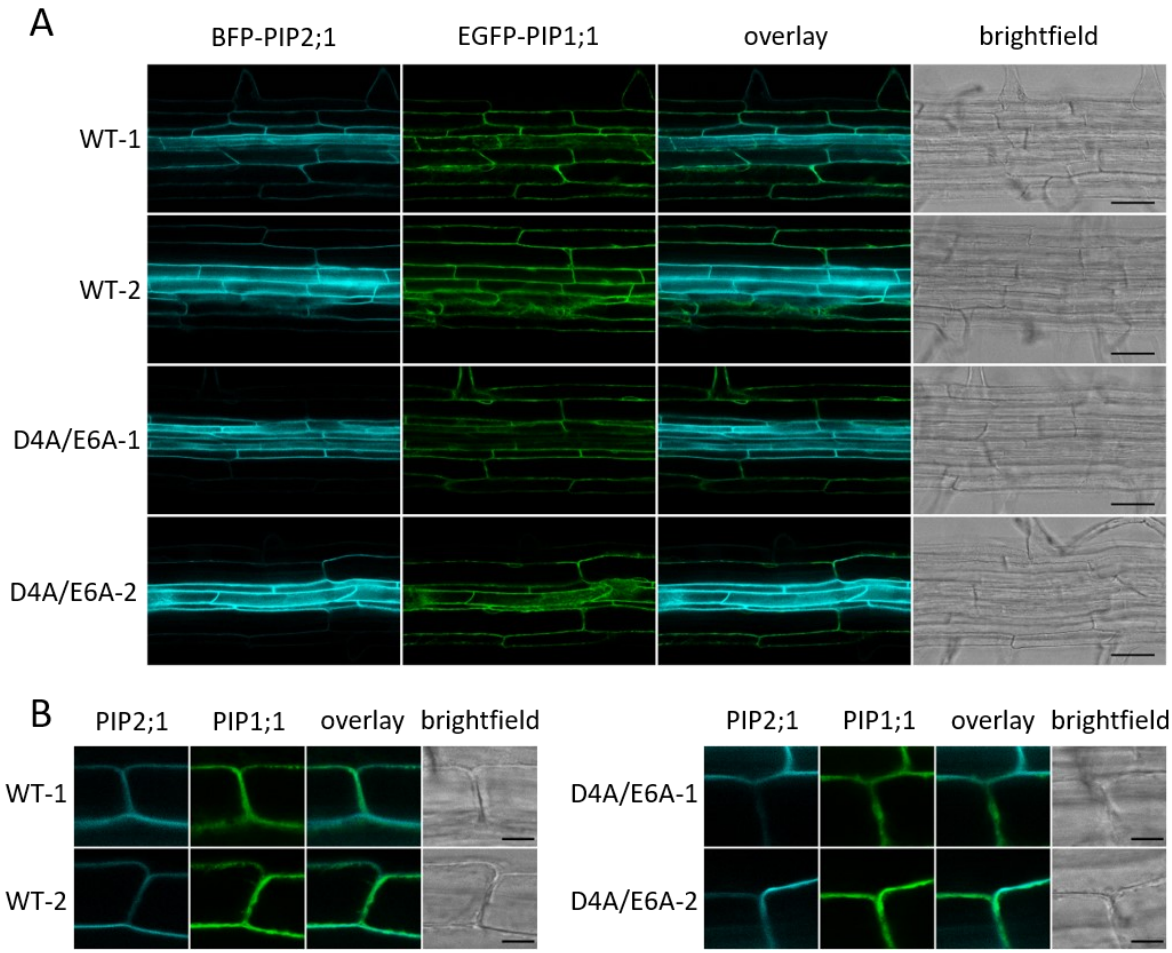

Figure 7: ***Diacidic mutant of BFP-PIP2;1 in the EGFP-PIP1;1 line.*** *(A) Cross-sections of 5-day-old* A. thaliana *roots expressing BFP-PIP2;1 and EGFP-PIP1;1 were used to analyze the effect of a mutated diacidic motif (D4A/E6A) on the localization of both isoforms. All lines are stable single insertion lines and two independent lines (-1/ -2) were used to exclude the influence of the insertion site. A Leica SP8 microscope was used for imaging with the following settings for excitation and detection wavelength: 405 nm/440-480 nm (BFP) and 488 nm/500-550 nm (EGFP). A four times higher excitation intensity was applied for WT-1 compared to the other roots to image the low signal in this line. Two biological replicates were performed. Scale bars, 50 µm. (B) Blow ups of (A) were performed to visualize subcellular localization. Scale bars, 10 µm.*

The lateral movement of proteins localized to the PM can differ between proteins. It has been shown by FRAP experiments that the recovery of NIP5;1 and PIPs attached to a fluorescence marker is slow (Takano *et al.*, 2010; Li *et al.*, 2011; Sorieul *et al.*, 2011). Therefore, one can assume that after bleaching a tangential optical section of a cell, the signal recovery is achieved by exocytosis of proteins with an unbleached fluorescence tag. This in turn means that all the proteins migrating into the bleached region of interest (ROI) were intracellular and not in the plasma membrane. With these prerequisites the relative amount of intracellular and PM localized proteins can be estimated.

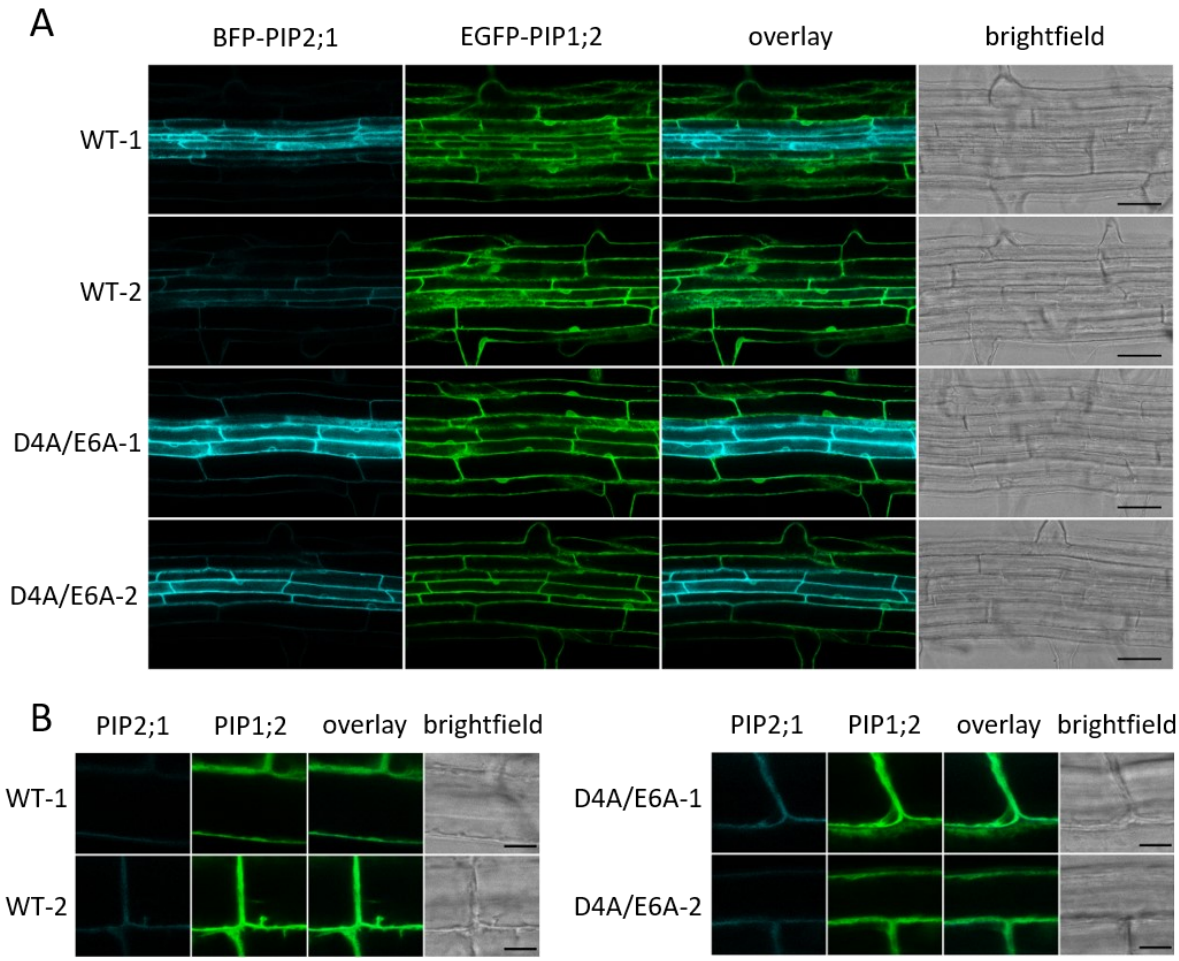

Figure 8: ***Diacidic mutant of BFP-PIP2;1 in the EGFP-PIP1;2 line.*** *(A) Cross-sections of five-day-old* A. thaliana *roots expressing BFP-PIP2;1 and EGFP-PIP1;2 were used to analyze the effect of a mutated diacidic motif (D4A/E6A) on the localization of both isoforms. All lines are stable single insertion lines and two independent lines (-1/ -2) were used to exclude the influence of the insertion site. A Leica SP8 microscope was used for imaging with the following settings for excitation and detection wavelength: 405 nm/440-480 nm (BFP) and 488 nm/500-550 nm (EGFP). Two biological replicates were performed. Scale bars, 50 µm. (B) Blow ups of (A) were performed to visualize subcellular localization. Scale bars, 10 µm.*

Five-day-old roots expressing wild-type PIP2;1 or the mutant modification were used for FRAP experiments to determine the subcellular localization of the PIP proteins (compare **Figure 9 A** and **B** for the PIP1;1 line and Figure 10 **A** and **B** for the PIP1;2 line). The root cells were imaged before bleaching (t_b), immediately after bleaching (t_a) and 5 min after bleaching (t_5) to monitor the bleaching and recovery effects. For PIP2;1 a large signal reduction could be observed after bleaching in the region of interest (ROI, yellow boxes) and after 5 min signal recovery was detected.

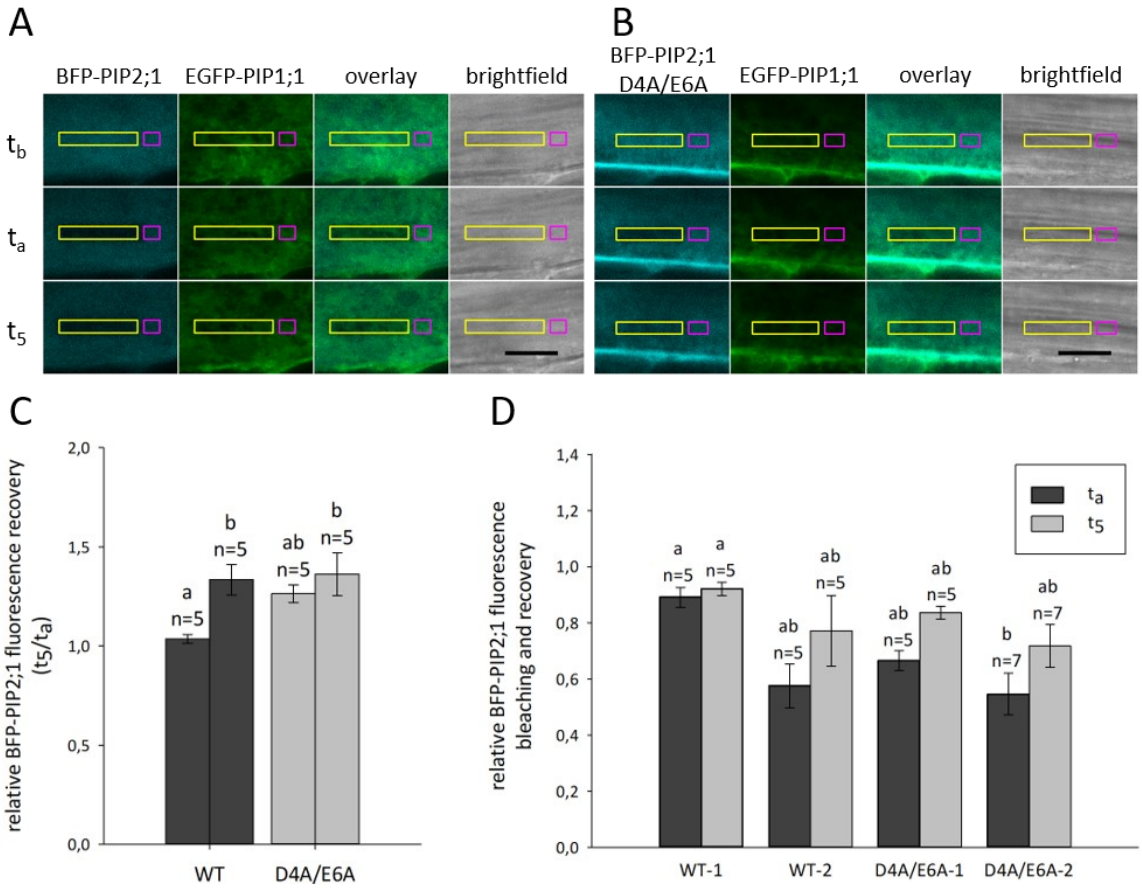

Figure 9: ***FRAP experiments to estimate the intracellular labelling of BFP-PIP2;1.*** *(A, B) Tangential optical sections of 5-day-old* A. thaliana *root cells expressing EGFP-PIP1;1 and WT or D4A/E6A BFP-PIP2;1 constructs were imaged before (t_b), immediately after (t_a) and 5 min after photobleaching (t_5) the region of interest (ROI, shown by yellow boxes). In addition, a nonbleached region (NBR, shown by magenta boxes) was recorded at all time points to use as a reference to measure photobleaching independent fluorescence intensity changes. All lines are stable single insertion lines and two independent lines (-1/ -2, only one displayed as representative) were used to exclude the influence of the insertion site. A Leica SP8 microscope was used for imaging with the following settings for excitation and detection wavelength: 405 nm/440-480 nm (BFP) and 488 nm/500-550 nm (EGFP). Scale bars, 10 µm. (C) Fluorescence recovery after photobleaching of ROI corresponds to intracellular labeled BFP-PIP2;1 trafficking into the ROI. The ratio of t_5 and t_a (t_5/t_a) gives an estimate of relative intracellular labelling, where "1" means no recovery and thus no intracellular labelling and higher values equal higher amounts of intracellular labelling. Standard error values, the number of independent cells studied (n) and significant differences between the lines are shown. Significance ($P<0.05$) was determined by Kruskal-Wallis One Way Analysis of Variance on Ranks with the Dunn's method as the all pairwise multiple comparison procedure. (D) The success of the bleaching experiment can be judged by calculating the relative fluorescence bleaching (t_a) and recovery (t_5) with t_b as the reference. By displaying these values, one can see, if a high reduction of fluorescence intensity is achieved after photobleaching, which is an essential factor to determine usability. Standard error values, the number of independent cells studied (n) and significant differences between the lines are shown. Significance ($P<0.05$) was determined by One Way Analysis of Variance with the Holm-Sidak method as the all pairwise multiple comparison procedure.*

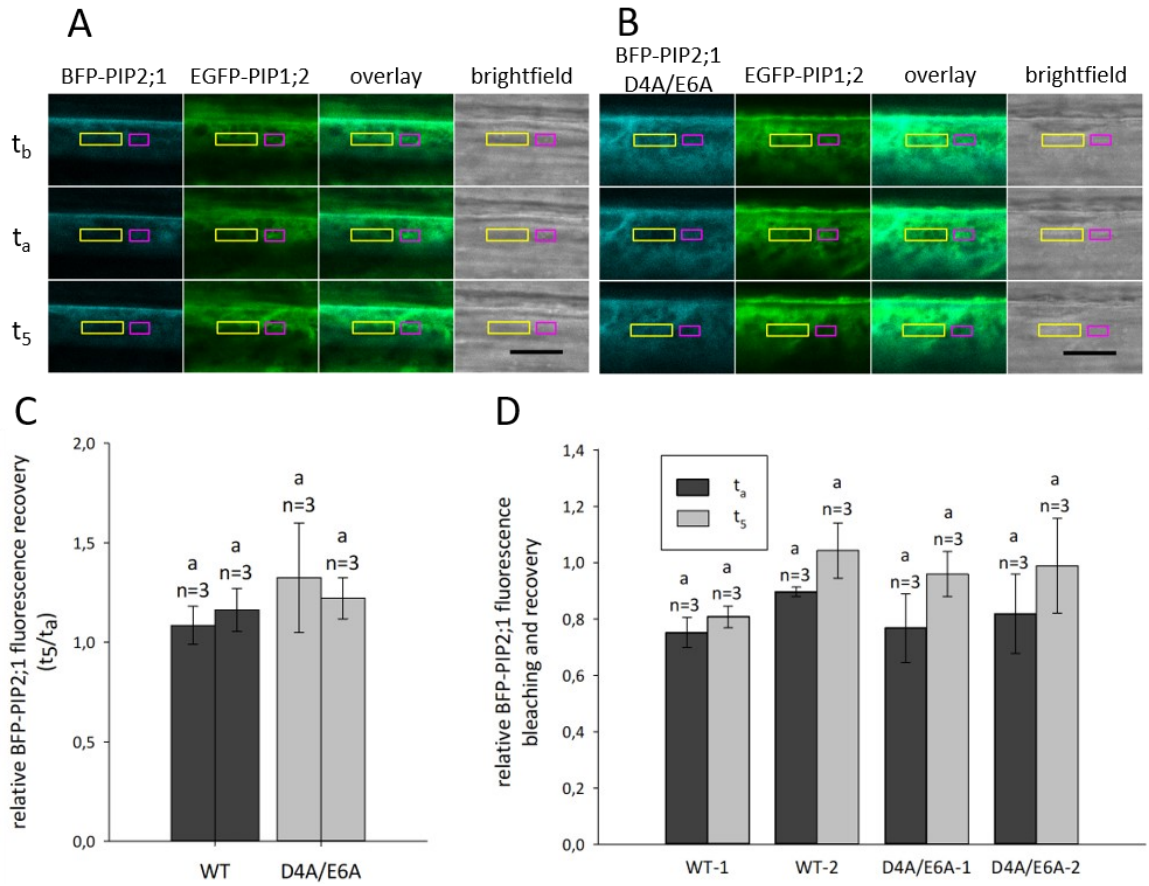

Figure 10: ***FRAP experiments to estimate the intracellular labelling of BFP-PIP2;1.*** *(A, B) Tangential optical sections of five-day-old* A. thaliana *root cells expressing EGFP-PIP1;2 and WT or D4A/E6A BFP-PIP2;1 constructs were imaged before (t_b), immediately after (t_a) and 5 min after photobleaching (t_5) the region of interest (ROI, shown by yellow boxes). In addition, a nonbleached region (NBR, shown by magenta boxes) was recorded at all time points to use as a reference to measure photobleaching independent fluorescence intensity changes. All lines are stable single insertion lines and two independent lines (-1/ -2, only one displayed as representative) were used to exclude the influence of the insertion site. A Leica SP8 microscope was used for imaging with the following settings for excitation and detection wavelength: 405 nm/440-480 nm (BFP) and 488 nm/500-550 nm (EGFP). Scale bars, 10 µm. (C) Fluorescence recovery after photobleaching of ROI corresponds to intracellular labeled BFP-PIP2;1 trafficking into the ROI. The ratio of t_5 and t_a (t_5/t_a) gives an estimate of relative intracellular labelling, where "1" means no recovery and thus no intracellular labelling and higher values equal higher amounts of intracellular labelling. Standard error values, the number of independent cells studied (n) and the lack of significant differences between the lines are shown. No statistically significant difference (P<0.05) was determined by One Way Analysis of Variance. (D) The success of the bleaching experiment can be judged by calculating the relative fluorescence bleaching (t_a) and recovery (t_5) with tb as the reference. By displaying these values one can see, if a high reduction of fluorescence intensity is achieved after photobleaching, which is an essential factor to determine usability. Standard error values, the number of independent cells studied (n) and the lack of significant differences between the lines are shown. No statistically significant difference (P<0.05) was determined by One Way Analysis of Variance.*

Sorieul et al. (2011) used the ratio of the bleached to the nonbleached region (ROI/NBR) at the 5 min timepoint to estimate the amount of intracellularly localized proteins. In the present case, data processing according to Sorieul *et al.* was not possible, because the bleaching did

not result in a complete extinction of the fluorescence signal. Therefore, the earlier timepoint t_a had to be taken into consideration to calculate how much the signal had increased within 5 min. Moreover, the imaging process already led to a weak bleaching. To solve this problem, NBR (**Figure 9** and **Figure 10**, magenta boxes) was used as a reference to calculate a corrected mean fluorescence value of the ROI. The relative amount of intracellular localized PIP2;1 in the different lines was compared by the ratio of t_5/t_a, where a higher value equals a higher amount. The results for the PIP1;1 – PIP2;1 combination show that the difference between the independent lines is significant whereas no differences between the wild-type and mutant can be observed (**Figure 9 C**). In addition, the calculated ratio in the EGFP-PIP1;2 lines is similar for the wild-type and mutated PIP2;1, questioning the influence of the diacidic motif on PIP2;1's trafficking (**Figure 10 C**).

A low bleaching efficiency would affect the ratio calculated in **Figure 9** and **Figure 10 C**, because for a signal which is not decreased, no recovery would be expected. In **Figure 9** and **Figure 10 D** t_a and t_5 were set in relation to t_b, to visualize the bleaching and recovery in the different lines. These experiments highlight, that almost no signal reduction could be detected in the first independent PIP2;1 WT line in the PIP1;1 – PIP2;1 combination (WT-1; **Figure 9 D**), proving that it should be excluded from the analysis. The other lines exhibited clear bleaching and recovery patterns and no significant difference between them could be detected.

The same FRAP experiment was performed for the PIP1 - PIP2;2 combinations, with similar results displayed in **Supplemental Figure 4** and **Supplemental Figure 5**. In summary, no significant difference was observed between the WT and mutated diacidic motif, showing that the mutation had no influence on the localization of PIP2;1 and PIP2;2.

The goal of this experiment was to determine whether the degradation of PIP1s can be prevented by the interaction with PIP2s, although less trafficking of the PIP1s to the plasma membrane is taking place. The mutation of the diacidic ER export motif of PIP2s was supposed to result in a changed routing pattern, but no difference to the WT situation was detected. Therefore, no new conclusions can be drawn on the degradation of PIP1.

To further address this question, it might help to adjust the FRAP conditions to achieve complete bleaching. Moreover, a change in the fluorescence tags might be considered, because mTagBFP is very photosensitive and bleaching already occurs during the imaging process. Fluorescence tags with a good balance between photostability and the ability to be efficiently bleached would be the best choice.

2.3 Can PIP2;3 or PIP2;7 prevent degradation of PIP1s in the absence of PIP2;1 and PIP2;2?

As described before, there is a decrease of the PIP1 protein level in the absence of PIP2;2 (compare **1.4.4**). To study the PIP2-specific down-regulation two PIP2 isoforms were chosen, PIP2;3 and PIP2;7 with the highest and lowest similarities to PIP2;2, respectively (compare **Supplemental Figure 6**). Constructs were designed with the regulatory regions of *PIP2;2* and the coding sequence of *PIP2;3* or *PIP2;7* and transformed into the *pip2;2* mutant. The generated hybrid lines were used to isolate microsomal fractions and to determine the PIP protein levels by an ELISA-based quantification. The regulatory domains of PIP2;2 ensure similar expression patterns and allow the focus on the different amino acid sequences between the three isoforms. This experimental setup can help to determine if the PIP2;1/PIP2;2-specific PIP1 regulation is dependent on a certain expression pattern and/or on characteristics in the amino acid sequence.

2.3.1 PIP2;3

PIP2;3 shows the highest similarity to PIP2;2 (96.8 % identity, compare **Supplemental Figure 6**), but its expression level is extremely low (Jang *et al.*, 2004; Alexandersson *et al.*, 2005; Monneuse *et al.*, 2011). This might be the reason why PIP2;3 is not able to compensate the loss of PIP2;2 and prevent PIP1s from degradation. To evaluate this theory, the capability of the *PIP2;2$_{pro}$:PIP2;3:tPIP2;2* hybrid construct to rescue the *pip2;2* mutant phenotype was analyzed. The microsomal membrane fraction of roots of 14-day-old plants were isolated and the protein levels were quantified by ELISA. Two different primary antibodies were used: anti-PIP1, to measure the combined PIP1 protein level and anti-PIP2;1/PIP2;3/PIP2;3, which can detect those three PIP2 isoforms. Two independent single insertion lines were tested and wild type, *pip2;1* and *pip2;1 pip2;2* lines were included as controls. If PIP2;3 could complement the loss of PIP2;2 in the *pip2;1 pip2;2* mutant, the PIP1 protein level in the hybrid lines should be comparable to the *pip2;1* single mutant.

The PIP1 protein level in the *pip2;1 pip2;2* double mutant is significantly reduced compared to the wild type, whereas the *pip2;1* value lies as expected in between (compare **Figure 11 A**). Both independent hybrid lines exhibit increased PIP1 levels, comparable to the *pip2;1* single mutant, indicating that the *PIP2;2$_{pro}$:PIP2;3:tPIP2;2* hybrid construct can complement the loss

of PIP2;2. To ensure that the increased PIP1 level can be traced back to the higher abundance of PIP2;3, the PIP2;1/PIP2;2/PIP2;3 protein level was analyzed (**Figure 11 B**). The same tendencies in the three control lines could be observed for the PIP2 level, with the highest amount in the wild type and the lowest in the double mutant. The hybrid lines exhibit an elevated amount of PIP2 proteins compared to *pip2;1 pip2;2*, confirming that the increased PIP1 protein level can be linked to the modified expression of PIP2;3.

Taken together, these data confirm that PIP2;3 can protect PIP1 proteins from degradation, if expressed at the same level and with the same expression pattern as PIP2;2.

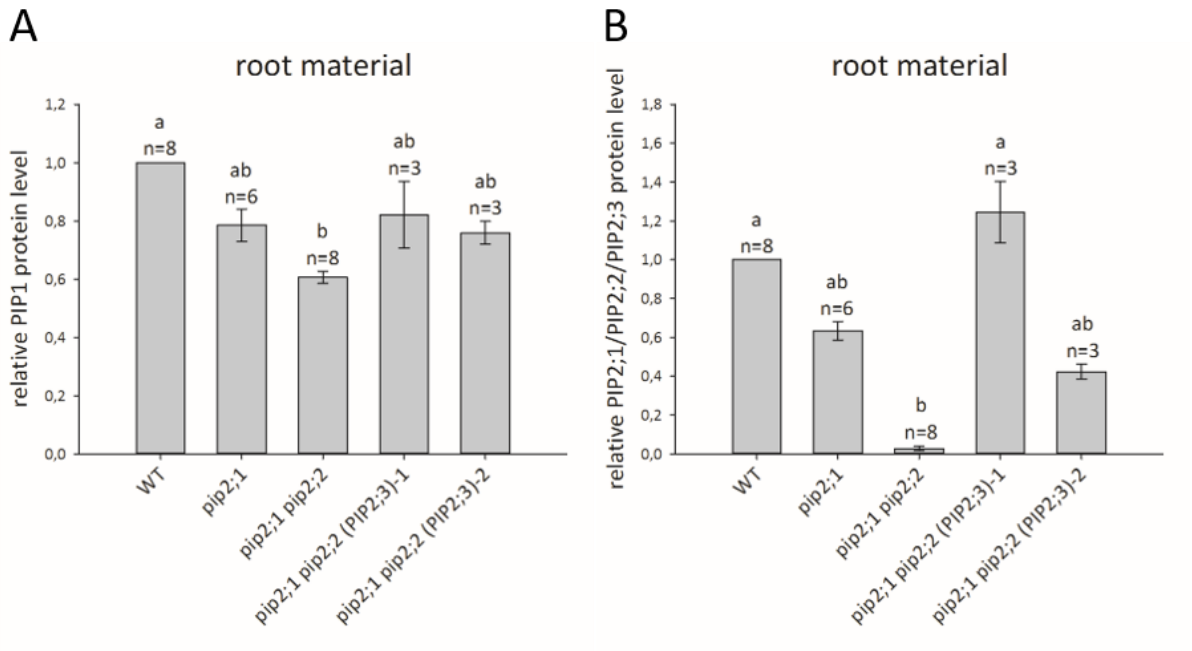

Figure 11: ***Complementation of the* pip2;2 *mutant with PIP2;3.*** *Microsomal fractions of the wild type line and* pip2 *mutants with or without complementation with PIP2;3 were isolated from roots of 14-day-old plants grown on vertical ½ MS plates. An ELISA-based quantification using anti-PIP1 antiserum or anti-PIP2;1/PIP2;2/PIP2;3 antiserum was performed to determine the PIP1 and PIP2;1/PIP2;2/PIP2;3 protein levels, respectively. The relative results are displayed with the wild type line as the reference. (A) PIP1 protein levels in roots. (B) PIP2;1/PIP2;2/PIP2;3 protein levels in roots. Standard error values, the number of independent microsomal fractions studied (n) and significant differences between the lines are shown. Significance (P<0.05) was determined by Kruskal-Wallis One Way Analysis of Variance on Ranks with the Dunn's method as the all pairwise multiple comparison procedure.*

2.3.2 PIP2;7

In contrast to PIP2;2, which is highly abundant in the roots, PIP2;7 is equally present both in leaves and roots, but at a lower total level (Monneuse *et al.*, 2011). Moreover, it has the highest amino acid deviation from PIP2;2 (77.4 % identity, compare **Supplemental Figure 6**). By using the hybrid construct *PIP2;2$_{pro}$:PIP2;7:tPIP2;2*, PIP2;7's expression pattern should equal PIP2;2's pattern and allow the study of the PIP2 sequence specificity on the PIP1 regulation. The experiment was performed as described in **2.3.1** for PIP2;3. If PIP2;7 could complement the loss of PIP2;2 in the *pip2;1 pip2;2* mutant, the PIP1 protein level in the hybrid lines should be comparable to the *pip2;1* single mutant.

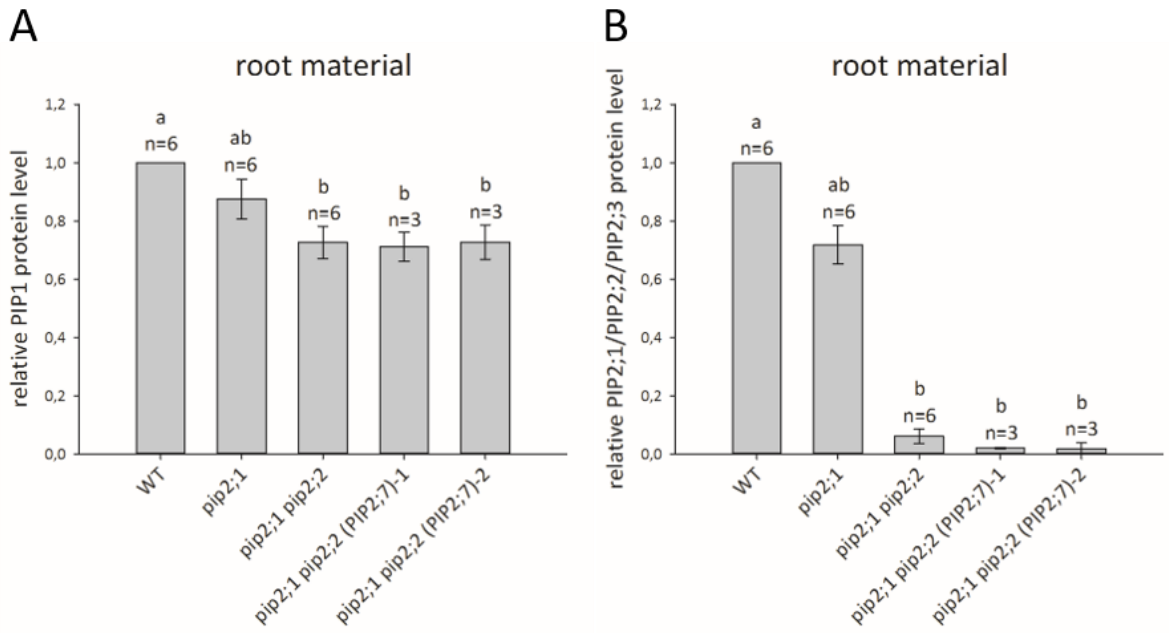

Figure 12: ***Complementation of the* pip2;2 *mutant with PIP2;7.*** *Microsomal fractions of the wild type line and* pip2 *mutants with or without complementation with PIP2;7 were isolated from roots of 14-day-old plants grown on vertical ½ MS plates. An ELISA-based quantification using anti-PIP1 antiserum or anti-PIP2;1/PIP2;2/PIP2;3 antiserum was performed to determine the PIP1 and PIP2;1/PIP2;2/PIP2;3 protein levels, respectively. The relative results are displayed with the wild type line as the reference. (A) PIP1 protein levels in roots. (B) PIP2;1/PIP2;2/PIP2;3 protein levels in roots. Standard error values, the number of independent microsomal fractions studied (n) and significant differences between the lines are shown. Significance (P<0.05) was determined by One Way Analysis of Variance with the Holm-Sidak method as the all pairwise multiple comparison procedure for (A) and by Kruskal-Wallis One Way Analysis of Variance on Ranks with the Dunn's method as the all pairwise multiple comparison procedure for (B).*

The PIP1 protein level is significantly reduced in the double mutant compared to the wild type (**Figure 12 A**) with the *pip2;1* mutant in between. The complementation of *pip2;1 pip2;2* with the hybrid construct results in no change at the PIP1 protein level. This leads to the assumption that the differences in the amino acid sequence between PIP2;7 and PIP2;2 prevent PIP2;7 from regulating PIP1. Therefore, expressing PIP2;7 in the PIP2;2 specific pattern is not sufficient to prevent the degradation of PIP1s.

pip2;1 exhibits a reduction of the PIP2;1/PIP2;2/PIP2;3 protein level in comparison to the wild type which is even more pronounced in the double mutant (compare **Figure 12 B**). As expected, no effect for the addition of PIP2;7 in the hybrid lines could be observed in the analysis of the PIP2 protein level, since the used antiserum can only detect PIP2;1, PIP2;2 and PIP2;3.

In summary, these hybrid studies show that the regulation of PIP1s by PIP2s depends not only on specific expression patterns, but also on the amino acid sequence of the PIP2s', as the PIP2;3 hybrid construct could rescue the *pip2;2* phenotype in contrast to the PIP2;7 construct.

2.4 Which degradation pathway is involved in PIP1 degradation in the absence of PIP2s?

Liu (2015) provided evidence that PIP1 proteins are synthesized at the same amount in the wild type and in the *pip2;1 pip2;2* mutant. The difference in the measured protein level in these mutants arises from degradation of PIP1s in the absence of these PIP2s. To determine which degradation pathway is involved different approaches are possible. In this study published proteomics data (PRIDE database) related to degradation was taken into consideration, an inhibitor was used to block the proteasomal degradation and mutants impairing ERAD or autophagy were crossed with *pip2* mutants.

2.4.1 Influence of the proteasome inhibitor syringolin A on PIP protein level

Svozil *et al.* (2014) performed studies on protein changes in response to the inhibition of the 26S proteasome by syringolin A. They isolated proteins of treated and untreated leaves at three different time points (at the end of the day, midnight and the end of the night) and subjected them to mass spectrometry measurements. The fold change of protein levels, where at least 10 spectra were detected, was calculated and the significance was determined by a paired Students's t-test.

Table 2: ***Influence of syringolin A on PIP1 protein levels.*** A. thaliana *plants grown under short-day conditions for 55 days were treated and leaves were harvested after 8 h at the end of the day, at midnight and after 16 h of treatment at the end of the night. Mass spectrometry was performed, but only proteins with at least 10 spectra were taken into consideration. Treated and untreated samples were compared with a paired t-test, showing no significant differences for all found PIP isoforms.*

	end of day		midnight		end of night	
	p-value	fold change	p-value	fold change	p-value	fold change
PIP1;2	0.772	0.93	0.918	1.01	0.453	1.22
PIP1;5	0.423	0.55			0.184	0.50
PIP2;1	0.938	1.01	0.648	1.09	0.333	1.26
PIP2;2	0.423	0.72			0.185	1.63
PIP2;6	0.915	1.01	0.995	1.00	0.240	1.12
PIP2;7	0.441	0.96	0.428	1.30	0.828	1.03

Eight PIP isoforms were detected in this study, but only six of them met the before mentioned prerequisite (PIP1;3: 9 spectra, PIP1;1: 4 spectra). Fold changes were measured for some isoforms, but no statistically significant differences were detected. At the midnight time point no spectrum of PIP1;5 could be identified in the treated samples and none of PIP2;2 in the control. If proteins were degraded by the 26S proteasome, an inhibition of this pathway should result in an accumulation of these proteins. Interestingly, the fold change seemed to differ more between the PIP isoforms, than between the three observed time points. For example, PIP1;5 showed a decreased amount of protein after treatment with syringolin A, whereas PIP2;1 was slightly increased. The PIP protein levels were not increased as a result of the inhibition of the proteasome for any of the detected PIP isoforms. Therefore, a direct connection between the proteasome pathway and PIP protein degradation could not be identified.

However, the studies of Svozil *et al*. lack an important factor required for achieving the aims of this work, where the focus lies on the degradation pathway of PIP1s in the absence of PIP2s, which were present in this case. The degradation pathway may depend on the availability of PIP2s, leading to the conclusion that involvement of the proteasome cannot be excluded.

2.4.2 PIP1 protein degradation in the presence of proteasome inhibitor (MG132) and/or protein biosynthesis inhibitor (CHX)

The endoplasmic reticulum has a quality-control mechanism to prevent misfolded proteins from exiting the ER and targeting them for degradation by the ER-associated degradation pathway. The proteins are detected, ubiquitinated and transported to the proteasome for disassembly. MG132 is a synthetic peptide aldehyde which inhibits the proteasome activity and blocks the degradation of ubiquitinated proteins (compare **1.5.1**).

As a next step the role of the proteasome in PIP1 degradation in the absence of PIP2;1 and PIP2;2 was assessed. Therefore, mesophyll protoplasts from four-week-old plants were isolated and treated with MG132. To visualize the protein abundance in the protoplast, a line expressing EGFP tagged PIP1;1 in the pip1;1 background was used (*pip1;1* (EGFP-PIP1;1)). The loss of PIP2;1 and PIP2;2 was achieved in a second line harboring in addition the *pip2;1* and *pip2;2* mutations (*pip1;1 pip2;1 pip2;2* (EGFP-PIP1;1)). Taken together these lines supply a wild-type-like and a double mutant-like background with a trackable PIP1;1. The isolated protoplasts were treated without or with MG132 and the fluorescence was measured over the time course of 8 h. To exclude the effect of newly synthesized proteins, cycloheximide (CHX), a protein synthesis inhibitor, was added simultaneously.

Figure 13 A shows that blocking of the 26S proteasome leads to a slightly slower degradation rate of PIP1;1 compared to the mock and untreated controls in the wild-type-like situation. This effect is more pronounced in the double mutant-like background (**Figure 13 B**), showing a significant difference in the PIP1;1 protein level between the MG132 treated and untreated protoplasts. These findings indicate an involvement of the ERAD pathway in PIP1;1 protein degradation, especially in the absence of PIP2;1 and PIP2;2.

In contrast to the treatment with MG132, there is no change of the PIP1;1 protein level after addition of CHX. The amount of PIP1;1 protein synthesized within the 8 h time span of observation might not have been high enough to result in a detectable change by CHX supplementation. To verify the action of CHX a positive control could be included in future experiments.

Taken together these results suggest an involvement of the ERAD pathway in the degradation of the PIP1;1 protein in the presence and absence of PIP2;1 and PIP2;2, but further studies are required to strengthen this theory.

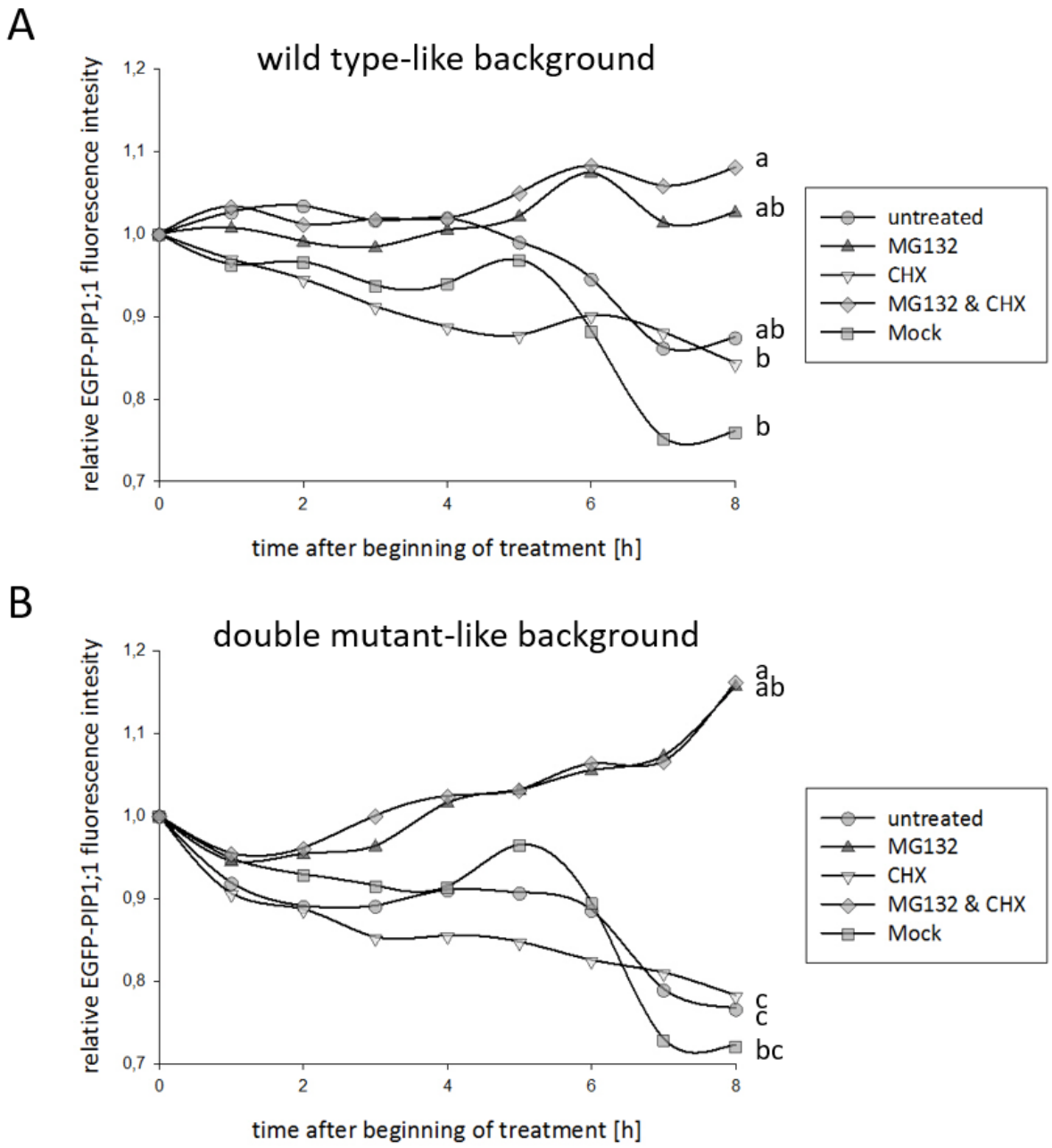

Figure 13: ***Influence of proteasomal degradation on the PIP1;1 protein.*** *Mesophyll protoplasts were isolated from 4-week-old* pip1;1 *(EGFP-PIP1;1) and* pip1;1 pip2;1 pip2;2 *(EGFP-PIP1;1) plants. The fluorescence intensity was measured every hour after treatment with inhibitors (MG132, CHX) or mock (DMSO, EtOH) for 8 h to determine the influence of the proteasome on the PIP1;1 protein level in the wild-type-like (A) and double mutant-like (B) background. The measurement right after inhibitor addition served as a reference (signal intensity for (B) 53 % compared to (A)). Wild type protoplasts were monitored in parallel and the observed fluorescence intensity was used as the background value (17 % compared to* the pip1;1 *(EGFP-PIP1;1) signal). Four biological replicates were performed. Statistically significant differences between treatments (P<0.05) were determined by One Way Analysis of Variance with the time as a discreet factor and the Tukey method as the all pairwise multiple comparison procedure. Corresponding error bars are shown in* ***Supplemental Figure 7****.*

2.4.3 PIP1 protein level in different degradation mutant backgrounds

Autophagy is an important degradation pathway where proteins and whole organelles designated for degradation are enclosed by an autophagosome and transported to the vacuole for further processing. *A. thaliana* has two ubiquitin-like conjugation systems involving two ubiquitin-like proteins, ATG8 and ATG12. Both systems are activated by ATG7, an E1-like enzyme, and can therefore be blocked by the mutation of this single protein (*atg7-1;* Doelling *et al.*, 2002).

ER-associated degradation is a pathway to remove misfolded proteins from the ER (compare **2.4.2**). Hrd3a is an ERAD protein associated with the recognition of target proteins and a defect in this protein (*hrd3a*) leads to the inhibition of misfolded protein degradation and increased UPR (unfolded protein response; Liu *et al.*, 2011).

The degradation of PIP1s in the presence and absence of PIP2s is not necessarily achieved by the same pathway. To distinguish between both cases, not only degradation single mutants were analyzed, but also crossed lines including *pip2;1* and *pip2;2* (degradation mutant x *pip2;1 pip2;2,* compare **Table 4**). The PIP1 protein level was quantified in microsomal membrane fractions of two-week-old plants by ELISA. If a certain degradation pathway plays a role in degrading PIP1, an increased PIP1 protein level is expected. **Figure 14** shows no increase of the PIP1 protein level in any of the single or triple mutant lines, but even a significant decrease for *atg7-1* compared to the wild type. These results indicate no involvement of either ATG7 - dependent or HRD3a-dependent pathways in the degradation of PIP1s.

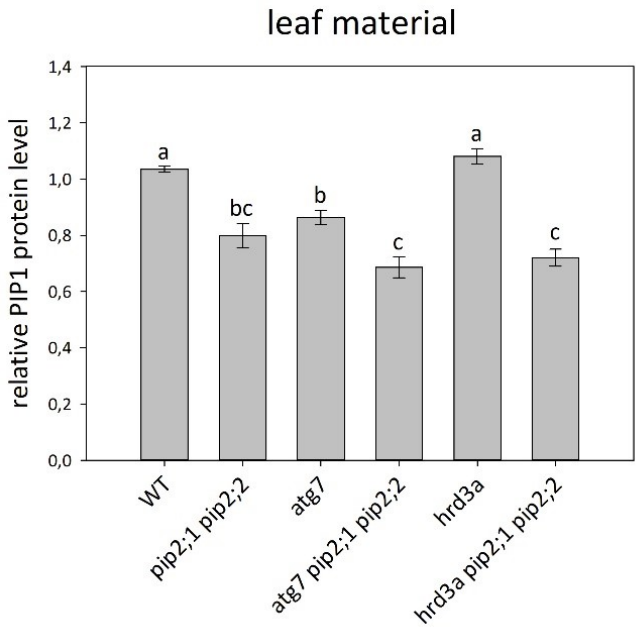

Figure 14: ***PIP1 protein level in degradation mutants.*** *Microsomal fractions of the wild type line and pip2 and degradation mutants were isolated from roots of 14-day-old plants grown on vertical ½ MS plates. An ELISA-based quantification using anti-PIP1 antiserum was performed to determine the PIP1 protein levels. The relative results of four independent biological replicates are displayed with the wild type line as the reference. Standard error values and significant differences between the lines are shown. Significance (P<0.05) was determined by One Way Analysis of Variance with the Holm-Sidak method as the all pairwise multiple comparison procedure.*

2.5 When does the degradation take place?

It is known that the PIP2-dependent PIP1 regulation takes place on the post-translational level, but is it degraded right after synthesis or first transported to the PM? To address this question, the exocytosis rate can be determined by the cFRAPc (corrected fluorescence recovery of after photoconversion; Luo *et al*., 2016) method, where the protein of interest is tagged with a photoconvertible fluorescence protein (mEosFP). The conversion from green to red is achieved by irreversible conformational changes in response to excitation with specific wavelengths (405 nm) and results in a shift in the emission wavelength (Wiedenmann *et al.*, 2004; Nienhaus *et al.*, 2006). The fluorescence of a PM region is quantified, the fluorescence protein converted and the fluorescence of both channels is monitored. Synthesis of new proteins that are transported to the PM leads to the recovery in the green channel and can therefore be used to estimate the exocytosis rate. However, other protein movements are taking place, for example endocytosis, reducing the amount of tagged proteins at the plasma membrane and resulting in the calculation of a too low exocytosis rate. The endocytosis rate can be determined by the fluorescence reduction in the red channel and therefore a corrected exocytosis rate is obtained.

In the case of the PIP1s, the exocytosis rate in the presence and absence of PIP2s can be compared to determine if degradation takes place before or after trafficking to the PM.

2.5.1 Expression and localization of newly generated mEosFP-PIP1 lines

To study the exocytosis rate of PIP1s, new transgenic lines had to be generated (mEosFP lines in **Table 4**). PIP1;1 and PIP1;2 were N-terminally tagged with mEosFP and transformed into the *pip1;1 pip2;1 pip2;2* and *pip1;2 pip2;1 pip2;2* mutant background, respectively, resulting in a double mutant-like background. To receive the wild-type-like background with the insertion at the same site, crossings were performed with *pip1;1* for *pip1;1 pip2;1 pip2;2* (mEosFP-PIP1;1) and *pip1;2* for *pip1;2 pip2;1 pip2;2* (mEosFP-PIP1;2). The following experiments were performed to check the existing lines and optimize conversion settings.

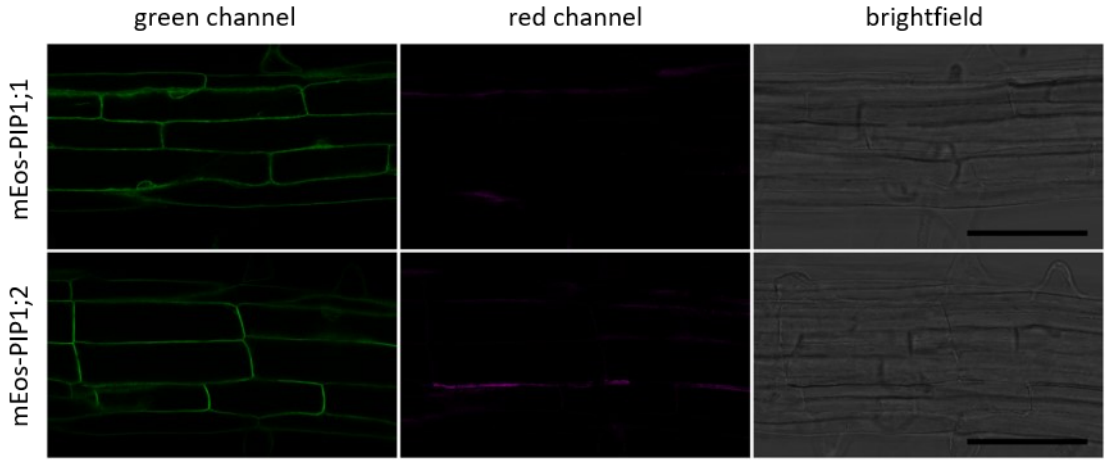

Figure 15: ***mEosFP tagged PIP1;1 and PIP1;2 lines.*** *Cross-sections of five-day-old* A. thaliana *roots expressing mEos-PIP1;1 or mEos-PIP1;2 in the double mutant-like background were imaged in the green and red channel to assess the localization of both proteins and the signal abundance in the red channel without conversion. Two independent lines were generated for each isoform to exclude the influence of the insertion site and one of each is shown above. All lines are stable homozygous single insertion lines. A Leica SP8 microscope was used for imaging with the following settings for excitation and detection wavelength:488 nm/500-550 nm (green mEos) and 570 nm/590-680 nm (red mEos). The expression of PIP1;1 was much lower than PIP1;2. To compensate this difference, a 16 times higher excitation intensity was applied for the mEos-PIP1;1 line.*

Figure 15 shows the expression of the mEosFP tagged PIP1;1 and PIP1;2, where the mEosFP-PIP1;1 line required a much higher excitation intensity for imaging than mEosFP-PIP1;2, representing a lower protein level for this isoform. PIP1s are localized to the PM and intracellular structures, displayed in the green channel, confirming the expected expression and targeting in these lines. A fluorescence signal was detected in the red channel, even though no conversion was performed, but the signal pattern is different to the one in the green channel.

This leads to the conclusion that the red signal is no bleed-through from the green channel or by ambient light converted mEosFP, but autofluorescence. Since the region of interest can be set at a location where no red signal is present before conversion, the interpretation of the data is not further complicated by autofluorescence and the lines can be used for further experiments.

2.5.2 Photoconversion capability of mEosFP-PIP1

The lines shown in **2.5.1** were tested for their ability to photoconvert. To achieve this, a region of the PM was selected, imaged, converted and then imaged again. The results for PIP1;1 are depicted in **Figure 16 A** and **B** and in **Figure 17 A** and **B** for PIP1;2. A significant decrease of the green conformation and increase of the red one can be observed for PIP1;2 but not PIP1;1, indicating that there is a difference between both lines in their ability to photoconvert. To clarify the results, the mean fluorescence intensity before and after the conversion in both channels was measured (compare **Figure 16 C** and **Figure 17 C**), confirming the inability to convert mEosFP-PIP1;1. The green signal is not reduced, whereas the red signal only slightly increased, proving that no efficient conversion had occurred. In contrast to that, conversion was achieved for mEosFP-PIP1;2 (strong mean fluorescence decrease in the green channel, increase in the red channel) where the same settings were applied. Since PIP1;2 shows a higher expression in the root than PIP1;1 and efficient conversion for the attached mEosFP can be performed, only the mEosFP-PIP1;2 line will be used for further studies.

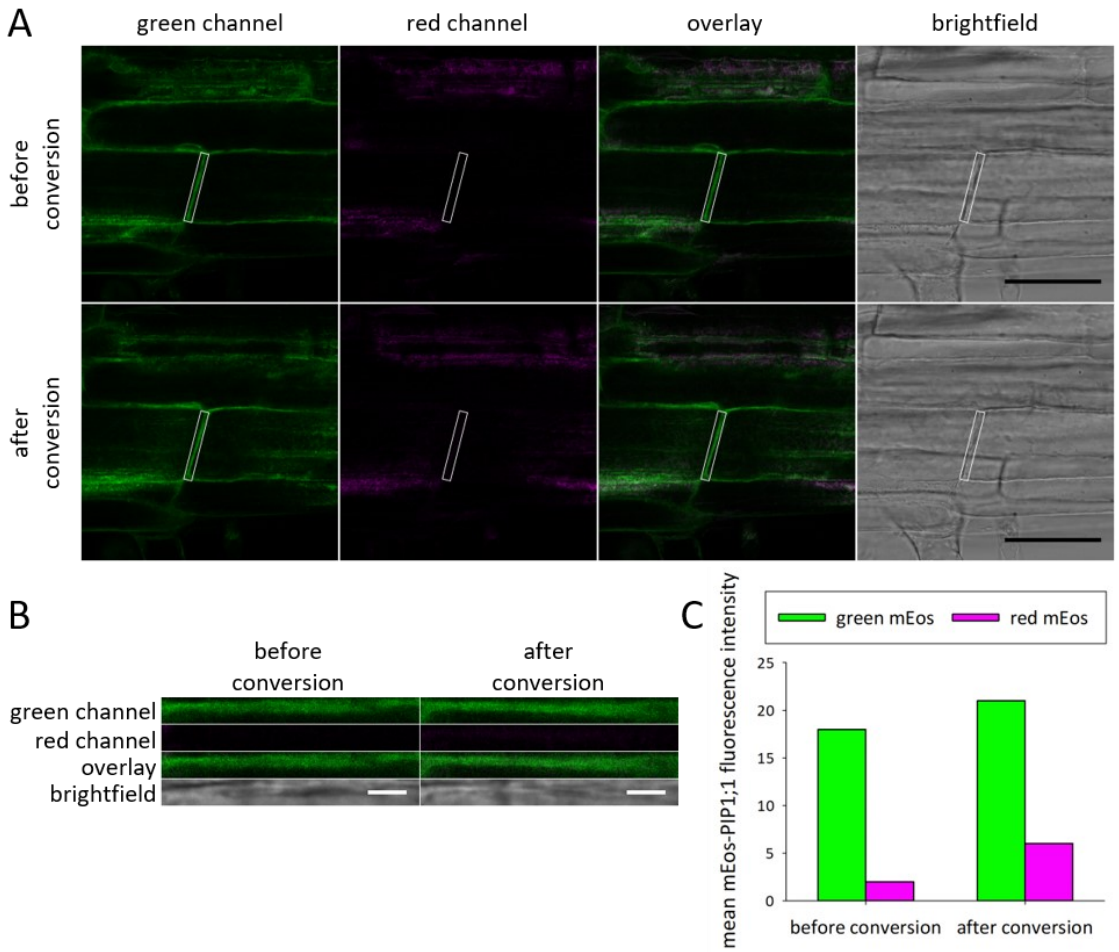

Figure 16: ***cFRAPc imaging of mEos-PIP1;1.*** *Cross-sections of 5-day-old* A. thaliana *roots expressing mEos-PIP1;1 were used to analyze the localization of PIP1;1 and the ability to photoconvert mEosFP. The line displayed is a stable single insertion line and chosen as a representative for four independent lines. A Leica SP8 microscope was used for imaging with the following settings for excitation and detection wavelength:488 nm/500-550 nm (green mEos) and 570 nm/590-680 nm (red mEos). (A) For photoconversion a section of the PM was selected (ROI, shown in the white boxes) and scanned twenty times with 50% excitation intensity at 405 nm. The root was imaged before and after scanning. A successful photoconversion shows a shift from green to red, which was not the case for all four independent lines. Scale bars, 50 µm. (B) is a magnified image of the photoconversion region in (A). Scale bars, 2 µm. (C) The mean fluorescence intensity of the ROI was measured in the green and red channel at both time points, visualizing the inability to photoconvert mEos in this line.*

The photoconversion is achieved by scanning the ROI with 405 nm wavelength several times, leading to a higher amount of converted proteins with each scan, but damaging the samples at the same time. To determine the optimal scan number, the mean fluorescence intensity of the region of interest was measured after each scan in the mEosFP-PIP1;2 line. No change in the intensity between successive scans marks the minimal scan number needed for efficient conversion. As displayed in **Figure 18** the signal remained staticly after 18 scans. For further experiments a number of 20 scans was chosen to ensure a high conversion rate.

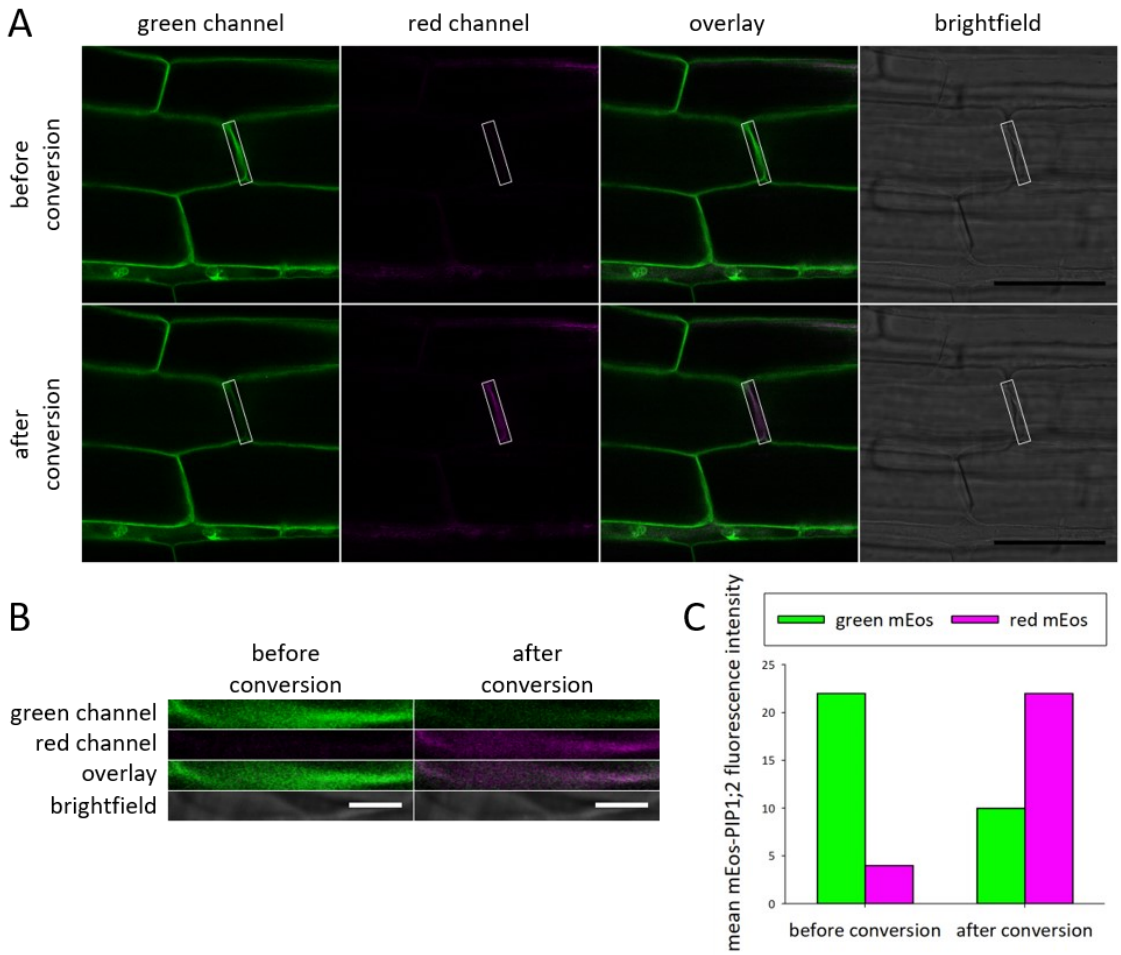

Figure 17: ***cFRAPc imaging of mEos-PIP1;2.*** *Cross-sections of 5-day-old* A. thaliana *roots expressing mEos-PIP1;2 were used to analyze the localization of PIP1;2 and the ability to photoconvert mEosFP. The line displayed is a stable single insertion line and chosen as a representative for two independent lines. A Leica SP8 microscope was used for imaging with the following settings for excitation and detection wavelength:488 nm/500-550 nm (green mEos) and 570 nm/590-680 nm (red mEos). (A) For photoconversion a section of the PM was selected (ROI, shown in the white boxes) and scanned twenty times with 50% excitation intensity at 405 nm. The root was imaged before and after scanning. A successful photoconversion shows a shift from green to red, which was the case for both independent lines. Scale bars, 50 µm. (B) is a magnified image of the photoconversion region in (A). Scale bars, 2 µm. (C) The mean fluorescence intensity of the ROI was measured in the green and red channel at both time points, visualizing the ability to photoconvert mEos in this line.*

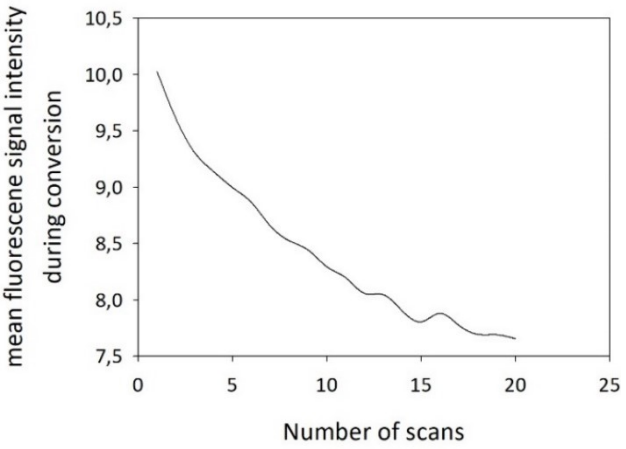

Figure 18: ***Determination of necessary scan number for efficient conversion.*** *Scanning the region of interest with 405 nm wavelength results in conversion of mEosFP. The fluorescence intensity in the ROI was measured after each scan to determine the optimal scan number for conversion.*

2.5.3 Recovery of green mEosFP-PIP1 signal 1h after photoconversion

After photoconverting a region in the plasma membrane, the green signal should recover by the exocytosis of newly synthesized proteins. The aim of this whole experiment is to determine if there is a difference in the exocytosis rate of PIP1;2 in the absence or presence of PIP2;1 and PIP2;2 and to accomplish this a detectable amount of not converted mEosFP-PIP1;2 has to reach the PM. To get an impression on the time line of PIP1;2 synthesis, a pilot study was performed. A root region was imaged before, immediately after and 1 h after conversion and the mean fluorescence intensity in the green and red channels were recorded. A large root section was converted to ensure that the photoconverted region could be found and reassessed after 1 h.

Figure 19 A shows the root section before, after and 1 h after conversion in both the green and red channel. A clear decrease in the green mEos and increase in the red mEos conformation can be detected after photoconversion but no change after 1 h is visible. The mean fluorescence intensity was measured to quantify the changes. The results displayed in **Figure 19 B** show a significant decrease of the green signal after conversion and no change after 1 h, implying that not enough PIP1;2 was synthesized within 1 h to lead to a detectable recovery. This means that the photoconverted root section has to be measured again after a longer period of time.

Taken together, this chapter provides optimized tools for measuring the exocytosis rate and preliminary results on the kinetics for PIP1;2, where 1 h is not sufficient to observe exocytosis. The next step will be to develop a method to attach the seedlings to coverslips without damaging them to allow longer periods of observation.

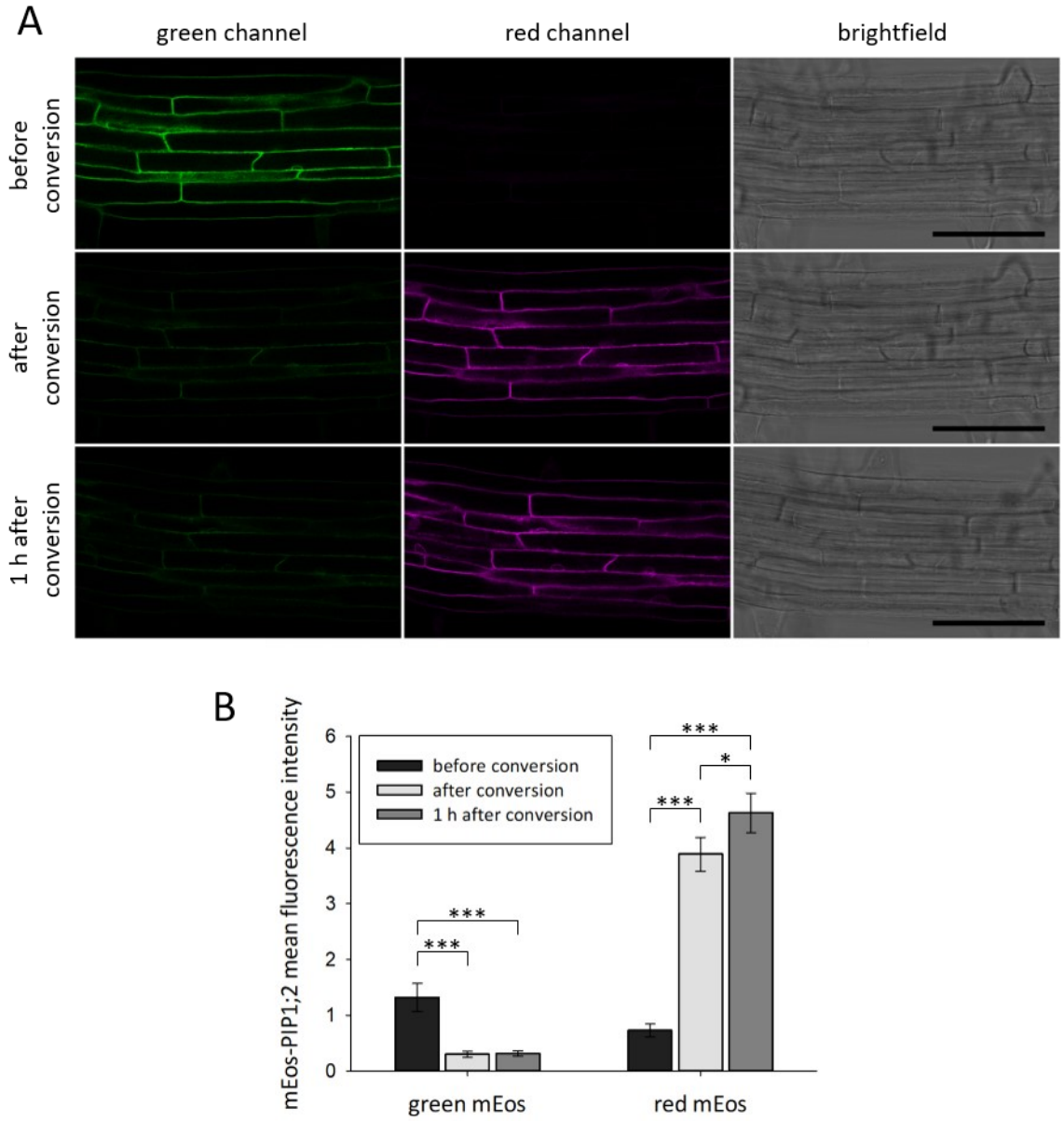

Figure 19: ***Determination of newly synthesized mEos-PIP1;2 within one hour.*** *Cross-sections of 5-day-old* A. thaliana *roots expressing mEos-PIP1;2 were used to measure the amount of newly synthesized mEos-PIP1;2 within one hour. (A) The visible root section was first imaged (t_b) and then photoconverted by using the microscope's DAPI filter. Both channels were documented right after conversion (t_a) and one hour after conversion (t_5). A Leica SP8 microscope was used for imaging with the following settings for excitation and detection wavelength: 488 nm/500-550 nm (green mEos) and 570 nm/590-680 nm (red mEos). Scale bars, 100 µm. (B) The mean fluorescence intensity of the whole root section was measured for both channels at the three time points. The experiment was repeated seven times independently. Standard error values and the significant differences between the time points are shown. The statistically significant difference (P<0.05) was determined by One Way Repeated Measures Analysis of Variance with the Bonferroni t-test as the all pairwise multiple comparison procedure (p ≤ 0.05: *, p ≤ 0.01: **, p ≤ 0.001: ***).*

3 Discussion

The interaction between PIPs in plants has been studied in several publications. Especially the dependence of PIP1s on PIP2s to reach the PM and the influence on the water transport activity was addressed (Fetter *et al.*, 2004; Zelazny *et al.*, 2007; Mut *et al.*, 2008; Sorieul *et al.*, 2011; Bienert *et al.*, 2018). In this thesis the focus was on PIP1 regulation on the protein level dependent on PIP2s. Therefore, the role of interaction, the amino acid sequence specificity of PIP2s, the involved degradation pathways and the exocytosis rate of PIP1 were studied.

3.1 The role of interaction in PIP1 and PIP2 co-regulation

In vitro studies showed that ZmPIP2;1 transiently expressed in maize protoplasts reaches the PM whereas ZmPIP1;1 and ZmPIP1;2 remain at the ER. Only co-expression of ZmPIP2;1 with ZmPIP1s lead to a PM localization pattern for ZmPIP1s (Zelazny *et al.*, 2007). To investigate the role of interaction between PIP1s and PIP2s for PIP1 trafficking in *A. thaliana*, BiFC was performed. The interaction studies revealed physical contact between PIP1;2 and PIP2;1/PIP2;2 both at the PM and the ER, supporting the theory that interaction already appears at the ER and plays a key role in the guided trafficking of PIP1;2.

Furthermore, the question was addressed if interaction of PIP2s with PIP1s is enough to protect PIP1s from degradation or if export from the ER is necessary in addition. Therefore, PIP2 mutants were generated with a reduced ER exiting ability. The effect on the PIP1 protein level could answer the question. If interaction as such is sufficient, there should be no change in the PIP1 protein level between the WT and mutated PIP2 line. PIP1 reduction would show that protection is achieved by trafficking to the PM (compare **Figure 20**). The important key part for this experiment was the changed routing for the mutated PIP2;1 and PIP2;2 compared to the WT situation. This difference could not be observed in any of the generated lines (compare **Figure 9**, **Figure 10**, **Supplemental Figure 4** and **Supplemental Figure 5**).

Sorieul *et al.* (2011) showed a clear difference between the WT PIP2;1 and the PIP2;1 with the mutated diacidic motif (D4A/E6A) regarding the trafficking. There are two major differences between the expression system of Sorieul *et al*. and the experiment in this thesis. (1) For the expression of the WT and mutated PIP2s the endogenous promoter was used in this study. In

contrast to that, the Sorieul lab expressed under a double enhanced CaMV35S. (2) Sorieul *et al*. tagged PIP2;1 with GFP, whereas mTagBFP was fused to PIP2;1 and PIP2;2 in this thesis.

The aim of this experiment was to determine the effect of the changed routing of PIP2 on the PIP1 protein level. Therefore, the expression of the involved proteins should be as close to the WT situation as possible, preventing the use of an enhanced expression system. Therefore, the retention of PIP2 for Sorieul *et al*. could be a result of the artificial flooding of the system and ER retention might endogenously not play a role. In contrast to that, changing the fluorescence tag might be a viable option for improvement. A high fluorescence intensity and the ability to be used for photobleaching experiments would be prerequisites for choosing a new fluorescence protein. Another factor for optimization could be the mutation of the diacidic motif itself. Sorieul *et al*. showed the highest retention rate for D4A PIP2;1, leading to the assumption that a change from D4A/E6A to D4A would enhance the difference between the WT and the mutated phenotype. Chevalier *et al.* (2014) address the importance of another ER export signal in plant aquaporins. They present the LxxxA export motif located to the third transmembrane domain, essential for trafficking. Mutating both motifs (diacidic and LxxxA) should increase the ER retention rate even further and provide the ideal tool to study the role of interaction in the PIP2-dependent PIP1 regulation.

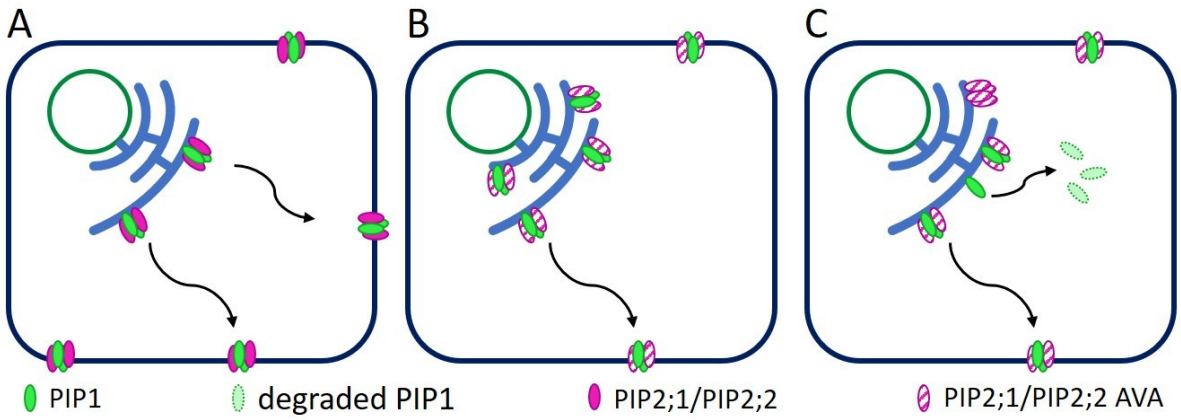

Figure 20: ***Influence of mutation of PIP2s' diacidic motif on the stability of PIP1s.*** *(A) PIP1s and PIP2s form heterotetramers at the ER (light blue) and travel to the PM (dark blue). If the diacidic motif, responsible for ER exiting, is mutated in PIP2s (AVA), their trafficking to the PM is reduced. This could have two possible consequences for PIP1s: (B) The interaction with PIP2s remaining at the ER is enough to stabilize PIP1s. (C) PIP1s are targeted for degradation as a result of the reduced capacity for trafficking from the ER. The nucleus is depicted in dark green.*

In the past it has been shown that on the one hand the ERAD degradation pathway can be activated to prevent accumulation of a certain protein at the ER (Pollier *et al.*, 2013). On the other hand interaction with another protein was shown to prevent degradation (Park *et al.*,

2005; Zschauer *et al.*, 2011). Therefore, both described theories for PIP1 protein regulation (interaction or trafficking, **Figure 20**) are possible options according to the literature.

3.2 Regulation of PIP1s relies on PIP2s' amino acid sequence

The PIP2-dependent down-regulation of PIP1s seems to be connected to PIP2;1 and PIP2;2, since no significant change in the PIP1 protein level was detected in other PIP2 single mutants such as *pip2;3*, *pip2;4* and *pip2;7* (Da Ines and Geist, unpublished data, **Supplemental Figure 1**). Understanding on which factor the co-regulation depends on, the amino acid sequence or the expression pattern, can help to unravel the underlying mechanisms. PIP2;3 shares a high sequence similarity with PIP2;2 but is expressed at low levels, whereas PIP2;7 deviates the most from PIP2;2 and even though it is highly abundant as well, there are differences in the cellular localization patterns between those two isoforms (Da Ines, 2008; Monneuse *et al.*, 2011; Prado *et al.*, 2013). Therefore, the necessary factor for the co-regulation can be determined by expressing *PIP2;3* and *PIP2;7* under the regulatory domains of *PIP2;2* in the absence of PIP2;2 and measuring the resulting PIP1 protein level.

The PIP2;3 hybrid construct can complement the *pip2;2* mutant phenotype, whereas the PIP1 protein level remains unchanged in the PIP2;2$_{pro}$:PIP2;7:tPIP2;2 hybrid lines (compare **Figure 11** and **Figure 12**, respectively). Therefore, adding ectopic expression of PIP2;7 under the control of the *PIP2;2* regulatory domains was not sufficient to protect PIP1 proteins from degradation and a specific amino acid sequence is required to achieve the regulatory function of PIP2;2. Furthermore, it is sufficient to alter the PIP2;3 expression to increase the PIP1 level and complement the *pip2;2* mutant phenotype, because of the high similarity between PIP2;3 and PIP2;2. Hence, a specific amino acid sequence of PIP2s is required for PIP1 regulation. Switching different regions of PIP2;2 with PIP2;7 and examining the effect on PIP1 could help in determining which domain is necessary for the co-regulation.

The anti-PIP2 antiserum only detects the three related isoforms PIP2;1, PIP2;2 and PIP2;3; thus no change in the measured PIP2 signal is expected when *pip2;1 pip2;2* and the PIP2;7-expressing *pip2;1 pip2;2* are compared (compare **Figure 12**). The protein data related to the PIP2;7 expression is essential to prove that no complementation is taking place even though the PIP2;7 hybrid construct is present. To verify PIP2;7 expression, an antibody for PIP2;7 is needed. Only then a reliable statement can be made.

3.3 Degradation of PIP1s in the absence of PIP2s

The PIP1 protein level is strongly reduced in *pip2;1* and *pip2;2* mutants. No down-regulation of *PIP1s'* transcription and no change in the translation could be observed, indicating a post-translational regulation between those two aquaporin groups (Liu, 2015). Polysome-associated *PIP1* gene expression shows an expression of all five *PIP1* genes in the *pip2;1 pip2;2* double mutant at similar or even higher levels compared to WT (Komal Jhala, unpublished results). Determining the degradation pathway involved in the PIP1 protein down-regulation can help to get an insight into the mechanisms behind that co-regulation.

There is not much known about the degradation of PIP proteins in general, but some studies provide information concerning PIP2;1 and, more recently, PIP2;7 (Kleine-Vehn *et al.*, 2008; Lee *et al.*, 2009; Hachez *et al.*, 2014; Ueda *et al.*, 2016). Rma1, a E3 ubiquitin ligase, is induced by drought stress, ubiquitinates PIP2;1 and prevents the trafficking of PIP2;1 from the ER to the PM. PIP2;1 is subsequently degraded by the 26S proteasome. Moreover, it has been shown that dark treatment and salt stress lead to the targeting of PIP2;1 to the lytic vacuole for degradation. In addition, the autophagy related pathway has been suggested for the stress induced degradation of PIP2;7 dependent on TSPO, a multi-stress regulator. Taken together, the 26S proteasome and autophagy represent viable options for degradation mechanisms involved in the PIP2 dependent PIP1 regulation.

3.3.1 Progress in determining the degradation pathway

The first step in determining the degradation pathway of PIP1 proteins in this thesis was to check proteomics data published in the PRIDE database. Svozil *et al*. treated plants with syringolin, a proteasomal inhibitor, which should result in an increase in the protein level of 26S proteasome targets (Svozil *et al.*, 2014). Several PIP isoforms were detected in this study, but no significant fold change between treated and untreated samples was observed (see **Table 2**). Walton *et al.* (2016) implemented ubiquitin combined fractional diagonal chromatography (COFRADIC) to obtain ubiquitination sites. The resulting ubiquitination site mapping did not include any PIP isoforms. In contrast, however, the additionally performed affinity purification on *35S:HIS6UBQ10* plants revealed ubiquitination of PIP1;2 in four out of six samples. Moreover, ubiquitination has been shown for PIP2;1, proving that the post-translational modification of PIP1s cannot be excluded (Lee *et al.*, 2009). The contrasting

results between the first two studies and Lee *et al*. might arise from the different prerequisites, since the ubiquitination of PIP2;1 was linked to abiotic stress conditions and neither Svozil *et al*. nor Walton *et al*. stressed the plants before sampling. PIP proteins are stable and have a low turnover rate under normal conditions, with higher degradation rates under certain stress conditions such as salt and drought (Liu, 2015; Boursiac *et al*., 2005; Hachez *et al*., 2014). The absence of PIPs in the proteasome inhibitor and ubiquitination site studies might therefore be explained by the low amount of PIP isoforms targeted for degradation in unstressed plants being below the detection range of the applied methods.

The second step was to study the influence of MG132 on the PIP1;1 protein level in the absence and presence of PIP2;1 and PIP2;2. A difference in the PIP1;1 protein level between treatment with MG132 and mock treated protoplasts could be detected in both background situations, but was more pronounced in the DM. Hence, an involvement of the proteasome in the degradation of PIP1;1 in the presence and particularly in the absence of PIP2s can be suggested. On the other hand, there was a high variation between the four replicates. As described before, stress has a high impact on the regulation of PIP proteins. To exclude the influence of stress on determining the degradation pathway dependent on PIP2s, the expression of stress markers could be measured in addition. Only replicates from plants with a low stress level should be taken into account. Moreover, the low turnover rate of PIPs makes monitoring over a long period of time necessary, but during this time the protoplast physiology changes as they are starting to regenerate cell walls and more severely, to die. Furthermore, the inhibitor might be another challenge, which is not very stable at RT. Prolonged treatment leads to a decreasing amount of functional MG132 and therefore an increased chance to lose the inhibitory effect on the proteasome. Continuously adding fresh MG132 would help to solve this problem. Nevertheless, a significantly slower decrease of the PIP1 protein level could be detected in the presence of MG132, indicating an involvement of the 26S proteasome in the degradation of PIP1;1 in the absence and presence of PIP2s.

The final experiment regarding the protein degradation was the determination of PIP1 protein levels in mutants deficient in autophagy or ERAD. If the affected degradation pathway is responsible for degrading PIP1s, PIP1 protein accumulation in the mutants is expected. No change between the WT and the ERAD mutant can be detected and even a decrease of PIP1 was observed for the autophagy mutant (compare **Figure 14**). The decrease could mean that a factor related to PIP1 degradation is usually degraded by autophagy and that inhibition of

this degradation pathway increases PIP1 protein processing. The more important question for this thesis was the regulation of PIP1 in the DM background, but no change in the protein level can be observed here. This could lead to the assumption that neither autophagy nor ERAD are involved in the PIP2 dependent PIP1 protein degradation, but recent discoveries give rise to explanations why they cannot be excluded.

Losing a degradation pathway can be challenging for the plant. Therefore, it stands to reason that other pathways can take over some of the targets of missing systems. When Svozil *et al*. (2014) inhibited the 26S proteasome an increase in the transcript levels of *NBR1* (Next to BRCA1 gene 1), responsible for targeting polyubiquitinated proteins to the autophagy pathway, and ATG8a was measured. This upregulation of autophagy marker genes could be a result of a higher demand on autophagy, degrading some of the proteins intended for the proteasome. A similar discovery was made in the human system by Houck *et al.* (2014), where they studied different mutant forms of a protein degraded in a proteasome dependent manner. A mutant version of GnRHR (a hormone receptor degraded by the proteasome) is resistant to proteasomal degradation and thus subjected to autophagy. Additionally, it has been shown that increased unfolded protein response can compensate the loss of Hrd3a (Li *et al.*, 2017). On the other hand, the autophagy deficient mutant *atg5* exhibited increased levels of proteasome sub-units, indicating a compensatory effect (Havé *et al.*, 2018).Therefore, the lack of change in PIP1 protein levels in the degradation mutants could be a result of compensation mechanisms between different degradation pathways. Further crossing to achieve a mutant line deficient in autophagy and proteasomal degradation could help clarify this issue. If PIP1 accumulates in the degradation double mutant, then either or both degradation pathways might be involved. No change in the PIP1 protein level could on one hand be explained by another degradation pathway being responsible for degradation or on the other hand a compensation by a third degradation machinery. However, such a cross between the autophagy and ERAD mutants might not be capable of surviving because two major degradation pathways are deficient. Therefore, a pharmacological approach such as treating the autophagy mutant with a proteasome inhibitor might be a viable alternative.

The ERAD mutant used in this thesis is an insertion line for the *Hrd3a* gene. Hrd3a is responsible for Hrd1 substrate recruitment and should therefore directly interact with PIP1s, if they are degraded by ERAD. Co-immunoprecipitation of Hrd3a and its interaction partners might be a viable alternative to analyze the involvement of the proteasomal degradation in

the PIP2-dependent PIP1 down-regulation. Since there are still open questions regarding ERAD in plants, there could be an alternative protein recruiting targets for Hrd1 (Li *et al.*, 2017). If this is the case, the utilization of the *hrd1a hrd1b* double mutant could be a viable alternative. However, a study in yeast revealed a stabilizing role of Hrd3 on Hrd1, where the Hrd1 protein level was strongly reduced in the *hrd3* mutant (Gardner *et al.*, 2000). If the same is true in plants, a *hrd3* mutant would in addition be at least a *hrd1* knock-down mutant and no new insights could be expected from the newly generated *hrd1a hrd1b pip2;1 pip2;2* line.

The difference between the treatment with MG132 and the *hrd3a* mutant studies could be explained by the duration the plant has to cope with the loss of the proteasomal degradation. A knock-out mutant line is deficient in this degradation pathway. Alternative routes for degradation can be activated and continuously take over the role of the absent pathway. In contrast to that, the treatment with an inhibitor like MG132 results in a sudden change in the plant's degradation system. Other routes might be activated as described above, but this process takes time and therefore the change in the PIP1 protein level could still be detected within the first 8 hours after treatment.

In summary, a clear hint for the proteasome-dependent degradation of PIP1;1 in the absence and presence of PIP2s was discovered. By performing the above suggested experiments, the mechanisms behind the PIP2 dependent PIP1 regulation might be further elucidated.

3.3.2 Time point of degradation (exocytosis rate)

Determining when the degradation of PIP1s in the absence of PIP2s is happening would help in finding the degradation pathway involved and get us one step closer to unraveling the mechanics of this co-regulation between the two aquaporin isoforms. The exocytosis rate is a measured value describing the amount of proteins reaching the PM. Therefore, determining this rate in the absence and presence of PIP2;1 and PIP2;2 can help figuring out when the degradation is taking place. A lower exocytosis rate and no change in the endocytosis rate in the DM background would mean that PIP1s are degraded before reaching the PM.

To get an idea how fast the newly synthesized proteins reach the PM the exocytosis rate for mEos-PIP1;2 in the DM background was measured over a time span of 1 h (**Figure 19**). However, no increase of the unconverted protein at the PM could be detected after 1 h, showing that no quantifiable exocytosis had taken place within this period of time. On the one

hand, the exocytosis rate in the DM background might be so low, that it cannot be detected with this method. The WT background has to be analyzed in comparison to study if exocytosis can be measured in these lines. If this is the case, the consequence would be that the exocytosis rate of PIP1;2 is decreased in the absence of PIP2s, leading to the assumption that PIP1s are degraded before they reach the PM. If there is no exocytosis measurable in the WT background this means that the exocytosis rate of PIP1;2 is so low that it cannot be detected within 1 h. Thus, a system where mEos-PIP1;2 can be observed over a longer period of time would be necessary.

As expected, mean fluorescence of the red conformation increased significantly after conversion, but increased even further within 1 h. Since no additional excitation at 405 nm wavelengths was applied to the material, the increase might have another reason than photoconversion. In **Figure 15** a signal in the red channel was detected before conversion and as described in **2.5.1**, that signal was not caused by a bleed-through from the green channel or conversion by ambient light. It might reflect the damage to the tissue, because of the increased fluorescence after keeping the seedling on the microscope slide covered with a coverslip for 1 h. The roots are quite fragile and immediately damaged upon drying. The roots were continually supplied with liquid ½ MS to prevent desiccation, leading to another kind of stress: hypoxia. Therefore, the increased signal in the red channel might reflect the tissue damage in the roots.

3.4 Potential physiological role of co-regulation

The DM of *pip2;1* and *pip2;2* is an artificial situation for the plant. By studying circumstances where PIP2 protein levels are reduced under natural conditions, the physiological role of the co-regulation between PIP1s and PIP2s might be discovered. It has been observed that such a reduction of most PIP proteins occurs when plants are stressed for example by cold, drought and salt (Jang *et al.*, 2004; Monneuse *et al.*, 2011). It would be interesting to compare the PIP1 protein level in stressed plants of the WT and DM background. If there is a further reduction for the stressed plants in the absence of PIP2;1 and PIP2;2, this would be a hint for an independent role of the co-regulation apart from stress conditions. The alternative outcome would be the same PIP1 protein levels in the WT and DM background. This could be explained by a reduction of PIP2s under the stress condition which leads to a subsequent PIP1 degradation in the WT, resembling the DM phenotype. It is possible that a certain stress signal

can induce PIP2 degradation but has no influence on PIP1s. Therefore, a co-regulation would transmit the signal for degradation from PIP2s to PIP1s and an overall reduction would be achieved (compare **Figure 21**).

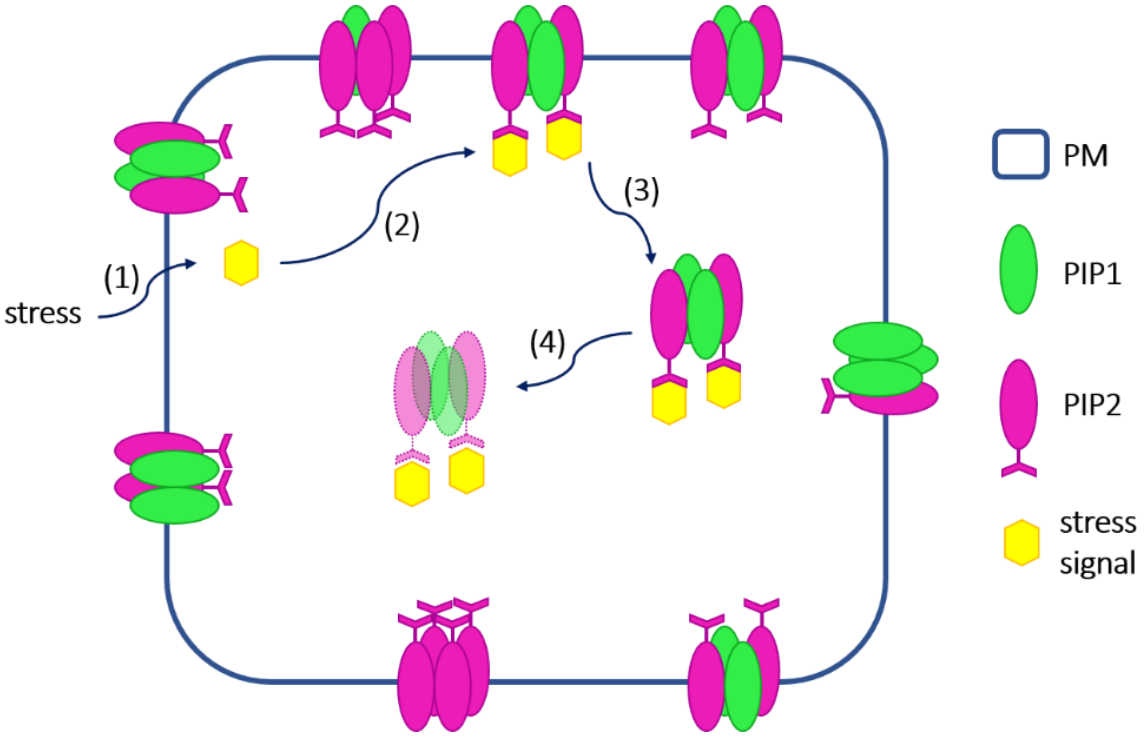

Figure 21: ***Scheme for the putative role of PIP2-PIP1 co-regulation.*** *If* A. th. *is subjected to stress conditions, a stress signal is produced in the cell (1) and recognized by PIP2 but not PIP1 (2). Signal binding results in a removal of the aquaporin tetramer, containing isoforms of both PIP subgroups, from the PM (3). The endocytosed PIPs are degraded (4) and therefore the PIP protein level is reduced.*

4 Outlook

Plants are sessile lifeforms that need to have a tightly regulated water regulation to cope with stresses like drought and heat. One of the key factors to achieve this are aquaporins, water channels which can facilitate the water flow across membranes. The focus in this work was on the co-regulation of PIP1s and PIP2s and the underlying mechanisms to get a better understanding on the control of water flow. The results suggest an ERAD dependent regulation of PIP1s which are directed for degradation in the absence of PIP2 proteins. Specifically, PIP2;1 and PIP2;2 isoforms contribute to this regulation, which can be complemented by highly similar PIP2 like PIP2;3, whereas the more divergent PIP2;7 protein could not replace PIP2;2.

Future work will focus on three main issues: 1) assessing the role of trafficking to the PM in preventing PIP1 down-regulation by studying PIP2 ER exiting mutants (combination of DVE and LxxxA mutations), 2) deepening the knowledge about the mechanisms involved in the PIP2-dependent PIP1 down-regulation by determining the involved degradation pathways (crossing degradation mutants, co-immunoprecipitation of Hrd3a) and the time point of degradation (cFRAPc) and 3) investigating the physiological role of the co-regulation by comparing the PIP2-dependent PIP1 protein level in stressed and unstressed plants.

5 Material and Methods

5.1 Material

5.1.1 Plant material

Table 3: Plant lines used in this work, which were ordered or already present in the lab

Plant line	Ecotype	Description
Wild type	Col-0	Wild type line
pip2;1 pip2;2	Col-0	plasma membrane intrinsic protein 2;1 and 2;2 knock-out line
pip1;1 pip1;2 pip2;1 pip2;2	Col-0	plasma membrane intrinsic protein 1;1 knock-down and plasma membrane intrinsic protein 1;2, 2;1 and 2;2 knock-out line
atg7-1 (SAIL)	Col-0	autophagy related protein 7 knock-out line
hrd3a (SALK)	Col-0	HMG-CoA reductase degradation 3a knock-out line
pip1;1 (EGFP-PIP1;1)	Col-0	plasma membrane intrinsic protein 1;1 knock-down complemented with N-terminally EGFP tagged PIP1;1
pip1;1 pip2;1 pip2;2 (EGFP-PIP1;1)	Col-0	plasma membrane intrinsic protein 1;1 knock-down and plasma membrane intrinsic protein 2;1 and 2;2 knock-out line complemented with N-terminally EGFP tagged PIP1;1
pip1;2 (EGFP-PIP1;2)	Col-0	plasma membrane intrinsic protein 1;2 knock-out line complemented with N-terminally EGFP tagged PIP1;2
pip1;2 pip2;1 pip2;2 (EGFP-PIP1;2)	Col-0	plasma membrane intrinsic protein 1;2, 2;1 and 2;2 knock-out line complemented with N-terminally EGFP tagged PIP1;2
pip2;1 pip2;2 (PIP2;2$_{pro}$:PIP2;3: tPIP2;2)-1	Col-0	plasma membrane intrinsic protein 2;1 and 2;2 knock-out line complemented with a hybrid construct of the PIP2;3 coding region and PIP2;2 regulatory domains (independent line 1)
pip2;1 pip2;2 (PIP2;2$_{pro}$:PIP2;3: tPIP2;2)-1	Col-0	plasma membrane intrinsic protein 2;1 and 2;2 knock-out line complemented with a hybrid construct of the PIP2;3 coding region and PIP2;2 regulatory domains (independent line 2)

Table 4: Plant lines generated in this work

Plant line	Description	Generated by
pip2;1 pip2;2 (PIP2;2$_{pro}$:PIP2;7: tPIP2;2)-1	plasma membrane intrinsic protein 2;1 and 2;2 knock-out line complemented with a hybrid construct of the PIP2;7 coding region and PIP2;2 regulatory domains (independent line 1)	Floral Dip
pip2;1 pip2;2 (PIP2;2$_{pro}$:PIP2;7: tPIP2;2)-2	plasma membrane intrinsic protein 2;1 and 2;2 knock-out line complemented with a hybrid construct of the PIP2;7 coding region and PIP2;2 regulatory domains (independent line 2)	Floral Dip
atg7-1 pip2;1 pip2,2	autophagy related protein 7, plasma membrane intrinsic protein 2;1 and 2;2 knock-out line	crossing
hrd3a pip2;1 pip2;2	EMS-mutagenized BRI1 suppressor 5, plasma membrane intrinsic protein 2;1 and 2;2 knock-out line	crossing
pip1;1 pip2;1 pip2;2 (mEos-PIP1;1)	plasma membrane intrinsic protein 1;1 knock-down and plasma membrane intrinsic protein 2;1 and 2;2 knock-out line complemented with N-terminally mEos tagged PIP1;1	Floral Dip
pip1;2 pip2;1 pip2;2 (mEos-PIP1;2)	plasma membrane intrinsic protein 1;2, 2;1 and 2;2 knock-out line complemented with N-terminally mEos tagged PIP1;2	Floral Dip
pip1;1 pip2;1 pip2;2 (EGFP-PIP1;1, BFP-PIP2;1)	plasma membrane intrinsic protein 1;1 knock-down and plasma membrane intrinsic protein 2;1 and 2;2 knock-out line complemented with N-terminally EGFP tagged PIP1;1 and N-terminally BFP-tagged PIP2;1	Floral Dip
pip1;1 pip2;1 pip2;2 (EGFP-PIP1;1, BFP-PIP2;1 D4A/E6A)	plasma membrane intrinsic protein 1;1 knock-down and plasma membrane intrinsic protein 2;1 and 2;2 knock-out line complemented with N-terminally EGFP tagged PIP1;1 and N-terminally BFP-tagged PIP2;1 D4A/E6A	Floral Dip
pip1;1 pip2;1 pip2;2 (EGFP-PIP1;1, BFP-PIP2;2)	plasma membrane intrinsic protein 1;1 knock-down and plasma membrane intrinsic protein 2;1 and 2;2 knock-out line complemented with N-terminally EGFP tagged PIP1;1 and N-terminally BFP-tagged PIP2;2	Floral Dip
pip1;1 pip2;1 pip2;2 (EGFP-PIP1;1, BFP-PIP2;2 D4A/E6A)	plasma membrane intrinsic protein 1;1 knock-down and plasma membrane intrinsic protein 2;1 and 2;2 knock-out line complemented with N-terminally EGFP tagged PIP1;1 and N-terminally BFP-tagged PIP2;2 D4A/E6A	Floral Dip

Plant line	Description	Generated by
pip1;2 pip2;1 pip2;2 (EGFP-PIP1;2, BFP-PIP2;1)	plasma membrane intrinsic protein 1;2, 2;1 and 2;2 knock-out line complemented with N-terminally EGFP tagged PIP1;2 and N-terminally BFP-tagged PIP2;1	Floral Dip
pip1;2 pip2;1 pip2;2 (EGFP-PIP1;2, BFP-PIP2;1 D4A/E6A)	plasma membrane intrinsic protein 1;2, 2;1 and 2;2 knock-out line complemented with N-terminally EGFP tagged PIP1;2 and N-terminally BFP-tagged PIP2;1 D4A/E6A	Floral Dip
pip1;2 pip2;1 pip2;2 (EGFP-PIP1;2, BFP-PIP2;2)	plasma membrane intrinsic protein 1;2, 2;1 and 2;2 knock-out line complemented with N-terminally EGFP tagged PIP1;2 and N-terminally BFP-tagged PIP2;2	Floral Dip
pip1;2 pip2;1 pip2;2 (EGFP-PIP1;2, BFP-PIP2;2 D4A/E6A)	plasma membrane intrinsic protein 1;2, 2;1 and 2;2 knock-out line complemented with N-terminally EGFP tagged PIP1;2 and N-terminally BFP-tagged PIP2;2 D4A/E6A	Floral Dip

Used insertion lines: *pip1;1* (At3g61430): GABI_437B11*, pip1;2* (At2g45960)*:* SALK_019794*, pip2;1* (At3g53420)*:* SM_3_35928*, pip2;2* (At2g37170)*:* SAIL_169_A03, *atg7-1* (At5g45900): SAIL_11H07/0/2, *hrd3a* (At1g18260): SALK_109430/0/X

5.1.2 Bacteria

Table 5: Bactria strain

Strain	Chromosomal genotype	Source	Purpose
E. coli DH5α	*phoA glnV44 Φ80' lacZ(del)M15 gyrA96 recA1 relA1 endA1 thi-1 hsdR17*	Lab	Cloning
E. coli DB3.1	*F- gyrA462 endA1 glnV44 Δ(sr1-recA) mcrB mrr hsdS20(rB-, mB-) ara14 galK2 lacY1 proA2 rpsL20(Smr) xyl5 Δleu mtl1*	Lab	Maintaining gateway vectors
Agrobacterium tumefaciens GV3101 pMP90	chromosomally encoded resistance against rifampicin and pMP90 (cured, stably inherited Ti plasmid encoding resistance against gentamycin)	Lab	Expression and plant transformation

5.1.3 Kits

Table 6: Applied kits

Kit	Company
Gateway® BP Clonase™ Enzyme Mix, No.11789-013	Invitrogen, Karlsruhe, Germany
Gateway® LR Clonase™ Enzyme Mix, No.11791-019	Invitrogen, Karlsruhe, Germany
QIAprep® Spin Miniprep Kit, No. 27104	Qiagen GmbH, Hilden, Germany
QIAGEN® Plasmid Midi Kit, No. 12143	Qiagen GmbH, Hilden, Germany
QIAquick® PCR Purification Kit, No. 28104	Qiagen GmbH, Hilden, Germany
innuPREP Gel Extraction Kit, No. 845-KS-50300	Analytik Jena, Jena, Germany

5.1.4 Media

Table 7: Media used for growing bacteria or plants

Medium	Composition
LB	1% (w/v) tryptone, 0.5% (w/v) yeast extract, 0.5% (w/v) NaCl, 1.5% (w/v) agar for solid media Adjust to pH 7.0
½ MS	2.2 g/L Murashige-Skoog basal salt mixture, 1% (w/v) sucrose Adjust to pH 5.8 with KOH 0.5% (w/v) gelrite for solid media
MS + Hyg (hygromycin selection)	4.3 g/L Murashige-Skoog salts incl. vitamins, 1% (w/v) sucrose, 0.5 g/L MES hydrate adjust to pH 5.7 (with KOH) 1.2% (w/v) phytoagar for solid media after autoclaving: add 30 µg/ml hygromycin to hand warm medium
RB	1% (w/v) Tryptone, 0.5% (w/v) yeast extract, 0.5% (w/v) NaCl, 0.2% (w/v) 1 M NaOH
TFB1 (transformation buffer 1)	100 mM RbCl, 50 mM $MnCl_2$, 30 mM KOAc (potassium acetate), 10 mM $CaCl_2$, 15% (v/v) Glycerin adjust to pH 5.8 (with acetic acid), use 0.45 µm filter to sterilize

Medium	Composition
TFB2 (transformation buffer 2)	10 mM MOPS, 75 mM $CaCl_2$, 10 mM RbCl, 15% (v/v) Glycerin adjust to pH 6.5 (with KOH), use 0.45 µm filter to sterilize

All media were prepared with ddH_2O and autoclaved for sterilization before use. Plant tissue culture grade chemicals were used.

5.1.5 Buffer

Table 8: Prepared buffers

Buffer name	Composition
Enzyme solution (protoplast isolation)	1-1.5% (w/v) cellulase R10, 0.2-0.4% (w/v) macerozyme R10, 0.4 M mannitol, 20 mM KCl, 20 mM MES (pH 5.7) Incubate at 55 °C for 10 min and cool down to RT 10 mM $CaCl_2$, 0.1% BSA Filter through 0.45 µm syringe filter device
W5 (protoplast isolation)	154 mM NaCl, 125 mM $CaCl_2$, 5mM KCl
PEG (protoplast transformation)	40% (w/v) PEG 4000, 0.2 M mannitol, 100 mM $CaCl_2$ Filter through 0.45 µm syringe filter device
MMg (protoplast transformation)	0.4 M mannitol, 15mM $MgCl_2$
CTAB	1.4 M NaCl, 100mM Tris-HCl (pH 8), 20mM EDTA (pH 8), 2% (w/v) cetyltrimethylammoniumbromid (CTAB), 1% (w/v) polyvinylpyrrolidone (PVP-40)
TE	10 mM Tris-HCl (pH 8), 1mM EDTA (pH 8)
Homogenization buffer (microsomal fraction isolation)	50 mM Hepes-KOH (pH 7.5), 5 mM EDTA (pH 8), 1 mM phenylmethane sulfonyl fluoride (PMSF), 0.01% (w/v) butylated hydroxytoluene (BHT), 2 mM dithiothreitol (DTT), 0.5 M sucrose, cOmplete™ Mini Protease Inhibitor Cocktail 1 tablet/ ml
Resuspension buffer (microsomal fraction isolation)	0.33 M sucrose, 5 mM K_3PO_4 (pH 7.8), 4mM KCl, 2mM dithiothreitol (DTT)
Carbonate-Bicarbonate buffer (ELISA)	3.5% (w/v) Na_2CO_3, 5.6% (w/v) $NaHCO_3$
ABTS (ELISA)	0.1 M citric acid, 0.05% (w/v) 2,2'-azino-bis(3-ethylbenzothiazoline-6-sulphonic acid) (ABTS)

Buffer name	Composition
Phosphate buffered saline (PBS, ELISA)	4 mM KH_2PO_4, 16 mM Na_2HPO_4, 115 mM NaCl
PBS-T (ELISA)	0.1% (v/v) Tween-20 in PBS
PBS-TB (ELISA)	0.1% (v/v) Tween-20 and 1% (w/v) bovine serum albumin (BSA) in PBS
Transformation solution (floral dip)	5% sucrose, 0.05% Silwet L-77
50x TAE buffer	2.0 M Tris, 5.71% (v/v) glacial acetic acid, 50 mM EDTA

Buffers supplied in kits are not listed.

5.1.6 Chemicals

Common chemicals were from SIGMA, Merck, Serva, Roche or Roth with the highest available purity.

Table 9: Chemicals

Chemical	Company
Phenylmethane sulfonyl fluoride (PMSF)	Sigma
Dithiothreitol (DTT)	Roth
Butylated hydroxytoluene (BHT)	Sigma
Cycloheximide (CHX)	Sigma
MG132	Sigma
Cellulase “Onozuka” R-10	Serva
Macerozyme R-10	Serva
Bradford reagent	Bio-Rad
BSA stock solution (20 mg/ml)	New England Biolabs
2,2'-Azino-bis(3-ethylbenzothiazoline-6-sulphonic acid) (ABTS)	Sigma
Cetyltrimethylammoniumbromid (CTAB)	SIGMA

5.1.7 Antibiotics

Table 10: Antibiotics

Antibiotic	Stock concentration	Working concentration
Ampicillin (Amp)	100 mg/ml (in ddH_2O)	100 µg/ml
Spectinomycin (Spec)	10 mg/ml (in ddH_2O)	100 µg/ml
Gentamycin (Gent)	50 mg/ml (Carl-Roth)	25 µg/ml
Rifampicin (Rif)	10 mg/ml (in Methanol)	100 µg/ml
Hygromycin (Hyg)	50 mg/ml (Carl-Roth)	30 µg/ml
Carbenicillin (Car)	100 mg/ml (in ddH_2O)	100 µg/ml
Kanamycin (Kan)	50 mg/ml (in ddH_2O)	50 µg/ml

5.1.8 Enzymes

Table 11: Enzymes

Enzyme	Company
Phusion High Fidelity DNA Polymerase, No. M0530	New England Biolabs
iProof High-fidelity™ Phusion Polymerase, No. 1725300	Bio-Rad
MangoTaq™, No. BIO-21083	Bioline GmbH
Gibson Assembly® Master Mix, No. E2611	New England Biolabs
NcoI, No. ER0571	Thermo Scientific
DraIII, No. R3510S	New England Biolabs
Bsp1470I, No. ER0931	Thermo Scientific
PvuI, No. ER0621	Thermo Scientific
EcoRV, No. ER0301	Thermo Scientific
DpnI, No. ER1701	Thermo Scientific

5.1.9 Antibodies

Table 12: Antibodies

Antibody	Species	Dilution	Source
Anti-rabbit-IgG HRP conjugate, No. W401B	mouse	1:2500	Promega
Anti-PIP1	rabbit	1:2000	Henzler *et al.*, 1999
Anti-PIP2;1/PIP2;2/PIP2;3	rabbit	1:2000	Da Ines, 2008*

*An independent antiserum for the same epitope was kindly provided by Christophe Maurel (Montpellier, France, Santoni *et al*., 2003).

5.1.10 Primer

Primer used for genotyping obtained from SALK-institute:

iSect Primers tool: http://signal.salk.edu/tdnaprimers.2.html

Table 13: Genotyping primer for the WT allele

Plant line	LP primer	RP primer
atg7-1 (SAIL)	CAGCGTGATCTGTGAGAACTG	TTCTTGGAGCTGGTACATTGG
hrd3a (SALK)	TTGTCTACGTTGTCTTTCCCG	TGCGTCTATCCATTAAGGCAG
pip2;1-2 (SM)	AACATATAACGTTGGCAAAAA	TGGTTAAGACAGGGTTAGTCA
pip2;2-3 (SAIL)	AAGTTATAGAAATGGCCAAAGAC	CTCAAACGTTGGCTGCACTTCTG

Table 14: Genotyping primer for insertion

Plant line	Insertion specific primer	RP primer
atg7-1 (SAIL)	TTCATAACCAATCTCGATACAC	TTCTTGGAGCTGGTACATTGG
hrd3a (SALK)	GGTTCACGTAGTGGGCCATC	TGCGTCTATCCATTAAGGCAG
pip2;1-2 (SM)	CTTATTTCAGTAAGAGTGTGGGGTTTTGG	TGGTTAAGACAGGGTTAGTCA
pip2;2-3 (SAIL)	TTCATAACCAATCTCGATACAC	CTCAGCTATTCCGGCTCTGT

Table 15: Primer used for mutagenesis

Name	Mutation	Sequence 5’ → 3’
PIP2;1_MUT_F	D4 → A/ E6 → A	GGAGAAGGATTTCAGACAAGAGACTATCAAGATCCG
PIP2;1_MUT_R	D4 → A/ E6 → A	GGGAACGGCTGCCACAGCCTTTGCCAT
PIP2;2_MUT_F	D4 → A/ E6 → A	GGATTTCAGACAAGAGACTACGAAGATCCGCC
PIP2;2_MUT_R	D4 → A/ E6 → A	CTCAGGTCCTGCCACGGCTTTGGCCAT

Table 16: Primer used for cloning

Name	Sequence 5’ → 3’	Purpose
Att_PIP2;1_PRO_F	GGGGACAAGTTTGTACAAAAAAGCAGGCgaaaatg caaatgattggtg	BFP-PIP2;1
PIP2;1_PRO_BFP_R	ccttaatcagctcgctCATagttaacttcttcttctttca	BFP-PIP2;1
PIP2;1_PRO_BFP_F	tgaaagaagaagaagttaactATGagcgagctgattaagg	BFP-PIP2;1
BFP_PIP2;1_R	TTCCACATCCTTTGCCATtcctgcaccattaagcttgtgccc cagtt	BFP-PIP2;1
BFP_PIP2;1_F	aactggggcacaagcttaatggtgcaggaATGGCAAAGGA TGTGGAA	BFP-PIP2;1
PIP2;1_GW_CO_r	GGGGACCACTTTGTACAAGAAAGCTGG GTtcgagcatttcctatatgatt	BFP-PIP2;1
PIP2;2_PRO_2;3Hy_GW_F	GGGGACAAGTTTGTACAAAAAAGCAGGCtggttgtg agatgaagaataaa	BFP-PIP2;2
PIP2;2_PRO_BFP_R	ccttaatcagctcgctCATttctataacttttttttgttatatat	BFP-PIP2;2
PIP2;2_PRO_BFP_F	atatataacaaaaaagttatagaaATGagcgagctgattaagg	BFP-PIP2;2
BFP_PIP2;2_R	TTCCACGTCTTTGGCCATtcctgcaccattaagcttgtgcc ccag	BFP-PIP2;2
BFP_PIP2;2_F	ctggggcacaagcttaatggtgcaggaATGGCCAAAGACG TGGAA	BFP-PIP2;2
PIP2;2_3U_2;3Hy_GW_R	GGGGACCACTTTGTACAAGAAAGCTGGGTacgatct taccaattgacttg	BFP-PIP2;2
PIP1;1_Pro_GW_B1_F	GGGGACAAGTTTGTACAAAAAAGCAGGCTaaagca tggtaaaattggtg	mEos-PIP1;1

Name	Sequence 5’ → 3’	Purpose
EosFP_PIP1;1_Pro_R 2	TAATCGCACTCATatcttcgatctctgtagagag	mEos-PIP1;1
PIP1;1_Pro_EosFP_F 2	agagatcgaagatATGAGTGCGATTAAGCCAG	mEos-PIP1;1
PIP1;1_EosFP_R 2	CTTCCATtcctgcaccCCGTCTGGCATTGTCAGG	mEos-PIP1;1
EosFP_PIP1;1_F 2	CAATGCCAGACGGgtgcaggaATGGAAGGCAAGG AAGAAG	mEos-PIP1;1
PIP1;1_TER_GW_B2_R	GGGGACCACTTTGTACAAGAAAGCTGGGTctcgtgg aatgatcaaactt	mEos-PIP1;1
PIP1;2_Pro_GW_B1_F	GGGGACAAGTTTGTACAAAAAAGCAGGCTtgagag gaccgatcatgt	mEos-PIP1;2
EosFP_PIP1;2_Pro_R 2	taatcgcactcatCTCTCTCTCTCTTTCTCTCTAG	mEos-PIP1;2
PIP1;2_Pro_EosFP_F 2	aagagagagagagATGAGTGCGATTAAGCCAG	mEos-PIP1;2
PIP1;2_EosFP_R 2	cttccattcctgcaccCCGTCTGGCATTGTCAGG	mEos-PIP1;2
EosFP_PIP1;2_F 2	caatgccagacggggtgcaggaATGGAAGGTAAAGAAG AAGATG	mEos-PIP1;2
PIP1;2_TER_GW_B2_R	ggggaccactttgtacaagaaagctgggtATGCCTTGGTAA TTCAGACA	mEos-PIP1;2

5.1.11 Vectors and plasmids

Table 17: Vectors

Vector	Company	Description
pDONR221	Thermo Fisher Scientific	Donor vector
pDONR221-P1P4	Grefen, University Tübingen	Donor vector
pDONR221-P2P3	Grefen, University Tübingen	Donor vector
pBiFC-2in1-NN	Grefen, University Tübingen	2in1 destination vector
pBiFC-2in1-NC	Grefen, University Tübingen	2in1 destination vector
pHGW	Karimi *et al.*, 2002	Binary destination vector

Table 18: Plasmids

Plasmid	Description
BFP-PIP2;1_pDONR221	N-terminally BFP tagged PIP2;1 with endogenous promotor and 3'-UTR in pDONR221
BFP-PIP2;1 D4A/E4A_pDONR221	N-terminally BFP tagged PIP2;1 D4A/E4A with endogenous promotor and 3'-UTR in pDONR221
BFP-PIP2;2_pDONR221	N-terminally BFP tagged PIP2;2 with endogenous promotor and 3'-UTR in pDONR221
BFP-PIP2;2 D4A/E4A_pDONR221	N-terminally BFP tagged PIP2;2 D4A/E4A with endogenous promotor and 3'-UTR in pDONR221
BFP-PIP2;1_pHGW	N-terminally BFP tagged PIP2;1 with endogenous promotor and 3'-UTR in pHGW
BFP-PIP2;1 D4A/E4A_pHGW	N-terminally BFP tagged PIP2;1 D4A/E4A with endogenous promotor and 3'-UTR in pHGW
BFP-PIP2;2_pHGW	N-terminally BFP tagged PIP2;2 with endogenous promotor and 3'-UTR in pHGW
BFP-PIP2;2 D4A/E4A_pHGW	N-terminally BFP tagged PIP2;2 D4A/E4A with endogenous promotor and 3'-UTR in pHGW
mEos-PIP1;1_pDONR221	n-terminally mEos tagged PIP1;1 with endogenous promotor and 3'-UTR in pDONR221
mEos-PIP1;2_pDONR221	n-terminally mEos tagged PIP1;2 with endogenous promotor and 3'-UTR in pDONR221
mEos-PIP1;1_pHGW	n-terminally mEos tagged PIP1;1 with endogenous promotor and 3'-UTR in pHGW
mEos-PIP1;2_pHGW	n-terminally mEos tagged PIP1;2 with endogenous promotor and 3'-UTR in pHGW
PIP1;1_pDONR221-P1P4*	PIP1;1 cDNA in pDONR221-P1P4
PIP1;1_pDONR221-P2P3*	PIP1;1 cDNA in pDONR221-P2P3
PIP1;2_pDONR221-P1P4*	PIP1;2 cDNA in pDONR221-P1P4
PIP2;1_pDONR221-P1P4*	PIP2;1 cDNA in pDONR221-P1P4
PIP2;2_pDONR221-P1P4*	PIP2;2 cDNA in pDONR221-P1P4
AHA1_pDONR221-P1P4*	AHA1 cDNA in pDONR221-P1P4

Plasmid	Description
PIP1;1+PIP1;1_pBiFC-2in1-NN*	N-terminally YFP^N tagged PIP1;1 and N-terminally YFP^C tagged PIP1;1 in pBiFC-2in1-NN
PIP1;1+PIP1;2_pBiFC-2in1-NN*	N-terminally YFP^N tagged PIP1;1 and N-terminally YFP^C tagged PIP1;2 in pBiFC-2in1-NN
PIP1;1+PIP2;1_pBiFC-2in1-NN*	N-terminally YFP^N tagged PIP1;1 and N-terminally YFP^C tagged PIP2;1 in pBiFC-2in1-NN
PIP1;1+PIP2;2_pBiFC-2in1-NN*	N-terminally YFP^N tagged PIP1;1 and N-terminally YFP^C tagged PIP2;2 in pBiFC-2in1-NN
PIP1;1+AHA1_pBiFC-2in1-NC*	N-terminally YFP^N tagged PIP1;1 and C-terminally YFP^C tagged AHA1 in pBiFC-2in1-NC

* Generated by Chen Lui

5.1.12 Instruments

Table 19: Instruments

Instrument	Type	Company
Autoclave	EVO 150	MediTech
	HV 50	HMC
Balance	CPA225D	Sartorius
	L 2200 P	Sartorius
Centrifuge	5430R	Eppendorf
	RC26+	Sorvall
	RC-5B	Sorvall
	Rotana 460R	Hettich
	Optima L-70	Beckmann Coultier
Rotors (for RC26+)	GS-3	Sorvall
	SS34	Sorvall
	SLA1500	Sorvall
DNA Electrophoresis Unit	Perfect Blue	Peqlab
Electroporator	Gene Pulser Electroporation	Bio-Rad

Instrument	Type	Company
Gel Documentation	Gel Doc 2000	Bio-Rad
Incubator	Innova4340 G25 ELL BM 200	New Brunswick Scientific New Brunswick Scientific Memmert
Magnetic stirrer	IKA-Combimag Ret	IKA
Microscope	TCS SP8 DMi8 CS	Leica
Microwave	Micromat	AEG
pH measurement	pH523	WTW
Shaker	Polymax 1040	Heidolph
Spectrophotometer	NanoDrop ND-1000 Infinite M1000 Pro	NanoDrop Technologies Tecan
Thermal cycler	T100 PTC-200	Bio-Rad Marshall Scientific
Thermoblock	ThermoMixer F 1.5	Eppendorf
Transilluminator	UV Transilluminator	UVP, Inc.
UltraPure water system	UltraClear	Siemens
Vacuum concentrator	Univapo 100H	UniEquip
Vacuum pump	TRIVAC D2,5E	Leybold
Vortexer	Vortex-Genie 2	Scientific industries
Waterbath	Haake DC1	Labequip

5.1.13 Internet tools and software

Table 20: Internet tools and software

Internet tools and software
www.pubmed.com (literature)
Vector NTI 9.1.0© 2004 Invitrogen Corporation
Fiji (ImageJ)

Internet tools and software
www.pubmed.com (literature)
Microsoft Office Professional Plus 2010 and 2016
iSect Primer tool http://signal.salk.edu/tdnaprimers.2.html (T-DNA primer selection)
SigmaPlot 14
Blast ® U.S. National Library of Medicine
http://elisaanalysis.com/app (ELISA analysis)

5.2 Methods

5.2.1 Plant methods

5.2.1.1 Cultivation on soil

A soil (Floragard) and silica sand mixture in a ratio of 8:1 was prepared and poured in 4-well pots aligned in the trays for normal plant growth. After the soil-sand mixture was wetted with water containing BT-toxin (toxic to fly larvae), seeds were placed with a toothpick on the surface of wet soil and stratified for 2 days at 4°C in the dark before transfer into the plant chamber (200 µE/m^2s light intensity, 22°C and 60% relative air humidity). To keep the air humidity high in the beginning, the trays were covered with cling film for one week.

Plants for protoplast isolation and stable transformation were grown under short-day conditions (10 h light/ 14h dark cycle). Long-day conditions (16 h light/ 8 h dark cycle) were applied to plants designated for seed amplification, genotyping and crossing.

5.2.1.2 Cultivation on plates

Seeds on filter paper were surface sterilized by applying 80% ethanol and letting them dry under the sterile hood. This process was performed two times. The seeds were placed on squared Petri dishes (120 mm x 120 mm x 17 mm Greiner bio-one Germany) containing medium with a sterile toothpick and stratified for 2 days at 4°C in the dark. Afterwards they were transferred to the plant chamber with long-day conditions (16 h light/ 8 h dark cycle, 200 µE/m^2s light intensity, 22°C and 60% relative air humidity). Growth periods and the used medium for the different methods are listed in **Table 21**.

Table 21: growth conditions on plates

experiment	medium	Days of growth
Microscopy of roots	½ MS basal salt mixture	5
Microsomal fraction isolation	½ MS basal salt mixture	14
Characterization of transgenic lines	MS incl. vitamins and 50 µM Hyg	14

5.2.1.3 Generation of multiple mutants and backcrossing of single mutants

To generate multiple mutant lines, plants with the desired single mutations have to be crossed. When plants have developed 5-6 inflorescences they are at the right stage for crossing. To avoid self-fertilization all the immature anthers around the stigma of the recipient flower have to be removed. Afterwards, this stigma was dabbed with pollen obtained from the donor plant. If the pollination was successful, a silique developed that could be harvested, after turning completely yellow. Seeds were dried and planted to obtain the segregating F2 generation. Homozygous multiple mutant plants were selected by isolation of genomic DNA and genotyping (compare **5.2.2.1** and **5.2.2.2**).

T-DNA insertion lines were backcrossed with the wild type (Col) using the same method as described above.

5.2.1.4 Generation and characterization of transgenic lines

The constructs were generated by PCR amplification of the desired parts and joined by the Gibson assembly (compare **5.2.2.2** and **5.2.2.5**). The GATEWAY system (Invitrogen) was used to get the construct into the pDONR vector (see **5.2.2.6**) and then transformed into *E. coli* DH5α (see **5.2.2.9**). After verification by sequencing (**5.2.2.14**), the fragment was cloned into the destination vector (pHGW, provides hygromycin resistance to plants) (compare **5.2.2.7**) and transformed into *Agrobacterium tumefaciens* (see **5.2.2.11**).

The *Agrobacterium tumefaciens*-mediated transformation was performed using the floral dip method (Clough and Bent, 1998). Selection was carried out by growing the seedlings on plates containing hygromycin (see **5.2.1.2**). After selection of successfully transformed plants, segregation analysis was used to identify single insertion lines (3:1 ratio) in the T2 generation. Two independent and homozygous (checked in T3) single insertion lines were selected for each transformation for further characterization.

5.2.2 Molecular methods

5.2.2.1 Isolation of genomic DNA (CTAB method)

Plant tissue was ground and 250 µl CTAB buffer was added. The samples were vortex to mix them properly and then incubated for at least 10 min at 65°C. To remove proteins 200µl chloroform/isoamylacohol (24:1) were added and vortexed for 1 min. After centrifugation at 13,000 rpm the supernatant was transferred (without disturbing the interphase) into a new vessel. The DNA was precipitated by adding 600 µl 100% ethanol and an incubation step at - 20°C for at least 20 min. The DNA was pelleted by centrifugation at 13,000 rpm and 4°C for 10 min. After removing the supernatant, the pellet was washed with 200 µl 70% ethanol, which was removed by centrifugation at 13,000 rpm and 4°C for 10 min. The supernatant was removed and the DNA pellet dried at 37°C. 100 µl TE buffer was used to dissolve the genomic DNA and it was stored at -20°C.

5.2.2.2 Polymerase chain reaction

The amplification of DNA fragments from a double stranded DNA template was achieved by the polymerase chain reaction (PCR). This method is based on denaturation, primer annealing and elongation cycles. The annealing temperature and the lengths of the elongation step depend on the used primers (see **5.1.10**) and the polymerase (see **5.1.8**), the enzyme catalyzing the elongation.

In this work three different polymerases were used according to the manufacturer's instructions. To determine the genotype of a plant, genomic DNA was isolated and PCR with the MangoTaq was performed. This enzyme has a high synthesis rate and no proofreading, which makes it a good choice for fast sample processing. To amplify fragments for cloning the iProof High-fidelity™ Polymerase was used, whereas the Phusion High Fidelity DNA Polymerase was employed for PCR-based mutation of plasmids. Both have a lower synthesis rate compared to the MangoTaq, but they have the advantage of the proofreading ability, which improves the accuracy of the copies. This characteristic is necessary, if the amplified fragment is later used for cloning.

5.2.2.3 Agarose gel electrophoresis

DNA samples were separated by size using 1% agarose gels (1 g of highly pure agarose in 100 ml of TAE buffer) supplemented with ethidium bromide. Gels were run at 120-140 V for 30–45 min. DNA was visualized on a UV transilluminator (Bio-Rad Gel Doc 2000).

5.2.2.4 Extraction of DNA from agarose gels

Gel extraction of DNA was performed using the innuPREP Gel Extraction Kit (Analytic Jena) according to the manufacturer´s instructions.

5.2.2.5 Gibson Assembly

The Gibson Assembly is a method to combine DNA fragments to one larger fragment. This process can be used to generate fusion constructs for cloning. The Gibson Assembly® Master Mix (New England Biolabs) was used according to the manufacturer's instructions.

5.2.2.6 BP reaction (Gateway)

The Gateway recombination technology was employed for cloning all constructs in this work. The cloning of the fragment of interest into the destination vector was performed by two steps of site-specific recombination reactions, BP and LR cloning.

The BP cloning is achieved with an attB-flanked DNA fragment and an attP containing donor vector to generate an entry clone.

Seventy-five ng of donor vector (pDONR221) were incubated with 50 fmol of attB-sites containing PCR product (ensuring a molar 1:1 ratio) together with 1 µl BP Clonase and 1 µl BP Clonase buffer in a total reaction volume of 5 µl overnight at 25°C (in a thermomixer with heated lid). BP reaction was stopped by adding 0.5 µl Proteinase K and incubating for 10 min at 37°C. 5 µl of the reaction were transformed into *E. coli* DH5α. Four colonies were picked and grown in 5 ml of LB medium at 37°C overnight. After plasmid purification (see **5.2.2.12**) the presence of the insert was verified by restriction digestion and sequencing (see **5.2.2.13** and **5.2.2.14**).

5.2.2.7 LR reaction (Gateway)

The LR cloning is achieved with an attL-contaning entry clone and an attR-containing destination vector to generate the final vector.

One hundred ng of entry clone was incubated with an equal molar amount of destination vector and 1 µl of LR Clonase and 1 µl of LR Clonase buffer in a total reaction volume of 5 µl. After incubation at 25°C overnight, LR reaction was stopped by incubating with 0.5 µl Protease K (37°C, 10 min). Five µl of the reaction was transformed into *E. coli* DH5 alpha. Five colonies were picked and grown in 5 ml of LB medium at 37°C overnight. The plasmid was isolated and the concentration was determined by spectrophotometry. Plasmids were sequenced (see **5.2.2.14**) and stored at – 20°C.

5.2.2.8 Preparation of chemically competent E. coli *DH5α cells*

Two hundred and fifty ml of RB media containing 20 mM $MgSO_4$ were inoculated with 2 ml overnight culture and grown at 37°C under continuous shaking (300 rpm) until an OD_{590} of 0.4-0.6. The cells were harvested by centrifugation at 500 rpm at 4°C for 5 min and the pellet was resuspended in 100 ml ice cold TFB1 buffer on ice. After 5 min incubation on ice and a centrifugation step (5000 rpm, 4°C, 5 min), the pellet was resuspended in 6 ml TFB2 buffer. The suspension was stored on ice for 60 min, aliquoted (50 µl), frozen in liquid N_2 and stored at -80°C.

5.2.2.9 Transformation of chemically competent E. coli *DH5α cells*

One to five µl plasmid DNA were added to 50 µl competent *E. coli* cells thawed on ice. After an incubation of 15 min on ice, a heat shock of 42°C for 30 sec was performed. The vessel was immediately transferred back on ice and 600 µl LB medium were added. The sample was incubated at 37°C for 1 h with shaking at 450 rpm. The cells were harvested by centrifugation at 7,000 rpm for 2 min and resuspended in 50 µl LB medium. Sterile glass beads were used to distribute the cell suspension on LB agar plates containing the corresponding antibiotics and the bacteria were grown overnight at 37°C.

5.2.2.10 Preparation of electro competent A. tumefaciens *GV3101 pMP90*

Three hundred ml LB media were inoculated with a 2 ml overnight culture of *A. tumefaciens* and grown at 28°C under continuous shaking until an OD_{600} of 0.5-0.7. Afterwards, the bacteria culture was cooled for 30 min on ice, centrifuged at 4°C for 20 min at 4000 rpm and the pellet was resuspended in ice cold 125 ml ddH_2O. The suspension was stored on ice for 60 min and again centrifuged. Subsequently, the pellet was resuspended in 3 ml ice cold 15% (v/v) glycerol, aliquoted (50 µl), frozen in liquid N_2 and stored at -80°C.

5.2.2.11 Transformation of electro competent A. tumefaciens *GV3101 pMP90*

One µl of plasmid DNA were added to 50 µl competent *A. tumefaciens* cells and mixed by gently tapping the vessel. The suspension was transferred to a pre-chilled electroporation cuvette (Bio-Rad, distance electrodes: 0.2 cm) and a pulse (25 µFD capacitance, 1.25 kV voltage, 400 Ω resistance) was applied. Immediately afterwards 2 ml LB medium were added and the cell culture was incubated at 28°C for 1 h at 220 rpm. Bacteria were harvested (7,000 rpm, 2 min) and the pellet was resuspended in 600 µl LB medium. Fifty µl of the suspension was plated on selective LB plates and incubated for 2 days at 28°C.

5.2.2.12 Plasmid isolation

QIAprep Spin Miniprer Kit or QIAGEN Plasmid Midi Kit (protoplast transformation) were used to purify plasmid DNA. The manufacturer's instructions were followed and the concentration was measured by spectrophotometry (NanoDrop).

5.2.2.13 Restriction digestion

Restriction digestion was applied in this work to analyze the plasmids obtained from Gateway cloning. Restriction enzymes cutting at the site of the inserted fragment and the vector backbone were used with the appropriate buffer and temperature according to the manufacturer's instructions (New England Biolabs, Thermo Scientific). After digestion, the fragment sizes were checked by agarose gel electrophoresis (see **5.2.2.3**).

5.2.2.14 DNA sequencing

To assess the precise order of nucleotides within a DNA fragment, the isolated plasmid DNA (see **5.2.2.12**) was prepared according to the manufacturer's instructions and processed by Eurofins MWG GmbH (Ebersberg, Germany).

5.2.2.15 PCR-based mutagenesis

A PCR-based mutagenesis can be applied to change single nucleotides of a plasmid's sequence. The first step of this method is to design primer (see **Table 15**) overlapping at the mutation site and perform a PCR (see **5.2.2.2**, **Table 22**). By restriction digestion with DpnI (50 µl PCR mix, 6 µl 10x Buffer Yellow, 2 µl DpnI, 2µl ddH_2O) all methylated DNA (template) is cut and only the newly synthesized mutagenized DNA remains as intact plasmid. 3 µl of the digestion reaction were used to transform competent *E. coli* cells (see **5.2.2.9**) and after plasmid isolation (see **5.2.2.12**), the success was checked by sequencing (see **5.2.2.14**).

Table 22: PCR program used for mutagenesis

temperature	time	step	cycles
94°C	3 min	Denaturation	1
94°C	1 min	Denaturation	
52°C*	1 min	Annealing	3
68°C	8 min*	Elongation	
68°C	1 h	Elongation	1

* Annealing temperature (should be lower to allow mismatch) and elongation depend on the primer and template

5.2.2.16 Agrobacterium tumefaciens *mediated plant transformation*

For stabile transformation (floral dip method; Clough and Bent, 1998) of *A. thaliana A. tumefaciens* was used. First a pre-culture was prepared by inoculating a colony in 2 ml LB medium containing antibiotics (Rif, Gent, Spec) and shaking overnight at 28°C and 220 rpm. The pre-culture was added to 300 ml fresh LB medium containing the antibiotics (Rif, Gent, Spec) and again incubated overnight at 28°C at 160 rpm. The cells of the overnight culture were harvested by centrifugation at 7,000 rpm and 4°C for 10 min and as much supernatant as possible was removed. Two ml transformation solution were used to resuspend the pellet thoroughly. OD_{600} was adjusted to 0.8 by diluting the suspension with transformation solution. The siliques of the plants (grown under short-day conditions in big pots until flowering) were removed and the inflorescences were dipped in the transformation solution containing the *A. tumefaciens*. The leaves were dried from the solution to avoid additional stress for the plant. To keep a high relative air humidity the plants were wrapped in clear plastic bags and kept under low light conditions for 24 h. Afterwards, the bag was removed and the plants were put to long-day conditions to allow fast ripening of the seeds. When the siliques were yellow and dry, the seeds (T1) were harvested and transformants were selected by hygromycin selection (see **5.2.1.4**).

5.2.2.17 Protoplast isolation

Protoplasts were isolated from 4-week-old *A. thaliana* plants grown under short-day conditions according to the Tape-Arabidopsis Sandwich method (Wu *et al.*, 2009). Leaves were fixed with the upper epidermal surface to Magic tape (Scotch M8101233 Klebeband Magic 810). Another strip of Magic tape was attached to the lower epidermal surface and carefully removed to peel away the lower epidermal cell layer. The leaves were transferred to a 6-well-plate containing 4 ml enzyme solution per well. To release the protoplast the leaves were incubated in the dark for 3 h while shaking at 40 rpm. The protoplasts were collected by centrifugation (3 min, 100 x g) and washed two times with buffer W5. After resuspension in 2 ml W5, the protoplasts were counted with a hemocytometer and kept on ice.

5.2.2.18 PEG-mediated transient protein expression

Freshly isolated protoplasts (see **5.2.2.17**) were centrifuged (1 min, 100 x g) and resuspended in MMg (concentration: 8 x 10^5 protoplasts/ml). Fifteen µg plasmid were mixed with 300 µl protoplasts and incubated for 5 min at RT. Three hundred µl PEG were carefully added and mixed by tapping the tube. After an incubation for 20 min at RT, 1 ml W5 was cautiously added and mixed by inverting the tube. The protoplasts were washed twice with W5, resuspended in 1 ml W5 and transferred to a 6-well-plate coated with 1% BSA. After an overnight incubation (14 - 20 h, RT, dark) the protoplasts were ready to be imaged.

5.2.3 Biochemical methods

5.2.3.1 Microsomal fraction isolation

All of the solutions, tubes and equipment were pre-cooled at 4°C before use. 0.5-1 g plant material was ground to a fine powder, mixed with 15 ml homogenization buffer and ground again for 3 min. The homogenate was filtered through two layers of miracloth. The mortar and pistil were rinsed with 15 ml homogenization buffer and filtered the same way resulting in a final volume of 30 ml. After centrifugation at 4°C and 8,000 x g for 10 min, the supernatant was filtered through one layer of miracloth into a Beckmann-Ultra clear tube (rotor SW 28) and centrifuged at 4°C and 110,000 x g for 1 h. The supernatant was carefully removed and 100 µl resuspension buffer was added to the pellet. Afterwards, an incubation on ice for 30 min was performed, the pellet was resuspended in the resuspension buffer and transferred to a douncer. The tube was rinsed with 100 µl resuspension buffer, which was then transferred to the douncer as well. After grinding by moving the douncer up and down 60 times, the homogenate was transferred to a new 1.5 ml tube. Another 100 µl resuspension buffer which was used to rinse the douncer were added to the tube for a final volume of 300 µl. The microsomal fraction was aliquoted into 3 tubes and stored at -80°C.

5.2.3.2 Determination of protein concentration with Bradford

The isolated microsomal fraction (MF) was centrifuged for 5 min at 9000 rpm and 4°C before measuring the protein concentration. The supernatant was transferred to a new tube and put on ice. For determination of protein concentration, a BSA standard curve was established. A BSA stock solution (20 mg/ml, New England BioLabs) was diluted to achieve the additional concentrations of 16 mg/ml, 10 mg/ml, 4 mg/ml and 2 mg/ml. The concentration measurement was performed with the Bio-Rad reagent (#500-0006) using a 96 well microtiter plate (Greiner Bio-one, 655101) in a Tecan Reader. The reagent was diluted with 62.5 mM NaOH in a ratio of 1:4 and 200 µl were added to the plate. Five µl of the standard or microsomal fractions were added to each well, performing 3 replicates for all samples. After an incubation at RT for 10 min, the plate was loaded into the Tecan Reader, shaken for 5 sec (amplitude: 2 mm, frequency: 306 rpm) and the absorbance measured at 595 nm (number of flashes: 25).

5.2.3.3 ELISA

Microsomal fractions were diluted to 1 µg/ml for leaf material und 0.5 µg/ml for root material with pre-chilled water right before applying the samples to the ELISA plate (NUNC-IMMUNO PLATE MAXISORP, 154110). The 96-well-plate was prepared for ELISA by supplying each well with 100 µl of carbonate buffer. 100 µl MF were added to the first well (0.1 M carbonate buffer) and mixed by pipetting up and down 3 times. One hunred µl of the first well were loaded into the second well, mixed three times and finally 100 µl were discarded. Each MF sample was loaded onto the plate in triplicates.

To determine the PIP concentration, a standard is needed. For PIP1 proteins 100 µl Peptide1 (40 ng/ml, peptide sequence present in all 5 PIP1 isoforms) were added to a well and diluted 7 times as described above. Peptide 2 (100 ng/ml, peptide sequence present in PIP2;1, PIP2;2 and PIP2;3) was diluted in the same way as Peptide 1 und used for PIP2;1/PIP2;2/PIP2;3 protein quantification. The standards were performed in triplicates as well. Three wells with carbonate buffer without the addition of MFs were used as blanks.

The binding of proteins to the sealed plate was performed overnight at 4 °C. The liquid in the plate was removed and the wells were washed with 200 µl PBS. Blocking was carried out with 200 µl PBS-TB for 30 min at RT and 2 rpm shaking. After washing with 200 µl PBS-T 3 times, 100 µl of the first antibody was added per well (anti-PIP1: 1:2000 or anti-PIP2;1/PIP2;2/PIP2;3:

1:2000). The plate was incubated for 2 h at 20 °C with shaking at 2 rpm and washed 5 times with 200 µl PBS-T. One hundred µl of the second antibody (anti-rabbit-IgG HRP conjugate) were added to each well, incubated for 2 h at 20 °C with shaking at 2 rpm and washed 5 times with 200 µl PBS. In the end, 100 µl activated ABTS (10.5 ml ABTS + 10 µl 30 % H_2O_2 for activation) were loaded onto the plate and incubated for 20 min. The absorbance measurement at 405 nm was performed with a Tecan Reader after shaking the plate for 10 sec.

To determine the unspecific binding of the first antibodies, 3 wells containing the MF of WT tissue were incubated with a blocked first antibody (5 ml first antibody + 1 µl Peptide (5 mg/ml), incubation for at least 10 min).

Analysis of the achieved data was performed with a 5-parameter logistic regression (http://elisaanalysis.com//app).

5.2.3.4 Degradation assay (CHX and MG132)

Freshly isolated protoplasts (see **5.2.2.17**) were diluted to 1-1.5 x 10^5 protoplasts/ml in W5 (see EGFP-PIP1;1 lines in **Table 3**). One hundred µl protoplasts were loaded to a 96-well-plate (Thermo Scientific, 164588) and different inhibitors (see **Table 23**) were added to study the degradation of PIP1. The mock controls were treated with DMSO or ethanol. Wild-type protoplasts were used to measure the background signal. The fluorescence measurement was performed with a plate reader (Tecan Infinite® M1000 PRO, settings: excitation/emission wavelengths of 484 / 507 nm, bandwidth:5 nm, gain:100, flash frequency:400Hz).

Table 23: Inhibitors used for the degradation assay

Inhibitor	Concentration	Solvent	Effect
MG132	10 µM	DMSO	Proteasome inhibition
Cycloheximide (CHX)	100 µM	ethanol	Protein biosynthesis inhibition

5.2.4 Microscopy

For all microscopic work the Leica microscope TCS SP8 DMi8 CS was used.

5.2.4.1 Ratiometric bimolecular fluorescence complementation (rBiFC)

The 2in1-rBiFC vector was used to transiently transform protoplasts with two proteins of interest and an RFP as transformation control and reference protein at the same time (compare **Figure 22**; Grefen and Blatt, 2012).

If the transformation was successful, the red fluorescence protein (RFP) could be seen. Moreover, interaction of the two proteins of interest would bring both halves of the split YFP (yellow fluorescence protein) attached to them in close proximity resulting in a yellow signal. In addition, the autofluorescence of chlorophyll can be detected. The microscope settings are shown in **Table 24**.

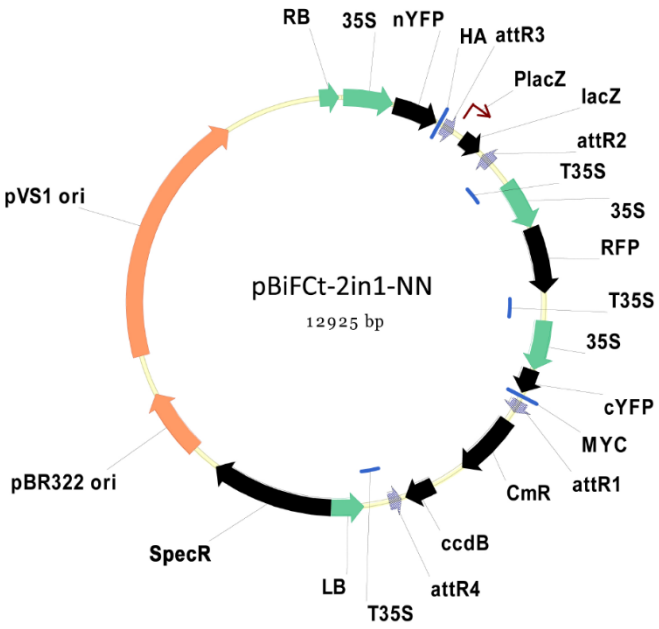

*Figure 22: **Vector map of the rBiFC system.** The vector contains 4 attR sites to insert two genes of interest fusing them with the nYFP half (attR3 + attR2) or the cYFP half (attR1 + attR4) at the n-terminus. Moreover, an RFP sequence is present to have a transformation control.*

Table 24: Microscope settings for rBiFC (WLL: white light laser)

Fluorophore	Excitation	Detector	Detection
YFP	WLL: 514 nm	Hybrid detector	520-550 nm
RFP	WLL: 590 nm	Hybrid detector	600-630 nm
chlorophyll	WLL: 514 nm	PMT detector	650-750 nm

5.2.4.2 Fluorescence recovery after photobleaching (FRAP)

Fluorescence recovery after photobleaching is a method to study the movement of proteins. A region of interest is bleached and the recovery after a certain time is measured to determine for example the migration speed of the protein into the region of interest.

In this work FRAP was used to estimate the ratio of protein localized to the membrane or to the ER (Sorieul *et al.*, 2011). It is known that there is hardly any movement of membrane proteins in the plasma membrane, whereas cytosolic or ER localized proteins are more mobile. The higher the relative amount of membrane proteins is in the ROI, the lower the measured recovery should be. The microscope settings are shown in **Table 25**.

For bleaching an area with high fluorescence was chosen. The microscope's zoom was set to 3, resolution to 512 x 512 and time scan was activated by switching to xyt. A region of interest was picked and bleaching was performed by scanning the ROI 10 times with the UV 405 nm DMOD laser at 100%.

The method applied in this work was slightly modified compared to the one used in (Sorieul *et al.*, 2011) because imaging already resulted in bleaching. To exclude the effect of bleaching by scanning the pictures, a region (NBR) in addition to the ROI was measured at each timepoint, which was not bleached intentionally. The only bleaching detected resulted from imaging. Images were taken at three different timepoints: before bleaching, right after bleaching and 5 min after bleaching. The mean fluorescence intensity was measured in both regions (ROI and NBR) and a corrected value for the ROI mean fluorescence intensity was obtained by using NBR as a reference.

A decrease in the value of the intensity of the region of interest from the image before to the image after bleaching shows that the bleaching was successful, whereas a higher increase from directly after to 5 min after bleaching equivalates a higher relative amount of ER or cytosolic localized proteins.

Table 25: Microscope settings for FRAP (UV: ultraviolet laser, WLL: white light laser)

Fluorophore	Excitation	Detector	Detection
BFP	UV: 405 nm	Hybrid detector	440-480 nm
EGFP	WLL: 488 nm	Hybrid detector	500-550 nm

5.2.4.3 Corrected fluorescence recovery after photoconversion (cFRAPc)

The corrected fluorescence recovery after photoconversion is similar to FRAP. The big difference is, that the fluorophore is not bleached but converted. This has the advantage to be able to observe what happens to proteins within the ROI, since they can still emit a signal. Moreover, signals from not converted and converted fluorophores can be distinguished, because the conversion results in a conformational change, leading to adjusted excitation and emission properties.

Conversion could be obtained by two different methods:

- Conversion of a small region of interest similar to the FRAP bleaching (see **5.2.4.2**) was performed. The microscope was set to xyt, zoomed to 3.5 and the resolution to 512 x 512. The conversion was performed by applying the UV-laser at 50% strength and scanning the ROI 20 times.
- Conversion of the whole field of vision could be achieved by excitation with the laser and the DAPI filter of the microscope for 3 min.

The laser and detector settings for image acquisition are shown in **Table 26**.

Table 26: Microscope settings for cFRAPc (WLL: white light laser)

Fluorophore	Excitation	Detector	Detection
Green mEos	Argon: 488 nm	Hybrid detector	500-550 nm
Red mEos	WLL: 570 nm	Hybrid detector	590-680 nm

6 Appendix

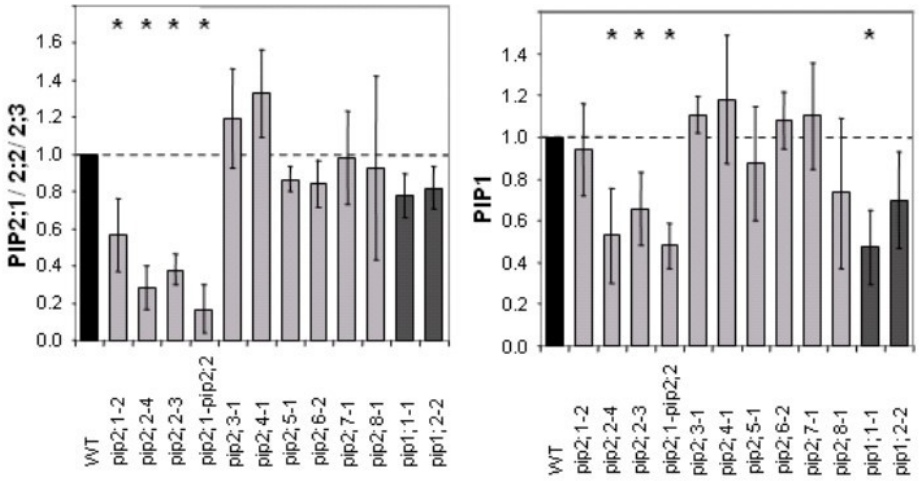

Supplemental Figure 1: ***PIP1 and PIP2 protein levels in*** **pip1** ***and*** **pip2** ***mutants.*** *PIP1 and PIP2 protein levels were determined by immunoblotting using anti-PIP1 and anti-PIP2;1/PIP2;2/PIP2;3 antibodies (unpublished data; Liu, Da Ines and Geist). Anti-PIP1 antiserum recognizes all five PIP1 members, which are highly similar; anti-PIP2;1/2;2/2;3 antiserum specifically recognizes these three PIP2 isoforms. Standard error values and the significant differences between WT and the mutants are shown ($p \leq 0.05$: *).*

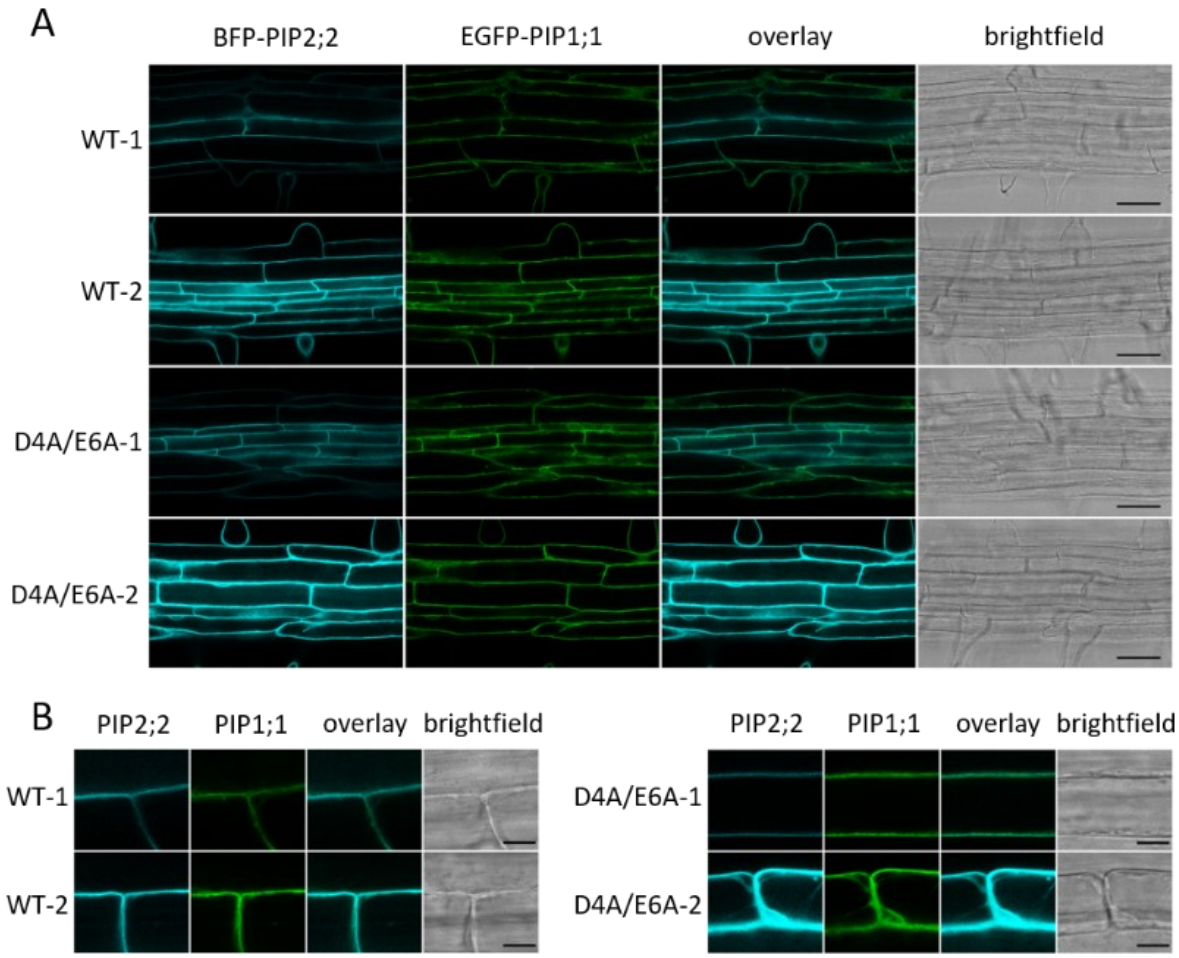

Supplemental Figure 2: ***Diacidic mutant of BFP-PIP2;2 in the EGFP-PIP1;1 line.*** *(A) Cross-sections of five-day-old* A. thaliana *roots expressing BFP-PIP2;2 and EGFP-PIP1;1 were used to analyze the effect of a mutated diacidic motif (D4A/E6A) on the localization of both isoforms. All lines are stable single insertion lines and two independent lines (-1/ -2) were used to exclude the influence of the insertion site. A Leica SP8 microscope was used for imaging with the following settings for excitation and detection wavelength: 405 nm/440-480 nm (BFP) and 488 nm/500-550 nm (EGFP). Two biological replicates were performed. Scale bars, 50 µm. (B) Blow ups of (A) were performed to visualize subcellular localization. Scale bars, 10 µm.*

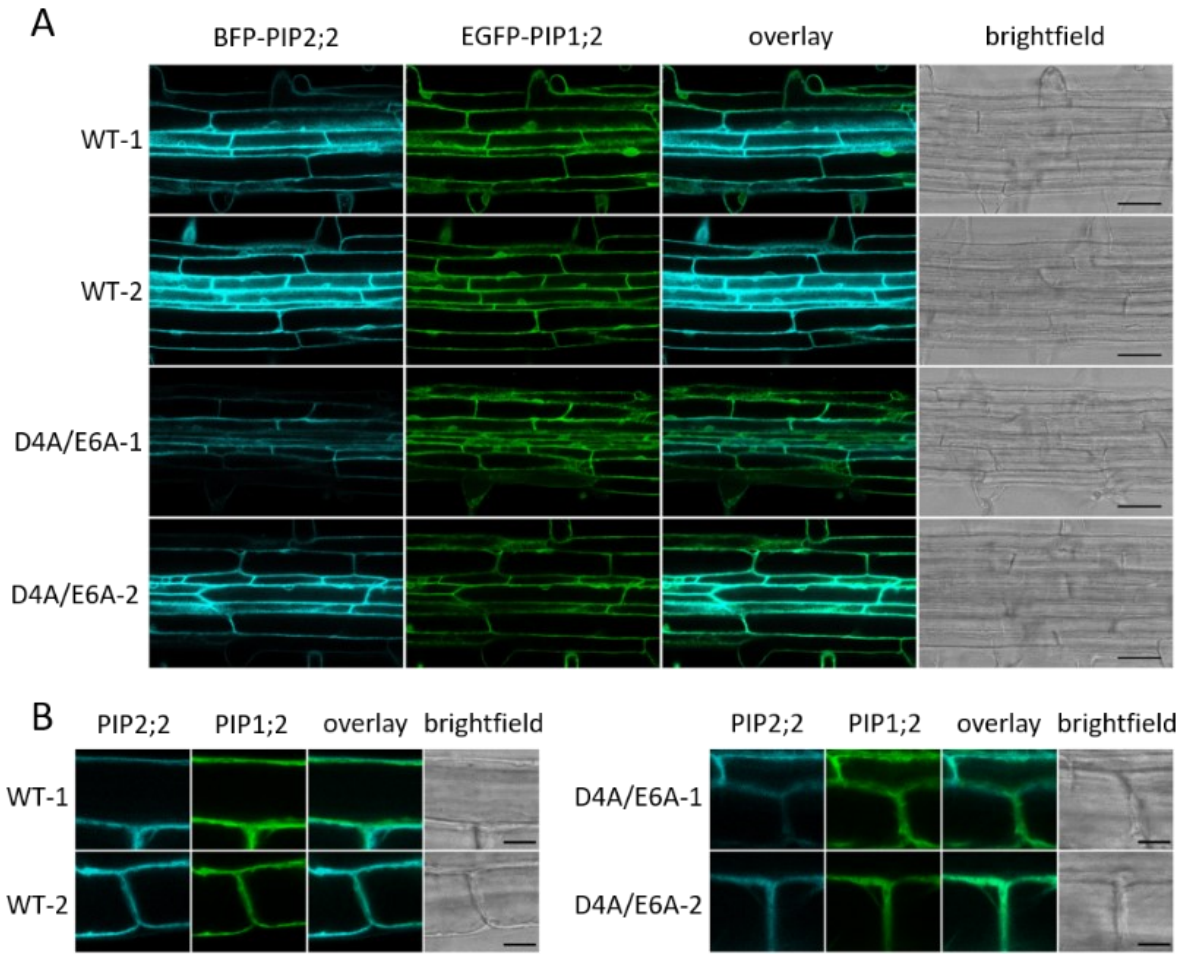

Supplemental Figure 3: ***Diacidic mutant of BFP-PIP2;2 in the EGFP-PIP1;2 line.*** *(A) Cross-sections of five-day-old* A. thaliana *roots expressing BFP-PIP2;2 and EGFP-PIP1;2 were used to analyze the effect of a mutated diacidic motif (D4A/E6A) on the localization of both isoforms. All lines are stable single insertion lines and two independent lines (-1/ -2) were used to exclude the influence of the insertion site. A Leica SP8 microscope was used for imaging with the following settings for excitation and detection wavelength: 405 nm/440-480 nm (BFP) and 488 nm/500-550 nm (EGFP). Two biological replicates were performed. Scale bars, 50 µm. (B) Blow ups of (A) were performed to visualize subcellular localization. Scale bars, 10 µm.*

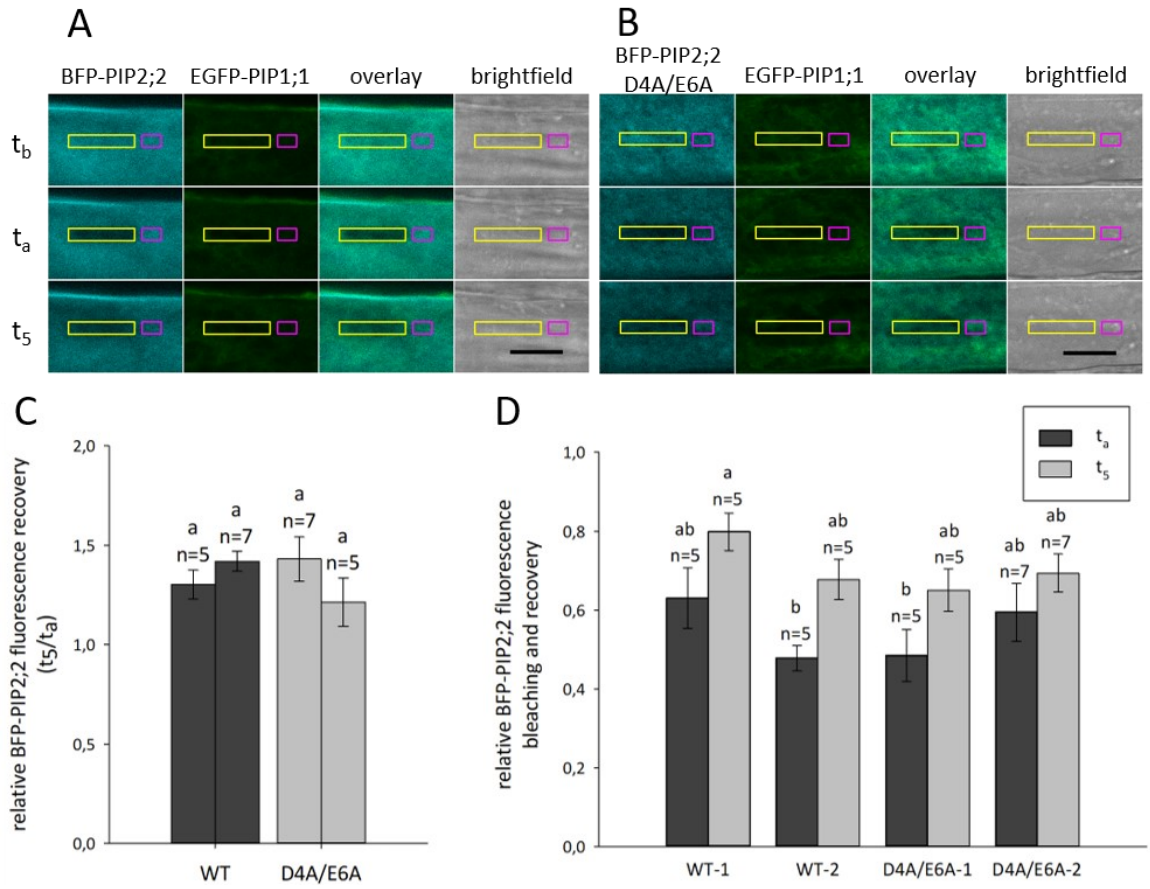

Supplemental Figure 4: ***FRAP experiments to estimate the intracellular labelling of BFP-PIP2;2.*** *(A, B) Tangential optical sections of five-day-old* A. thaliana *root cells expressing EGFP-PIP1;1 and WT or D4A/E6A BFP-PIP2;2 constructs were imaged before (t_b), immediately after (t_a) and 5 min after photobleaching (t_5) the region of interest (ROI, shown by yellow boxes). In addition, a nonbleached region (NBR, shown by magenta boxes) was recorded at all time points to use as a reference to measure photobleaching independent fluorescence intensity changes. All lines are stable single insertion lines and two independent lines (-1/ -2, only one displayed as representative) were used to exclude the influence of the insertion site. A Leica SP8 microscope was used for imaging with the following settings for excitation and detection wavelength: 405 nm/440-480 nm (BFP) and 488 nm/500-550 nm (EGFP). Scale bars, 10 µm. (C) Fluorescence recovery after photobleaching of ROI corresponds to intracellular labeled BFP-PIP2;2 trafficking into the ROI. The ratio of t_5 and t_a (t_5/t_a) gives an estimate of relative intracellular labelling, where "1" means no recovery and thus no intracellular labelling and higher values equal higher amounts of intracellular labelling. Standard error values, the number of independent cells studied (n) and the lack of significant differences between the lines are shown. No statistically significant difference (P<0.05) was determined by One Way Analysis of Variance. (D) The success of the bleaching experiment can be judged by calculating the relative fluorescence bleaching (t_a) and recovery (t_5) with t_b as the reference. By displaying these values one can see, if a high reduction of fluorescence intensity is achieved after photobleaching, which is an essential factor to determine usability. Standard error values, the number of independent cells studied (n) and significant differences between the lines are shown. Significance (P<0.05) was determined by One Way Analysis of Variance with the Holm-Sidak method as the all pairwise multiple comparison procedure.*

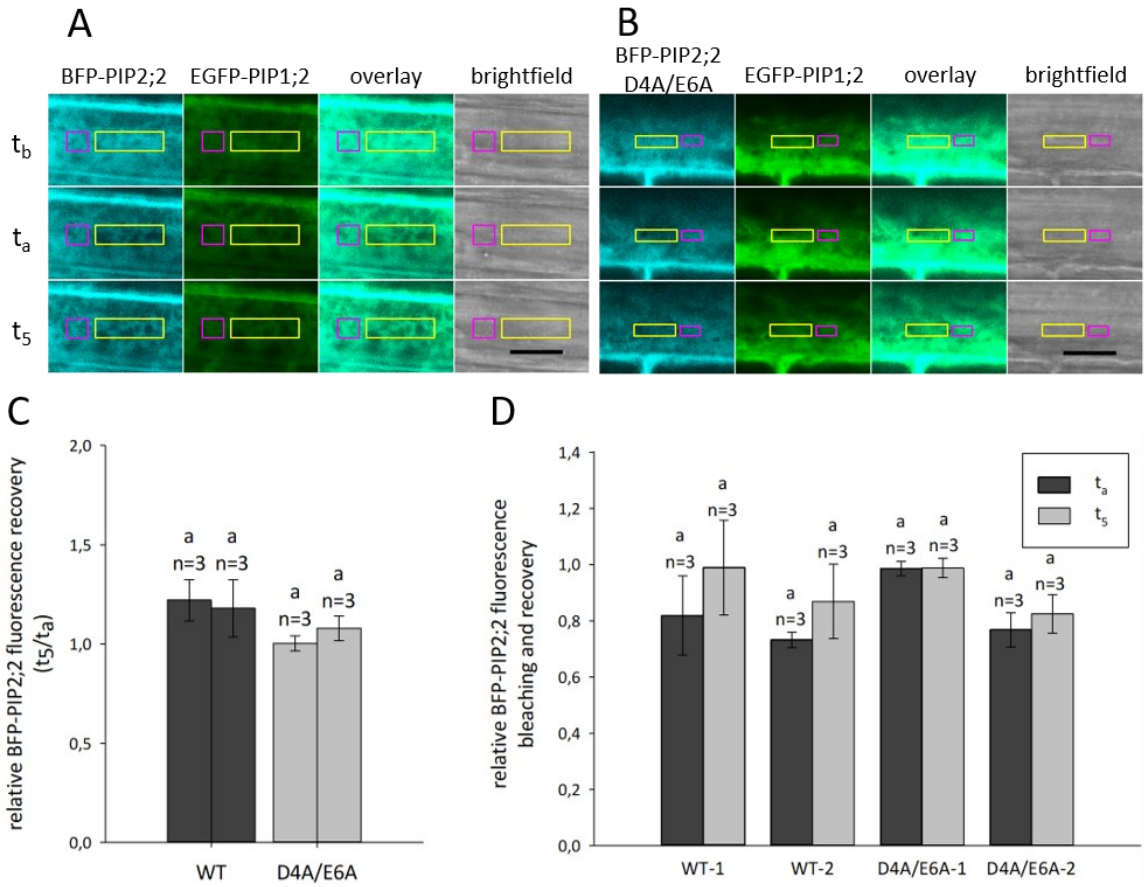

Supplemental Figure 5: ***FRAP experiments to estimate the intracellular labelling of BFP-PIP2;2.*** *(A, B) Tangential optical sections of five-day-old* A. thaliana *root cells expressing EGFP-PIP1;2 and WT or D4A/E6A BFP-PIP2;2 constructs were imaged before (t_b), immediately after (t_a) and 5 min after photobleaching (t_5) the region of interest (ROI, shown by yellow boxes). In addition, a nonbleached region (NBR, shown by magenta boxes) was recorded at all time points to use as a reference to measure photobleaching independent fluorescence intensity changes. All lines are stable single insertion lines and two independent lines (-1/ -2, only one displayed as representative) were used to exclude the influence of the insertion site. A Leica SP8 microscope was used for imaging with the following settings for excitation and detection wavelength: 405 nm/440-480 nm (BFP) and 488 nm/500-550 nm (EGFP). Scale bars, 10 µm. (C) Fluorescence recovery after photobleaching of ROI corresponds to intracellular labeled BFP-PIP2;2 trafficking into the ROI. The ratio of t_5 and t_a (t_5/t_a) gives an estimate of relative intracellular labelling, where "1" means no recovery and thus no intracellular labelling and higher values equal higher amounts of intracellular labelling. Standard error values, the number of independent cells studied (n) and the lack of significant differences between the lines are shown. No statistically significant difference (P<0.05) was determined by One Way Analysis of Variance. (D) The success of the bleaching experiment can be judged by calculating the relative fluorescence bleaching (t_a) and recovery (t_5) with t_b as the reference. By displaying these values one can see, if a high reduction of fluorescence intensity is achieved after photobleaching, which is an essential factor to determine usability. Standard error values, the number of independent cells studied (n) and the lack of significant differences between the lines are shown. No statistically significant difference (P<0.05) was determined by One Way Analysis of Variance.*

```
93.4% identity in 287 residues overlap; Score: 1387.0; Gap frequency: 0.7%

PIP2;2          1 MAKDVEGP--EGFQTRDYEDPPPTPFFDADELTKWSLYRAVIAEFVATLLFLYITVLTVI
PIP2;1          1 MAKDVEAVPGEGFQTRDYQDPPPAPFIDGAELKKWSFYRAVIAEFVATLLFLYITVLTVI
                  ******    ******** **** ** *  ** *** **********************

PIP2;2         59 GYKIQSDTKAGGVDCGGVGILGIAWAFGGMIFILVYCTAGISGGHINPAVTFGLFLARKV
PIP2;1         61 GYKIQSDTDAGGVDCGGVGILGIAWAFGGMIFILVYCTAGISGGHINPAVTFGLFLARKV
                  ******** ************************************************

PIP2;2        119 SLIRAVLYMVAQCLGAICGVGFVKAFQSSYYDRYGGGANSLADGYNTGTGLAAEIIGTFV
PIP2;1        121 SLPRALLYIIAQCLGAICGVGFVKAFQSSYYTRYGGGANSLADGYSTGTGLAAEIIGTFV
                  ** ** **  ********************** ************* **************

PIP2;2        179 LVYTVFSATDPKRNARDSHVPVLAPLPIGFAVFMVHLATIPITGTGINPARSFGAAVIYN
PIP2;1        181 LVYTVFSATDPKRSARDSHVPVLAPLPIGFAVFMVHLATIPITGTGINPARSFGAAVIYN
                  ************* ********************************************

PIP2;2        239 KSKPWDDHWIFWVGPFIGAAIAAFYHQFVLRASGSKSLGSFRSAANV
PIP2;1        241 KSKPWDDHWIFWVGPFIGAAIAAFYHQFVLRASGSKSLGSFRSAANV
                  *************************************************


96.8% identity in 285 residues overlap; Score: 1455.0; Gap frequency: 0.0%

PIP2;2          1 MAKDVEGPEGFQTRDYEDPPPTPFFDADELTKWSLYRAVIAEFVATLLFLYITVLTVIGY
PIP2;3          1 MAKDVEGPDGFQTRDYEDPPPTPFFDAEELTKWSLYRAVIAEFVATLLFLYVTVLTVIGY
                  ******** ****************** ********************** ********

PIP2;2         61 KIQSDTKAGGVDCGGVGILGIAWAFGGMIFILVYCTAGISGGHINPAVTFGLFLARKVSL
PIP2;3         61 KIQSDTKAGGVDCGGVGILGIAWAFGGMIFILVYCTAGISGGHINPAVTFGLFLARKVSL
                  ************************************************************

PIP2;2        121 IRAVLYMVAQCLGAICGVGFVKAFQSSYYDRYGGGANSLADGYNTGTGLAAEIIGTFVLV
PIP2;3        121 IRAVLYMVAQCLGAICGVGFVKAFQSSHYVNYGGGANFLADGYNTGTGLAAEIIGTFVLV
                  *************************** *  ****** **********************

PIP2;2        181 YTVFSATDPKRNARDSHVPVLAPLPIGFAVFMVHLATIPITGTGINPARSFGAAVIYNKS
PIP2;3        181 YTVFSATDPKRNARDSHVPVLAPLPIGFAVFMVHLATIPITGTGINPARSFGAAVIFNKS
                  ************************************************************ ***

PIP2;2        241 KPWDDHWIFWVGPFIGAAIAAFYHQFVLRASGSKSLGSFRSAANV
PIP2;3        241 KPWDDHWIFWVGPFIGATIAAFYHQFVLRASGSKSLGSFRSAANV
                  ***************** ****************************


86.9% identity in 268 residues overlap; Score: 1250.0; Gap frequency: 0.0%

PIP2;2         14 RDYEDPPPTPFFDADELTKWSLYRAVIAEFVATLLFLYITVLTVIGYKIQSDTKAGGVDC
PIP2;4         16 RDYKDPPPAPFFDMEELRKWPLYRAVIAEFVATLLFLYVSILTVIGYKAQTDATAGGVDC
                  *** **** ****  ** ** *****************   ******* * *  ******

PIP2;2         74 GGVGILGIAWAFGGMIFILVYCTAGISGGHINPAVTFGLFLARKVSLIRAVLYMVAQCLG
PIP2;4         76 GGVGILGIAWAFGGMIFVLVYCTAGISGGHINPAVTVGLFLARKVSLVRTVLYIVAQCLG
                  ***************** ****************** ********** * *** ******

PIP2;2        134 AICGVGFVKAFQSSYYDRYGGGANSLADGYNTGTGLAAEIIGTFVLVYTVFSATDPKRNA
PIP2;4        136 AICGCGFVKAFQSSYYTRYGGGANELADGYNKGTGLGAEIIGTFVLVYTVFSATDPKRNA
                  **** *********** ******* ****** **** **********************

PIP2;2        194 RDSHVPVLAPLPIGFAVFMVHLATIPITGTGINPARSFGAAVIYNKSKPWDDHWIFWVGP
PIP2;4        196 RDSHVPVLAPLPIGFAVFMVHLATIPITGTGINPARSFGAAVIYNNEKAWDDQWIFWVGP
                  ********************************************  * *** *******

PIP2;2        254 FIGAAIAAFYHQFVLRASGSKSLGSFRS
PIP2;4        256 MIGAAAAAFYHQFILRAAAIKALGSFGS
                   **** ******* ***   * **** *
```

```
78.7% identity in 286 residues overlap; Score: 1196.0; Gap frequency: 0.3%

PIP2;2          1 MAKDVEGPE-GFQTRDYEDPPPTPFFDADELTKWSLYRAVIAEFVATLLFLYITVLTVIG
PIP2;5          1 MTKEVVGDKRSFSGKDYQDPPPEPLFDATELGKWSFYRALIAEFIATLLFLYVTIMTVIG
                  * * * *    *   ** **** * *** ** *** *** **** ******* *  ****

PIP2;2         60 YKIQSDTKAGGVDCGGVGILGIAWAFGGMIFILVYCTAGISGGHINPAVTFGLFLARKVS
PIP2;5         61 YKSQTDPALNPDQCTGVGVLGIAWAFGGMIFILVYCTAGISGGHINPAVTFGLLLARKVT
                  ** * *       * *** ********************************** *****

PIP2;2        120 LIRAVLYMVAQCLGAICGVGFVKAFQSSYYDRYGGGANSLADGYNTGTGLAAEIIGTFVL
PIP2;5        121 LVRAVMYMVAQCLGAICGVALVKAFQSAYFTRYGGGANGLSDGYSIGTGVAAEIIGTFVL
                  * *** *************  ****** *  ******* * ***  *** **********

PIP2;2        180 VYTVFSATDPKRNARDSHVPVLAPLPIGFAVFMVHLATIPITGTGINPARSFGAAVIYNK
PIP2;5        181 VYTVFSATDPKRSARDSHVPVLAPLPIGFAVFIVHLATIPITGTGINPARSLGAAIIYNK
                  ************ ****************** ****************** *** ****

PIP2;2        240 SKPWDDHWIFWVGPFIGAAIAAFYHQFVLRASGSKSLGSFRSAANV
PIP2;5        241 DKAWDHHWIFWVGPFAGAAIAAFYHQFVLRAGAIKALGSFRSQPHV
                   * ** ********* ***************   * ******   *


80.2% identity in 273 residues overlap; Score: 1175.0; Gap frequency: 0.0%

PIP2;2          9 EGFQTRDYEDPPPTPFFDADELTKWSLYRAVIAEFVATLLFLYITVLTVIGYKIQSDTKA
PIP2;6         10 ESLSGKDYLDPPPVKTFEVRELKKWSFYRAVIAEFIATLLFLYVTVLTVIGFKSQTDINA
                  *     ** ****   *   ** *** ******** ******* ******* * * *  *

PIP2;2         69 GGVDCGGVGILGIAWAFGGMIFILVYCTAGISGGHINPAVTFGLFLARKVSLIRAVLYMV
PIP2;6         70 GGGACASVGLLGISWAFGGMIFILVYCTAGISGGHINPAVTFGLFLASKVSLVRAVSYMV
                  **  *  ** *** ********************************** **** *** ***

PIP2;2        129 AQCLGAICGVGFVKAFQSSYYDRYGGGANSLADGYNTGTGLAAEIIGTFVLVYTVFSATD
PIP2;6        130 AQCLGATCGVGLVKVFQSTYYNRYGGGANMLSDGYNVGVGVGAEIIGTFVLVYTVFSATD
                  ****** **** ** *** ** ******* * **** * *  ******************

PIP2;2        189 PKRNARDSHVPVLAPLPIGFAVFMVHLATIPITGTGINPARSFGAAVIYNKSKPWDDHWI
PIP2;6        190 PKRNARDSHIPVLAPLPIGFSVFMVHLATIPITGTGINPARSFGAAVIYNNQKAWDDQWI
                  ********* ********** ******************************  * *** **

PIP2;2        249 FWVGPFIGAAIAAFYHQFVLRASGSKSLGSFRS
PIP2;6        250 FWVGPFVGAAIAAFYHQFVLRAGAMKAYGSVRS
                  ****** ***************   *  ** **


77.4% identity in 270 residues overlap; Score: 1091.0; Gap frequency: 2.2%

PIP2;2         14 RDYEDPPPTPFFDADELTKWSLYRAVIAEFVATLLFLYITVLTVIGYKIQSDTKAGGVDC
PIP2;7         15 KDYVDPPPAPLLDMGELKSWSFYRALIAEFIATLLFLYVTVATVIGHKKQTG------PC
                   ** **** *  *  **  ** *** **** ******* ** **** * *        *

PIP2;2         74 GGVGILGIAWAFGGMIFILVYCTAGISGGHINPAVTFGLFLARKVSLIRAVLYMVAQCLG
PIP2;7         69 DGVGLLGIAWAFGGMIFVLVYCTAGISGGHINPAVTFGLFLARKVSLVRALGYMIAQCLG
                   *** ************ ****************************** **  ** *****

PIP2;2        134 AICGVGFVKAFQSSYYDRYGGGANSLADGYNTGTGLAAEIIGTFVLVYTVFSATDPKRNA
PIP2;7        129 AICGVGFVKAFMKTPYNTLGGGANTVADGYSKGTALGAEIIGTFVLVYTVFSATDPKRSA
                  ***********    *   *****  ****  ** * ********************** *

PIP2;2        194 RDSHVPVLAPLPIGFAVFMVHLATIPITGTGINPARSFGAAVIYNKSKPWDDHWIFWVGP
PIP2;7        189 RDSHIPVLAPLPIGFAVFMVHLATIPITGTGINPARSFGAAVIYNNEKAWDDQWIFWVGP
                  **** ***************************************  * *** *******

PIP2;2        254 FIGAAIAAFYHQFVLRASGSKSLGSFRSAA
PIP2;7        249 FLGALAAAAYHQYILRASAIKALGSFRSNA
                  * **  ** ***  ****  * ****** *
```

```
78.4% identity in 273 residues overlap; Score: 1106.0; Gap frequency: 2.2%

PIP2;2          9 EGFQTRDYEDPPPTPFFDADELTKWSLYRAVIAEFVATLLFLYITVLTVIGYKIQSDTKA
PIP2;8          8 EGRHGKDYVDPPPAPLLDMAELKLWSFYRAIIAEFIATLLFLYVTVATVIGHKNQTGP--
                  **    ** **** *  *  **  ** *** **** ******* ** **** * *

PIP2;2         69 GGVDCGGVGILGIAWAFGGMIFILVYCTAGISGGHINPAVTFGLFLARKVSLIRAVLYMV
PIP2;8         66 ----CGGVGLLGIAWAFGGMIFVLVYCTAGISGGHINPAVTFGLFLARKVSLPRAVAYMV
                      ***** ************ ***************************** *** ***

PIP2;2        129 AQCLGAICGVGFVKAFQSSYYDRYGGGANSLADGYNTGTGLAAEIIGTFVLVYTVFSATD
PIP2;8        122 AQCLGAICGVGLVKAFMMTPYKRLGGGANTVADGYSTGTALGAEIIGTFVLVYTVFSATD
                  *********** ****    * * *****  **** *** * ******************

PIP2;2        189 PKRNARDSHVPVLAPLPIGFAVFMVHLATIPITGTGINPARSFGAAVIYNKSKPWDDHWI
PIP2;8        182 PKRSARDSHVPVLAPLPIGFAVFMVHLATIPITGTGINPARSFGAAVIYNNEKAWDDHWI
                  *** ******************************************  * ******

PIP2;2        249 FWVGPFIGAAIAAFYHQFVLRASGSKSLGSFRS
PIP2;8        242 FWVGPFVGALAAAAYHQYILRAAAIKALASFRS
                  ****** **  ** ***  ***   * * ****
```

Supplemental Figure 6: ***Alignment of PIP2;2 with all other PIP2 isoforms.*** *Alignments were performed using BLAST® (blastp suite) by the National Library of Medicine. Asterisks show amino acid identity between the compared isoforms.*

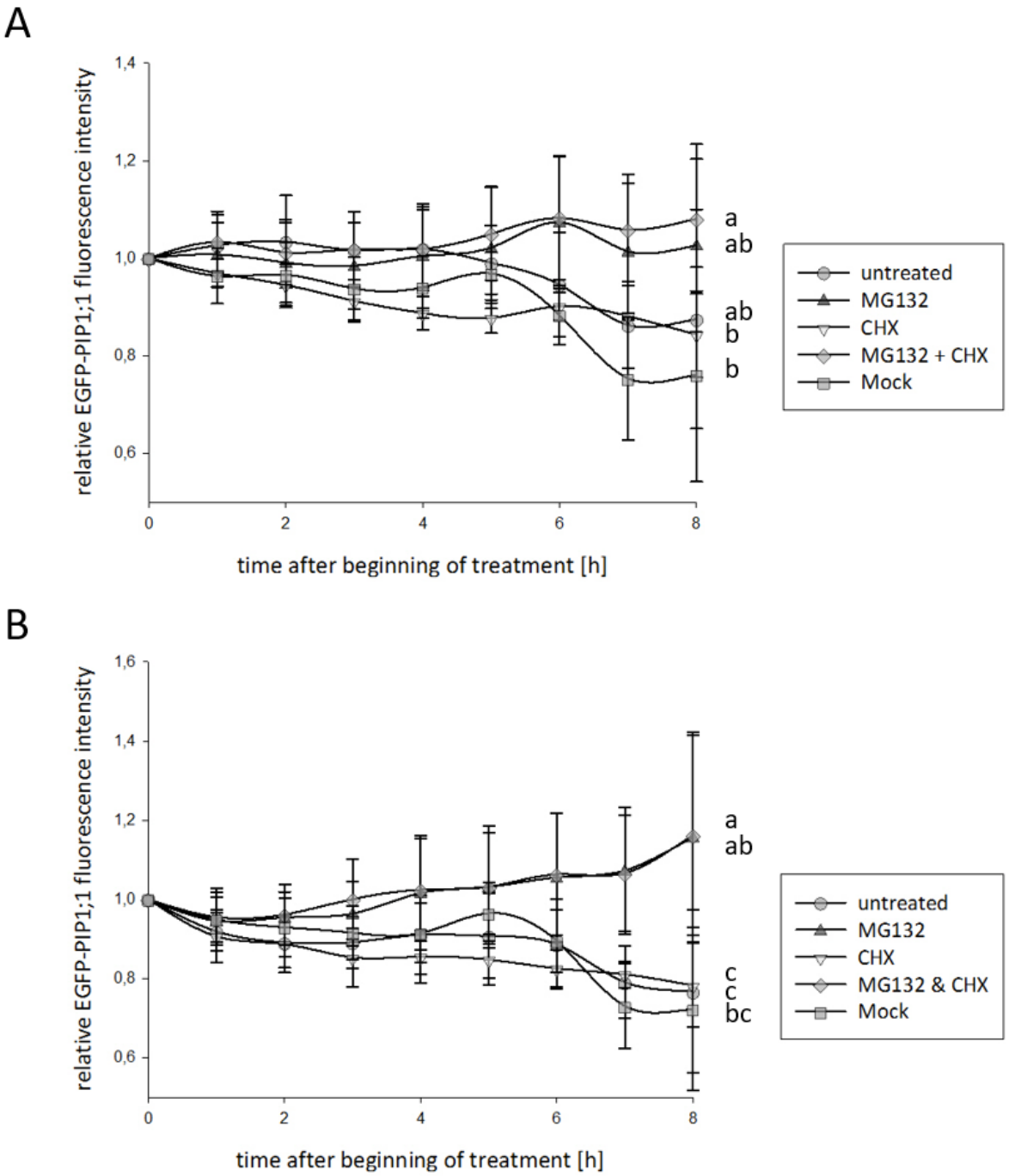

Supplemental Figure 7: ***Influence of proteasomal degradation on the PIP1;1 protein.*** *Mesophyll protoplasts were isolated from 4-week-old* pip1;1 *(EGFP-PIP1;1) and* pip1;1 pip2;1 pip2;2 *(EGFP-PIP1;1) plants. The fluorescence intensity was measured every hour after treatment with inhibitors (MG132, CHX) or mock (DMSO, EtOH) for 8 h to determine the influence of the proteasome on the PIP1;1 protein level in the wild-type-like (A) and double mutant-like (B) background. The measurement right after inhibitor addition served as a reference. Wild type protoplasts were monitored in parallel and the observed fluorescence intensity was used as the background value. Four biological replicates were performed and standard error values are shown. Statistically significant differences between treatments (P<0.05) were determined by One Way Analysis of Variance with the time as a discreet factor and the Tukey method as the all pairwise multiple comparison procedure.*

7 References

Aebi, M. (2013) 'N-linked protein glycosylation in the ER', *Biochimica et Biophysica Acta - Molecular Cell Research*. Elsevier B.V., 1833(11), pp. 2430–2437. doi: 10.1016/j.bbamcr.2013.04.001.

Alexandersson, E., Fraysse, L., Sjövall-Larsen, S., Gustavsson, S., Fellert, M., Karlsson, M., Johanson, U. and Kjellbom, P. (2005) 'Whole gene family expression and drought stress regulation of aquaporins', *Plant Molecular Biology*, 59(3), pp. 469–484. doi: 10.1007/s11103-005-0352-1.

Ampah-Korsah, H., Anderberg, H. I., Engfors, A., Kirscht, A., Norden, K., Kjellstrom, S., Kjellbom, P. and Johanson, U. (2016) 'The Aquaporin Splice Variant NbXIP1;1α Is Permeable to Boric Acid and Is Phosphorylated in the N-terminal Domain', *Frontiers in Plant Science*, 7(June), pp. 1–17. doi: 10.3389/fpls.2016.00862.

Azad, A. K., Sawa, Y., Ishikawa, T. and Shibata, H. (2004) 'Characterization of protein phosphatase 2A acting on phosphorylated plasma membrane aquaporin of tulip petals', *Bioscience, Biotechnology & Biochemistry*, 68(5), pp. 1170–1174. doi: 10.1271/bbb.68.1170.

Benga, G. and Popescu, O. (1986) 'Water permeability in human erythrocytes: identification of membrane proteins involved in water transport', *European Journal of Cell Biology*, 41, pp. 252–262.

Berny, M. C., Gilis, D., Rooman, M. and Chaumont, F. (2016) 'Single Mutations in the Transmembrane Domains of Maize Plasma Membrane Aquaporins Affect the Activity of Monomers within a Heterotetramer', *Molecular Plant*, 9(7), pp. 986–1003. doi: 10.1016/j.molp.2016.04.006.

Bertl, A. and Kaldenhoff, R. (2007) 'Function of a separate NH3-pore in Aquaporin TIP2;2 from wheat', *FEBS Letters*, 581(28), pp. 5413–5417. doi: 10.1016/j.febslet.2007.10.034.

Besserer, A., Burnotte, E., Bienert, G. P., Chevalier, A. S., Errachid, A., Grefen, C., Blatt, M. R. and Chaumont, F. (2012) 'Selective Regulation of Maize Plasma Membrane Aquaporin Trafficking and Activity by the SNARE SYP121', *The Plant Cell*, 24(8), pp. 3463–3481. doi: 10.1105/tpc.112.101758.

Biela, A., Grote, K., Otto, B., Hoth, S., Hedrich, R. and Kaldenhoff, R. (1999) 'The Nicotiana tabacum plasma membrane aquaporin NtAQP1 is mercury-insensitive and permeable for glycerol', *Plant Journal*, 18(5), pp. 565–570. doi: 10.1046/j.1365-313X.1999.00474.x.

Bienert, G. P., Bienert, M. D., Jahn, T. P., Boutry, M. and Chaumont, F. (2011) 'Solanaceae XIPs are plasma membrane aquaporins that facilitate the transport of many uncharged substrates', *Plant Journal*, 66(2), pp. 306–317. doi: 10.1111/j.1365-313X.2011.04496.x.

Bienert, G. P., Cavez, D., Besserer, A. and Berny, M. C. (2012) 'A conserved cysteine residue is involved in disulphide bond formation between plant plasma membrane aquaporin monomers', *Biochemical Journal*, 445(1), pp. 101-11. doi: 10.1042/BJ20111704.

Bienert, G. P., Schjoerring, J. K. and Jahn, T. P. (2006) 'Membrane transport of hydrogen peroxide', *Biochimica et Biophysica Acta - Biomembranes*, 1758(8), pp. 994–1003. doi: 10.1016/j.bbamem.2006.02.015.

Bienert, M. D., Diehn, T. A., Richet, N., Chaumont, F. and Bienert, G. P. (2018) 'Heterotetramerization of Plant PIP1 and PIP2 Aquaporins Is an Evolutionary Ancient Feature to Guide PIP1 Plasma Membrane Localization and Function', *Frontiers in Plant Science*, 9(March), pp. 1–15. doi: 10.3389/fpls.2018.00382.

Boursiac, Y., Chen, S., Luu, D.-T., Sorieul, M., Van Den Dries, N., Maurel, C., Dries, N. Van Den and Maurel, C. (2005) 'Early Effects of Salinity on Water Transport in Arabidopsis Roots . Molecular and Cellular Features of Aquaporin Expression 1', *Plant Physiology*, 139(October), pp. 790–805. doi: 10.1104/pp.105.065029.water.

Boursiac, Y., Boudet, J., Postaire, O., Luu, D. T., Tournaire-Roux, C. and Maurel, C. (2008) 'Stimulus-induced downregulation of root water transport involves reactive oxygen species-activated cell signalling and plasma membrane intrinsic protein internalization', *Plant Journal*, 56(2), pp. 207–218. doi: 10.1111/j.1365-313X.2008.03594.x.

Boursiac, Y., Prak, S., Boudet, J., Postaire, O., Luu, D., Tournaire-roux, C. and Santoni, V. (2008) 'The response of Arabidopsis root water transport to a challenging environment implicates reactive oxygen species- and phosphorylation-dependent internalization of aquaporins', *Plant Signaling & Behavior*, 3(12), pp. 1096–1098. doi: 10.4161/psb.3.12.7002.

Buck, T. M., Wright, C. M. and Brodsky, J. L. (2007) 'The Activities and Function of Molecular Chaperones in the Endoplasmic Reticulum', *Seminars in Cell & Developmental Biology*, 18(6), pp. 751–761. doi: 10.1016/j.asieco.2008.09.006.

Byrt, C. S., Zhao, M., Kourghi, M., Bose, J., Henderson, S. W., Qiu, J., Gilliham, M., Schultz, C., Schwarz, M., Ramesh, S. A., Yool, A. and Tyerman, S. (2017) 'Non-selective cation channel activity of aquaporin AtPIP2;1 regulated by Ca^{2+} and pH', *Plant, Cell & Environment*, 40(6), pp. 802–815. doi: 10.1111/pce.12832.

Carvalho, P., Stanley, A. M. and Rapoport, T. A. (2010) 'Retro-translocation of a misfolded luminal ER protein by the ubiquitin-ligase Hrd1p', *Cell*, 143(4), pp. 579–591. doi: 10.1016/j.cell.2010.10.028.

Chevalier, A. S., Bienert, G. P. and Chaumont, F. (2014) 'A New LxxxA Motif in the Transmembrane Helix3 of Maize Aquaporins Belonging to the Plasma Membrane Intrinsic Protein PIP2 Group Is Required for Their Trafficking to the Plasma Membrane', *Plant Physiology*, 166(1), pp. 125–138. doi: 10.1104/pp.114.240945.

Chiba, Y., Mitani, N., Yamaji, N. and Ma, J. F. (2009) 'HvLsi1 is a silicon influx transporter in barley', *Plant Journal*, 57(5), pp. 810–818. doi: 10.1111/j.1365-313X.2008.03728.x.

Chung, T., Phillips, A. R. and Vierstra, R. D. (2010) 'ATG8 lipidation and ATG8-mediated autophagy in Arabidopsis require ATG12 expressed from the differentially controlled ATG12A and ATG12B loci', *Plant Journal*, 62(3), pp. 483–493. doi: 10.1111/j.1365-313X.2010.04166.x.

Clerc, S., Hirsch, C., Oggier, D. M., Deprez, P., Jakob, C., Sommer, T. and Aebi, M. (2009) 'Htm1 protein generates the N-glycan signal for glycoprotein degradation in the endoplasmic reticulum', *Journal of Cell Biology*, 184(1), pp. 159–172. doi: 10.1083/jcb.200809198.

Clough, S. J. and Bent, A. F. (1998) 'Floral dip: A simplified method for Agrobacterium-mediated transformation of *Arabidopsis thaliana*.', *Plant Journal*, 16(6), pp. 735–743. doi: 10.1046/j.1365-313X.1998.00343.x.

D'Alessio, C., Caramelo, J. J. and Parodi, A. J. (2010) 'UDP-GLC:GLYCOPROTEIN GLUCOSYLTRANSFERASE- GLUCOSIDASE II, THE YING-YANG OF THE ER QUALITY CONTROL', *Seminars in Cell & Developmental Biology*, 21(5), pp. 491–499. doi: 10.1037/a0018493.

Daniels, M. J., Chrispeels, M. J. and Yeager, M. (1999) 'Projection structure of a plant vacuole membrane aquaporin by electron cryo-crystallography', *Journal of Molecular Biology*, 294(5), pp. 1337–1349. doi: 10.1006/jmbi.1999.3293.

Daniels, M. J. and Yeager, M. (2005) 'Phosphorylation of aquaporin PvTIP3;1 defined by mass spectrometry and molecular modeling', *Biochemistry*, 44(44), pp. 14443–14454. doi: 10.1021/bi050565d.

Danielson, J. Å. H. and Johanson, U. (2008) 'Unexpected complexity of the Aquaporin gene family in the moss Physcomitrella patens', *BMC Plant Biology*, 8, pp. 1–16. doi: 10.1186/1471-2229-8-45.

Dean, R. M., Rivers, R. L., Zeidel, M. L. and Roberts, D. M. (1999) 'Purification and functional reconstitution of soybean nodulin 26. An aquaporin with water and glycerol transport properties', *Biochemistry*, 38(1), pp. 347–353. doi: 10.1021/bi982110c.

Delporte, C. (2014) 'Aquaporins in salivary glands and pancreas', *Biochimica et Biophysica Acta - General Subjects*, 1840(5), pp. 1524–1532. doi: 10.1016/j.bbagen.2013.08.007.

Dhonukshe, P., Aniento, F., Hwang, I., Robinson, D. G., Mravec, J., Stierhof, Y. D. and Friml, J. (2007) 'Clathrin-Mediated Constitutive Endocytosis of PIN Auxin Efflux Carriers in Arabidopsis', *Current Biology*, 17(6), pp. 520–527. doi: 10.1016/j.cub.2007.01.052.

Doelling, J. H., Walker, J. M., Friedman, E. M., Thompson, A. R. and Vierstra, R. D. (2002) 'The APG8/12-activating enzyme APG7 is required for proper nutrient recycling and senescence in Arabidopsis thaliana', *Journal of Biological Chemistry*, 277(36), pp. 33105–33114. doi: 10.1074/jbc.M204630200.

Fauteux, F., Chain, F., Belzile, F., Menzies, J. G. and Belanger, R. R. (2006) 'The protective role of silicon in the Arabidopsis-powdery mildew pathosystem', *Proceedings of the National Academy of Sciences of the United States of America*, 103(46), pp. 17554–17559. doi: 10.1073/pnas.0606330103.

Feraru, E., Feraru, M. I., Asaoka, R., Paciorek, T., De Rycke, R., Tanaka, H., Nakano, A. and Friml, J. (2012) 'BEX5/RabA1b Regulates trans-Golgi Network-to-Plasma Membrane Protein Trafficking in Arabidopsis', *The Plant Cell*, 24(7), pp. 3074–3086. doi: 10.1105/tpc.112.098152.

Fetter, K. (2004) 'Interactions between Plasma Membrane Aquaporins Modulate Their Water Channel Activity', *The Plant Cell*, 16(1), pp. 215–228. doi: 10.1105/tpc.017194.

Frick, A., Järvå, M., Ekvall, M., Uzdavinys, P., Nyblom, M. and Törnroth-Horsefield, S. (2013) 'Mercury increases water permeability of a plant aquaporin through a non-cysteine-related mechanism', *Biochemical Journal*, 454(3), pp. 491–499. doi: 10.1042/BJ20130377.

Gardner, R. G., Swarbrick, G. M., Bays, N. W., Cronin, S. R., Wilhovsky, S., Seelig, L., Kim, C. and Hampton, R. Y. (2000) 'Endoplasmic reticulum degradation requires lumen to cytosol signaling: Transmembrane control of Hrd1p by Hrd3p', *Journal of Cell Biology*, 151(1), pp. 69–82. doi: 10.1083/jcb.151.1.69.

Di Giorgio, J. A. P., Bienert, G. P., Ayub, N. D., Yaneff, A., Barberini, M. L., Mecchia, M. A., Amodeo, G., Soto, G. C. and Muschietti, J. P. (2016) 'Pollen-Specific Aquaporins NIP4;1 and NIP4;2 Are Required for Pollen Development and Pollination in *Arabidopsis thaliana*', *The Plant Cell*, 28(5), pp. 1053–1077. doi: 10.1105/tpc.15.00776.

Grefen, C. and Blatt, M. R. (2012) 'A 2in1 cloning system enables ratiometric bimolecular fluorescence complementation (rBiFC)', *BioTechniques*, 53(5), pp. 311–314. doi: 10.2144/000113941.

De Groot, B. L. and Grubmüller, H. (2001) 'Water permeation across biological membranes: Mechanism and dynamics of aquaporin-1 and GlpF', *Science*, 294(5550), pp. 2353–2357. doi: 10.1126/science.1062459.

Gu, R., Chen, X., Zhou, Y. and Yuan, L. (2011) 'Isolation and characterization of three maize aquaporin genes ', *BMB reports*, (14), pp. 1–6. doi: 10.5483/BMBRep.2012.45.2.96.

Guenther, J. F., Chanmanivone, N., Galetovic, M. P., Wallace, I. S., Cobb, J. A. and Roberts, D. M. (2003) 'Phosphorylation of soybean nodulin 26 on serine 262 enhances water permeability and is regulated developmentally and by osmotic signals.', *The Plant Cell*, 15(4), pp. 981–91. doi: 10.1105/tpc.009787.

Gupta, A. B. and Sankararamakrishnan, R. (2009) 'Genome-wide analysis of major intrinsic proteins in the tree plant Populus trichocarpa: Characterization of XIP subfamily of aquaporins from evolutionary perspective', *BMC Plant Biology*, 9, pp. 1–28. doi: 10.1186/1471-2229-9-134.

Gustavsson, S., Lebrun, A.-S., Nordén, K., Chaumont, F. and Johanson, U. (2005) 'A novel plant major intrinsic protein in Physcomitrella patens most similar to bacterial glycerol channels.', *Plant Physiology*, 139(1), pp. 287–95. doi: 10.1104/pp.105.063198.

Hachez, C., Laloux, T., Reinhardt, H., Cavez, D., Degand, H., Grefen, C., De Rycke, R., Inzé, D., Blatt, M. R., Russinova, E. and Chaumont, F. (2014) '*Arabidopsis* SNAREs SYP61 and SYP121 Coordinate the Trafficking of Plasma Membrane Aquaporin PIP2;7 to Modulate the Cell Membrane Water Permeability', *The Plant Cell*, 26(7), pp. 3132–3147. doi: 10.1105/tpc.114.127159.

Hachez, C., Veljanovski, V., Reinhardt, H., Guillaumot, D., Vanhee, C., Chaumont, F. and Batoko, H. (2014) 'The *Arabidopsis* Abiotic Stress-Induced TSPO-Related Protein Reduces Cell-Surface Expression of the Aquaporin PIP2;7 through Protein-Protein Interactions and Autophagic Degradation', *The Plant Cell*, 26(12), pp. 4974–4990. doi: 10.1105/tpc.114.134080.

Hammond, C., Braakman, I. and Helenius, A. (1994) 'Role of N-linked oligosaccharide recognition, glucose trimming, and calnexin in glycoprotein folding and quality control.', *Proceedings of the National Academy of Sciences of the United States of America*, 91(3), pp. 913–917. doi: 10.1073/pnas.91.3.913.

Hanaoka, H. (2002) 'Leaf Senescence and Starvation-Induced Chlorosis Are Accelerated by the Disruption of an Arabidopsis Autophagy Gene', *Plant Physiology*, 129(3), pp. 1181–1193. doi: 10.1104/pp.011024.

Havé, M., Balliau, T., Cottyn-boitte, B., Dérond, E., Cueff, G., Soulay, F., Lornac, A., Reichman, P., Dissmeyer, N., Avice, J., Gallois, P., Rajjou, L., Zivy, M. and Masclaux-daubresse, C. (2018) 'Increases in activity of proteasome and papain-like cysteine protease in Arabidopsis autophagy mutants : back-up compensatory effect or cell-death promoting effect?', *Journal of Experimental Botany*, 69(6), pp. 1369–1385. doi: 10.1093/jxb/erx482.

Heckwolf, M., Pater, D., Hanson, D. T. and Kaldenhoff, R. (2011) 'The Arabidopsis thaliana aquaporin AtPIP1;2 is a physiologically relevant CO2 transport facilitator', *Plant Journal*, 67(5), pp. 795–804. doi: 10.1111/j.1365-313X.2011.04634.x.

Hemsley, P. A., Weimar, T., Lilley, K. S., Dupree, P. and Grierson, C. S. (2013) 'A proteomic approach identifies many novel palmitoylated proteins in Arabidopsis', *New Phytologist*, 197(3), pp. 805–814. doi: 10.1111/nph.12077.

Henzler, T., Waterhouse, R. N., Smyth, a. J., Carvajal, M., Cooke, D. T., a.R., S., Steudle, E. and Clarkson, D. T. (1999) 'Diurnal varia- tions in hydraulic conductivity and root pressure can be correlated with the expression of putative aquaporins in the roots of Lotus japonicus', *Planta*, C(210), pp. 50–60.

Hirsch, C., Gauss, R., Horn, S. C., Neuber, O. and Sommer, T. (2009) 'The ubiquitylation machinery of the endoplasmic reticulum', *Nature*, 458(7237), pp. 453–460. doi: 10.1038/nature07962.

Holm, L. M., Jahn, T. P., Møller, A. L. B., Schjoerring, J. K., Ferri, D., Klaerke, D. A. and Zeuthen, T. (2005) 'NH3 and NH4+ permeability in aquaporin-expressing Xenopus oocytes', *Pflugers Archiv European Journal of Physiology*, 450(6), pp. 415–428. doi: 10.1007/s00424-005-1399-1.

Horsefield, R., Nordén, K., Fellert, M., Backmark, A., Törnroth-Horsefield, S., Terwisscha van Scheltinga, A. C., Kvassman, J., Kjellbom, P., Johanson, U. and Neutze, R. (2008) 'High-resolution x-ray structure of human aquaporin 5', *Proceedings of the National Academy of Sciences of the United States of America*, 105(36), pp. 13327–32. doi: 10.1073/pnas.0801466105.

Hüttner, S., Veit, C., Schoberer, J., Grass, J. and Strasser, R. (2012) 'Unraveling the function of Arabidopsis thaliana OS9 in the endoplasmic reticulum-associated degradation of glycoproteins', *Plant Molecular Biology*, 79(1–2), pp. 21–33. doi: 10.1007/s11103-012-9891-4.

Ichimura, Y., Kirisako, T., Takao, T., Satomi, Y., Shimonishi, Y., Ishihara, N., Mizushima, N., Tanida, I., Kominami, E., Ohsumi, M., Noda, T. and Ohsumi, Y. (2000) 'A ubiquitin-like system mediates protein lipidation', *Nature*, 408(6811), pp. 488–492. doi: 10.1038/35044114.

Da Ines, O. (2008) 'Functional analysis of PIP2 aquaporins in Arabidopsis thaliana', *Thesis (LMU)*.

Da Ines, O., Graf, W., Franck, K. I., Albert, A., Winkler, J. B., Scherb, H., Stichler, W. and Schäffner, A. R. (2010) 'Kinetic analyses of plant water relocation using deuterium as tracer - reduced water flux of Arabidopsis pip2 aquaporin knockout mutants', *Plant Biology*, 12(SUPPL. 1), pp. 129–139. doi: 10.1111/j.1438-8677.2010.00385.x.

Ishikawa, F., Suga, S., Uemura, T., Sato, M. H. and Maeshima, M. (2005) 'Novel type aquaporin SIPs are mainly localized to the ER membrane and show cell-specific expression in Arabidopsis thaliana', *FEBS Letters*, 579(25), pp. 5814–5820. doi: 10.1016/j.febslet.2005.09.076.

Jang, J. Y., Kim, D. G., Kim, Y. O., Kim, J. S. and Kang, H. (2004) 'An expression analysis of a gene family encoding plasma membrane aquaporins in response to abiotic stresses in Arabidopsis thaliana', *Plant Molecular Biology*, 54(5), pp. 713–725. doi: 10.1023/B:PLAN.0000040900.61345.a6.

Javot, H., Lauvergeat, V., Santoni, V., Martin-laurent, F., Güçlü, J., Vinh, J., Heyes, J., Franck, K. I., Schäffner, A. R., Bouchez, D. and Maurel, C. (2003) 'Role of a Single Aquaporin Isoform in Root Water Uptake', *The Plant Cell*, 15(February), pp. 509–522. doi: 10.1105/tpc.008888.

Jian, F. M., Tamai, K., Yamaji, N., Mitani, N., Konishi, S., Katsuhara, M., Ishiguro, M., Murata, Y. and Yano, M. (2006) 'A silicon transporter in rice', *Nature*, 440(7084), pp. 688–691. doi: 10.1038/nature04590.

Jin, H., Yan, Z., Nam, K. H. and Li, J. (2007) 'Allele-Specific Suppression of a Defective Brassinosteroid Receptor Reveals an Essential Role of UDP-Glucose', *Molecular Cell*, 26(6), pp. 821–830. doi: 10.1016/j.asieco.2008.09.006.

Jin, H., Hong, Z., Su, W. and Li, J. (2009) 'A plant-specific calreticulin is a key retention factor for a defective brassinosteroid receptor in the endoplasmic reticulum.', *Proceedings of the National Academy of Sciences of the United States of America*, 106(32), pp. 13612–13617. doi: 10.1073/pnas.0906144106.

Johanson, U. (2001) 'The Complete Set of Genes Encoding Major Intrinsic Proteins in Arabidopsis Provides a Framework for a New Nomenclature for Major Intrinsic Proteins in Plants', *Plant Physiology*, 126(4), pp. 1358–1369. doi: 10.1104/pp.126.4.1358.

Johanson, U. and Gustavsson, S. (2002) 'A new subfamily of major intrinsic proteins in plants', *Molecular Biology and Evolution*, 19(4), pp. 456–461. doi: 10.1093/oxfordjournals.molbev.a004101.

Johansson, I., Karlsson, M., Shukla, V. K., Chrispeels, M. J., Larsson, C. and Kjellbom, P. (1998) 'Water Transport Activity of the Plasma Membrane Aquaporin PM28A Is Regulated by Phosphorylation', *The Plant Cell*, 10(3), pp. 451–459. doi: 10.1105/tpc.10.3.451.

Johnson, K. D. and Chrispeels, M. J. (1992) 'Tonoplast-bound protein kinase phosphorylates tonoplast intrinsic protein.', *Plant Physiology*, 100(4), pp. 1787–95. doi: 10.1104/pp.100.4.1787.

Jozefkowicz, C., Rosi, P., Sigaut, L., Soto, G., Pietrasanta, L. I., Amodeo, G. and Alleva, K. (2013) 'Loop A Is Critical for the Functional Interaction of Two Beta vulgaris PIP Aquaporins', *PLOS ONE*, 8(3). doi: 10.1371/journal.pone.0057993.

Jozefkowicz, C., Scochera, F. and Alleva, K. (2016) 'Two aquaporins, multiple ways of assembly', *Channels*, 10(6), pp. 438–439. doi: 10.1080/19336950.2016.1206371.

Karimi, M., Inzé, D. and Depicker, A. (2002) 'GATEWAY vectors for Agrobacterium-mediated plant transformation', *Trends in Plant Science,* 7(5), pp. 193–195.

Kirscht, A., Kaptan, S. S., Bienert, G. P., Chaumont, F., Nissen, P., de Groot, B. L., Kjellbom, P., Gourdon, P. and Johanson, U. (2016) 'Crystal Structure of an Ammonia-Permeable Aquaporin', *PLoS Biology*, 14(3), pp. 1–19. doi: 10.1371/journal.pbio.1002411.

Kleine-Vehn, J., Leitner, J., Zwiewka, M., Sauer, M., Abas, L., Luschnig, C. and Friml, J. (2008) 'Differential degradation of PIN2 auxin efflux carrier by retromer-dependent vacuolar targeting', *Proceedings of the National Academy of Sciences of the United States of America*, 105(46), pp. 17812–17817. doi: 10.1073/pnas.0808073105.

Kodama, Y. and Hu, C. (2012) 'Bimolecular fluorescence complementation (BiFC): A 5-year update and future perspectives', *Biotechniques*, 53(5), pp. 285-98. doi: 10.2144/000113943.

Kosinka Eriksson, U., Fischer, G., Friemann, R., Enkavi, G., Tajkhorshid, E. and Neutze, R. (2013) 'Subangstrom resolution x-ray structure details aquaporin-water interactions', *Science*, 340(6138), pp. 1346–1349. doi: 10.1126/science.1234306.

Laloux, T., Junqueira, B., Maistriaux, L. C., Ahmed, J., Jurkiewicz, A. and Chaumont, F. (2018) 'Plant and mammal aquaporins: Same but different', *International Journal of Molecular Sciences*, 19(2), pp. 521. doi: 10.3390/ijms19020521.

Lee, H. K., Cho, S. K., Son, O., Xu, Z., Hwang, I. and Kim, W. T. (2009) 'Drought Stress-Induced Rma1H1, a RING Membrane-Anchor E3 Ubiquitin Ligase Homolog, Regulates Aquaporin Levels via Ubiquitination in Transgenic Arabidopsis Plants', *The Plant Cell*, 21(2), pp. 622–641. doi: 10.1105/tpc.108.061994.

Li, G., Boudsocq, M., Hem, S., Vialaret, J., Rossignol, M., Maurel, C. and Santoni, V. (2015) 'The calcium-dependent protein kinase CPK7 acts on root hydraulic conductivity', *Plant, Cell & Environment*, 38(7), pp. 1312–1320. doi: 10.1111/pce.12478.

Li, L.-M., Lü, S.-Y. and Li, R.-J. (2017) 'The Arabidopsis endoplasmic reticulum associated degradation pathways are involved in the regulation of heat stress response.', *Biochemical and Biophysical Research Communications*, 487(2), pp. 362-367. doi: 10.1016/j.bbrc.2017.04.066.

Li, L., Wang, H., Gago, J., Cui, H., Qian, Z., Kodama, N., Ji, H., Tian, S., Shen, D., Chen, Y., Sun, F., Xia, Z., Ye, Q., Sun, W., Flexas, J. and Dong, H. (2015) 'Harpin Hpa1 Interacts with Aquaporin PIP1;4 to Promote the Substrate Transport and Photosynthesis in Arabidopsis', *Scientific Reports*, 5(October), pp. 1–17. doi: 10.1038/srep17207.

Li, X., Wang, X., Yang, Y., Li, R., He, Q., Fang, X., Luu, D.-T., Maurel, C. and Lin, J. (2011) 'Single-Molecule Analysis of PIP2;1 Dynamics and Partitioning Reveals Multiple Modes of Arabidopsis Plasma Membrane Aquaporin Regulation', *The Plant Cell*, 23(10), pp. 3780–3797. doi: 10.1105/tpc.111.091454.

Liu, C. (2015) 'The PIP1 protein expression is positively regulated by PIP2 ; 1 and PIP2 ; 2 in Arabidopsis thaliana', *Thesis (LMU)*.

Liu, L.-H. (2003) 'Urea Transport by Nitrogen-Regulated Tonoplast Intrinsic Proteins in Arabidopsis', *Plant Physiology*, 133(3), pp. 1220–1228. doi: 10.1104/pp.103.027409.

Liu, L., Cui, F., Li, Q., Yin, B., Zhang, H., Lin, B., Wu, Y., Xia, R., Tang, S. and Xie, Q. (2011) 'The endoplasmic reticulum-associated degradation is necessary for plant salt tolerance', *Cell Research,* 21(6), pp. 957–969. doi: 10.1038/cr.2010.181.

Lopez, D., Bronner, G., Brunel, N., Auguin, D., Bourgerie, S., Brignolas, F., Carpin, S., Tournaire-Roux, C., Maurel, C., Fumanal, B., Martin, F., Sakr, S., Label, P., Julien, J. L., Gousset-Dupont, A. and Venisse, J. S. (2012) 'Insights into Populus XIP aquaporins: Evolutionary expansion, protein functionality, and environmental regulation', *Journal of Experimental Botany*, 63(5), pp. 2217–2230. doi: 10.1093/jxb/err404.

Luo, N., Yan, A. and Yang, Z. (2016) 'Measuring Exocytosis Rate Using Corrected Fluorescence Recovery After Photoconversion', *Traffic*, 17(5), pp. 554–564. doi: 10.1111/tra.12380.

Luu, D. T., Martiniãre, A., Sorieul, M., Runions, J. and Maurel, C. (2012) 'Fluorescence recovery after photobleaching reveals high cycling dynamics of plasma membrane aquaporins in Arabidopsis roots under salt stress', *Plant Journal*, 69(5), pp. 894–905. doi: 10.1111/j.1365-313X.2011.04841.x.

Martinière, A., Li, X., Runions, J., Lin, J., Maurel, C. and Luu, D. T. (2012) 'Salt stress triggers enhanced cycling of Arabidopsis root plasma-membrane aquaporins', *Plant Signaling & Behavior*, 7(4), pp. 529–532. doi: 10.4161/psb.19350.

Matsumoto, T., Lian, H. L., Su, W. A., Tanaka, D., Liu, C. W., Iwasaki, I. and Kitagawa, Y. (2009) 'Role of the aquaporin PIP1 subfamily in the chilling tolerance of rice', *Plant & Cell Physiology*, 50(2), pp. 216–229. doi: 10.1093/pcp/pcn190.

Mitani, N., Yamaji, N. and Ma, J. F. (2008) 'Characterization of substrate specificity of a rice silicon transporter, Lsi1', *Pflugers Archiv European Journal of Physiology*, 456(4), pp. 679–686. doi: 10.1007/s00424-007-0408-y.

Mizushima, N., Noda, T., Yoshimori, T., Tanaka, Y., Ishii, T., George, M. D., Klionsky, D. J., Ohsumi, M. and Ohsumi, Y. (1998) 'A protein conjugation system essential for autophagy', *Nature*, 395(6700), pp. 395–398. doi: 10.1038/26506.

Mizutani, M., Watanabe, S., Nakagawa, T. and Maeshima, M. (2006) 'Aquaporin NIP2;1 is mainly localized to the ER membrane and shows root-specific accumulation in Arabidopsis thaliana', *Plant & Cell Physiology*, 47(10), pp. 1420–1426. doi: 10.1093/pcp/pcl004.

Monneuse, J. M., Sugano, M., Becue, T., Santoni, V., Hem, S. and Rossignol, M. (2011) 'Towards the profiling of the Arabidopsis thaliana plasma membrane transportome by targeted proteomics', *Proteomics*, 11(9), pp. 1789–1797. doi: 10.1002/pmic.201000660.

Mosa, K. A., Kumar, K., Chhikara, S., Musante, C., White, J. C. and Dhankher, O. P. (2016) 'Enhanced Boron Tolerance in Plants Mediated by Bidirectional Transport Through Plasma Membrane Intrinsic Proteins', *Scientific Reports*, 6(September 2015), pp. 1–14. doi: 10.1038/srep21640.

Murata, K., Mitsuoka, K., Hirai, T., Walz, T., Agre, P., Heymann, J. B., Engel, A. and Fujiyoshi, Y. (2000) 'Structural determinants of water permeation through aquaporin-1', *Nature*, 407(6804), pp. 599–605.

Mut, P., Bustamante, C., Martínez, G., Alleva, K., Sutka, M., Civello, M. and Amodeo, G. (2008) 'A fruit-specific plasma membrane aquaporin subtype PIP1;1 is regulated during strawberry (Fragaria x ananassa) fruit ripening', *Physiologia Plantarum*, 132(4), pp. 538–551. doi: 10.1111/j.1399-3054.2007.01046.x.

Nejsum, L. N., Kwon, T.-H., Jensen, U. B., Fumagalli, O., Frøkiaer, J., Krane, C. M., Menon, A. G., King, L. S., Agre, P. C. and Nielsen, S. (2002) 'Functional requirement of aquaporin-5 in plasma membranes of sweat glands.', *Proceedings of the National Academy of Sciences of the United States of America*, 99(1), pp. 511–6. doi: 10.1073/pnas.012588099.

Nienhaus, G. U., Nienhaus, K., Hölzle, A., Ivanchenko, S., Renzi, F., Oswald, F., Wolff, M., Schmitt, F., Röcker, C., Vallone, B., Weidemann, W., Heilker, R., Nar, H. and Wiedenmann, J. (2006) 'Photoconvertible Fluorescent Protein EosFP: Biophysical Properties and Cell Biology Applications', *Photochemistry and Photobiology*, 82(2), p. 351. doi: 10.1562/2005-05-19-RA-533.

Noda, Y. and Sasaki, S. (2006) 'Regulation of aquaporin-2 trafficking and its binding protein complex', *Biochimica et Biophysica Acta - Biomembranes*, 1758(8), pp. 1117–1125. doi: 10.1016/j.bbamem.2006.03.004.

Nuhse, T. S. (2004) 'Phosphoproteomics of the Arabidopsis Plasma Membrane and a New Phosphorylation Site Database', *The Plant Cell*, 16(9), pp. 2394–2405. doi: 10.1105/tpc.104.023150.

Nyblom, M., Frick, A., Wang, Y., Ekvall, M., Hallgren, K., Hedfalk, K., Neutze, R., Tajkhorshid, E. and Törnroth-Horsefield, S. (2009) 'Structural and Functional Analysis of SoPIP2;1 Mutants Adds Insight into Plant Aquaporin Gating', *Journal of Molecular Biology*, 387(3), pp. 653–668. doi: 10.1016/j.jmb.2009.01.065.

Park, S. J., Suetsugu, S. and Takenawa, T. (2005) 'Interaction of HSP90 to N-WASP leads to activation and protection from proteasome-dependent degradation', *The EMBO Journal*, 24(May), pp. 1557–1570. doi: 10.1038/sj.emboj.7600586.

Péret, B., Li, G., Zhao, J., Band, L. R., Voß, U., Postaire, O., Luu, D. T., Da Ines, O., Casimiro, I., Lucas, M., Wells, D. M., Lazzerini, L., Nacry, P., King, J. R., Jensen, O. E., Schäffner, A. R., Maurel, C. and Bennett, M. J. (2012) 'Auxin regulates aquaporin function to facilitate lateral root emergence', *Nature Cell Biology*, 14(10), pp. 991–998. doi: 10.1038/ncb2573.

di Pietro, M., Vialaret, J., Li, G.-W., Hem, S., Prado, K., Rossignol, M., Maurel, C. and Santoni, V. (2013) 'Coordinated Post-translational Responses of Aquaporins to Abiotic and Nutritional Stimuli in *Arabidopsis* Roots', *Molecular & Cellular Proteomics*, 12(12), pp. 3886–3897. doi: 10.1074/mcp.M113.028241.

Pilon, M., Schekman, R. and Römisch, K. (1997) 'Sec61p mediates export of a misfolded secretory protein from the endoplasmic reticulum to the cytosol for degradation', *The EMBO Journal*, 16(15), pp. 4540–4548. doi: 10.1093/emboj/16.15.4540.

Pollier, J., Moses, T., Miguel, G.-G., De Geyter, N., Lippens, S., Bossche, Robin Vanden Marhavy, P., Kremer, A., Morreel, K., Guerin, C. J., Tava, A., Oleszek, W., Thevelein, J. M., Campos, N., Goormachting, S. and Goossens, A. (2013) 'The protein quality control systemmanages plant defence compound synthesis', *Nature*, 504, pp. 148–152. doi: 10.1038/nature12685.

Postaire, O., Tournaire-Roux, C., Grondin, A., Boursiac, Y., Morillon, R., Schaffner, A. R. and Maurel, C. (2010) 'A PIP1 Aquaporin Contributes to Hydrostatic Pressure-Induced Water Transport in Both the Root and Rosette of Arabidopsis', *Plant Physiology*, 152(3), pp. 1418–1430. doi: 10.1104/pp.109.145326.

Prado, K., Boursiac, Y., Tournaire-Roux, C., Monneuse, J.-M., Postaire, O., Da Ines, O., Schaffner, A. R., Hem, S., Santoni, V. and Maurel, C. (2013) 'Regulation of Arabidopsis Leaf Hydraulics Involves Light-Dependent Phosphorylation of Aquaporins in Veins', *The Plant Cell*, 25(3), pp. 1029–1039. doi: 10.1105/tpc.112.108456.

Prak, S., Hem, S., Boudet, J., Viennois, G., Sommerer, N., Rossignol, M., Maurel, C. and Santoni, V. (2008) 'Multiple Phosphorylations in the C-terminal Tail of Plant Plasma Membrane Aquaporins', *Molecular & Cellular Proteomics*, 7(6), pp. 1019–1030. doi: 10.1074/mcp.M700566-MCP200.

Quigley, F., Rosenberg, J. M., Shachar-Hill, Y. and Bohnert, H. J. (2002) 'From genome to function: the Arabidopsis aquaporins', *Genome Biology*, 3(1), pp. research0001.1–research0001.17. doi: 10.1186/gb-2001-3-1-research0001.

Rancour, D. M., Dickey, C. E., Park, S. and Bednarek, S. Y. (2002) 'Characterization of AtCDC48. Evidence for Multiple Membrane Fusion Mechanisms at the Plane of Cell Division in Plants', *Plant Physiology*, 130(3), pp. 1241–1253. doi: 10.1104/pp.011742.

Rodrigues, O., Reshetnyak, G., Grondin, A., Saijo, Y., Leonhardt, N., Maurel, C. and Verdoucq, L. (2017) 'Aquaporins facilitate hydrogen peroxide entry into guard cells to mediate ABA- and pathogen-triggered stomatal closure', *Proceedings of the National Academy of Sciences of the United States of America*, 114(34), p. 201704754. doi: 10.1073/pnas.1704754114.

Santoni, V., Verdoucq, L., Sommerer, N., Vinh, J., Pflieger, D. and Maurel, C. (2006) 'Methylation of aquaporins in plant plasma membrane', *Biochemical Journal*, 400(1), pp. 189–197. doi: 10.1042/BJ20060569.

SANTONI, V., VINH, J., PFLIEGER, D., SOMMERER, N. and MAUREL, C. (2003) 'A proteomic study reveals novel insights into the diversity of aquaporin forms expressed in the plasma membrane of plant roots', *Biochemical Journal*, 373(1), pp. 289–296. doi: 10.1042/bj20030159.

Schey, K. L., Wang, Z., L. Wenke, J. and Qi, Y. (2014) 'Aquaporins in the eye: Expression, function, and roles in ocular disease', *Biochimica et Biophysica Acta - General Subjects*, 1840(5), pp. 1513–1523. doi: 10.1016/j.bbagen.2013.10.037.

Schoebel, S., Mi, W., Stein, A., Ovchinnikov, S., Pavlovicz, R., DImaio, F., Baker, D., Chambers, M. G., Su, H., Li, D., Rapoport, T. A. and Liao, M. (2017) 'Cryo-EM structure of the protein-conducting ERAD channel Hrd1 in complex with Hrd3', *Nature*, 548(7667), pp. 352–355. doi: 10.1038/nature23314.

Shin, K. D., Lee, H. N. and Chung, T. (2014) 'A Revised Assay for Monitoring Autophagic Flux in Arabidopsis thaliana Reveals Involvement of AUTOPHAGY-RELATED9 in Autophagy', *Molecules and Cells*, 37(5), pp. 399–405. doi: 10.14348/molcells.2014.0042.

Sjövall-Larsen, S., Alexandersson, E., Johansson, I., Karlsson, M., Johanson, U. and Kjellbom, P. (2006) 'Purification and characterization of two protein kinases acting on the aquaporin SoPIP2;1', *Biochimica et Biophysica Acta - Biomembranes*, 1758(8), pp. 1157–1164. doi: 10.1016/j.bbamem.2006.06.002.

Sláviková, S., Shy, G., Yao, Y., Glozman, R., Levanony, H., Pietrokovski, S., Elazar, Z. and Galili, G. (2005) 'The autophagy-associated Atg8 gene family operates both under favourable growth conditions and under starvation stresses in Arabidopsis plants', *Journal of Experimental Botany*, 56(421), pp. 2839–2849. doi: 10.1093/jxb/eri276.

Sorieul, M., Santoni, V., Maurel, C. and Luu, D. T. (2011) 'Mechanisms and Effects of Retention of Over-Expressed Aquaporin AtPIP2;1 in the Endoplasmic Reticulum', *Traffic*, 12(4), pp. 473–482. doi: 10.1111/j.1600-0854.2010.01154.x.

Srivastava, R., Li, Z., Russo, G., Tang, J., Bi, R., Muppirala, U., Chudalayandi, S., Severin, A., He, M., Vaitkevicius, S. I., Lawrence-Dill, C. J., Liu, P., Stapleton, A. E., Bassham, D. C., Brandizzi, F. and Howell, S. H. (2018) 'Response to Persistent ER Stress in Plants: a Multiphasic Process that Transitions Cells from Prosurvival Activities to Cell Death', *The Plant Cell*, 30(June), pp. 1220–1242. doi: 10.1105/tpc.18.00153.

Steudle, E. and Peterson, C. A. (1998) 'How does water get through roots?', *Journal of Experimental Botany*, 49(322), pp. 775–788. doi: 10.1093/jxb/49.322.775.

Su, W., Liu, Y., Xia, Y., Hong, Z. and Li, J. (2011) 'Conserved endoplasmic reticulum-associated degradation system to eliminate mutated receptor-like kinases in Arabidopsis.', *Proceedings of the National Academy of Sciences of the United States of America*, 108(2), pp. 870–5. doi: 10.1073/pnas.1013251108.

Sui, H., Han, B. G., Lee, J. K., Walian, P. and Jap, B. K. (2001) 'Structural basis of water-specific transport through the AQP1 water channel', *Nature*, 414(6866), pp. 872–878. doi: 10.1038/414872a.

Suzuki, K., Kirisako, T., Kamada, Y., Mizushima, N., Noda, T. and Ohsumi, Y. (2001) 'The pre-autophagosomal structure organized by concerted functions of APG genes is essential for autophagosome formation', *EMBO Journal*, 20(21), pp. 5971–5981. doi: 10.1093/emboj/20.21.5971.

Svozil, J., Hirsch-Hoffmann, M., Dudler, R., Gruissem, W. and Baerenfaller, K. (2014) 'Protein Abundance Changes and Ubiquitylation Targets Identified after Inhibition of the Proteasome with Syringolin A', *Molecular & Cellular Proteomics*, 13(6), pp. 1523–1536. doi: 10.1074/mcp.M113.036269.

Tajkhorshid, E., Nollert, P., Jensen, M., Miercke, L. J. W., O'Connell, J., Stroud, R. M. and Schulten, K. (2002) 'Control of the selectivity of the aquaporin water channel family by global orientational tuning', *Science*, 296(5567), pp. 525–530. doi: 10.1126/science.1067778.

Takano, J. (2006) 'The Arabidopsis Major Intrinsic Protein NIP5;1 Is Essential for Efficient Boron Uptake and Plant Development under Boron Limitation', *The Plant Cell*, 18(6), pp. 1498–1509. doi: 10.1105/tpc.106.041640.

Takano, J., Tanaka, M., Toyoda, A., Miwa, K., Kasai, K., Fuji, K., Onouchi, H., Naito, S. and Fujiwara, T. (2010) 'Polar localization and degradation of Arabidopsis boron transporters through distinct trafficking pathways', *Proceedings of the National Academy of Sciences of the United States of America*, 107(11), pp. 5220–5225. doi: 10.1073/pnas.0910744107.

Tanaka, M., Wallace, I. S., Takano, J., Roberts, D. M. and Fujiwara, T. (2008) 'NIP6;1 Is a Boric Acid Channel for Preferential Transport of Boron to Growing Shoot Tissues in Arabidopsis', *The Plant Cell*, 20(10), pp. 2860–2875. doi: 10.1105/tpc.108.058628.

Tian, S., Wang, X., Li, P., Wang, H., Ji, H., Xie, J., Qiu, Q., Shen, D. and Dong, H. (2016) 'Plant Aquaporin AtPIP1;4 Links Apoplastic H_2O_2 Induction to Disease Immunity Pathways', *Plant Physiology*, 171(3), pp. 1635–1650. doi: 10.1104/pp.15.01237.

Törnroth-Horsefield, S., Wang, Y., Hedfalk, K., Johanson, U., Karlsson, M., Tajkhorshid, E., Neutze, R. and Kjellbom, P. (2006) 'Structural mechanism of plant aquaporin gating', *Nature*, 439(7077), pp. 688–694. doi: 10.1038/nature04316.

Ueda, M., Tsutsumi, N. and Fujimoto, M. (2016) 'Salt stress induces internalization of plasma membrane aquaporin into the vacuole in Arabidopsis thaliana', *Biochemical and Biophysical Research Communications*, 474(4), pp. 742–746. doi: 10.1016/j.bbrc.2016.05.028.

Vashist, S. and Ng, D. T. W. (2004) 'Misfolded proteins are sorted by a sequential checkpoint mechanism of ER quality control', *Journal of Cell Biology*, 165(1), pp. 41–52. doi: 10.1083/jcb.200309132.

Wallace, I. S., Choi, W. G. and Roberts, D. M. (2006) 'The structure, function and regulation of the nodulin 26-like intrinsic protein family of plant aquaglyceroporins', *Biochimica et Biophysica Acta - Biomembranes*, 1758(8), pp. 1165–1175. doi: 10.1016/j.bbamem.2006.03.024.

Walton, A., Stes, E., Cybulski, N., Van Bel, M., Inigo, S., Nagels Durand, A., Timmerman, E., Heyman, J., Pauwels, L., De Veylder, L., Goossens, A., De Smet, I., Coppens, F., Goormachtig, S. and Gevaert, K. (2016) 'It's time for some "site"-seeing: novel tools to monitor the ubiquitin landscape in Arabidopsis thaliana', *The Plant Cell*, 28(January), pp. 6-16. doi: 10.1105/tpc.15.00878.

Wang, C., Hu, H., Qin, X., Zeise, B., Xu, D., Rappel, W.-J., Boron, W. F. and Schroeder, J. I. (2016) 'Reconstitution of CO_2 Regulation of SLAC1 Anion Channel and Function of CO_2 -Permeable PIP2;1 Aquaporin as CARBONIC ANHYDRASE4 Interactor', *The Plant Cell*, 28(2), pp. 568–582. doi: 10.1105/tpc.15.00637.

Wiedenmann, J., Ivanchenko, S., Oswald, F., Schmitt, F., Rocker, C., Salih, A., Spindler, K.-D. and Nienhaus, G. U. (2004) 'EosFP, a fluorescent marker protein with UV-inducible green-to-red fluorescence conversion', *Proceedings of the National Academy of Sciences of the United States of America*, 101(45), pp. 15905–15910. doi: 10.1073/pnas.0403668101.

Vander Willigen, C., Postaire, O., Tournaire-Roux, C., Boursiac, Y. and Maurel, C. (2006) 'Expression and inhibition of aquaporins in germinating Arabidopsis seeds', *Plant and Cell Physiology*, 47(9), pp. 1241–1250. doi: 10.1093/pcp/pcj094.

Wolf, D. H. and Stolz, A. (2012) 'The Cdc48 machine in endoplasmic reticulum associated protein degradation', *Biochimica et Biophysica Acta - Molecular Cell Research*, 1823(1), pp. 117–124. doi: 10.1016/j.bbamcr.2011.09.002.

Wu, F. H., Shen, S. C., Lee, L. Y., Lee, S. H., Chan, M. T. and Lin, C. S. (2009) 'Tape-arabidopsis sandwich - A simpler arabidopsis protoplast isolation method', *Plant Methods*, 5(1), pp. 1–10. doi: 10.1186/1746-4811-5-16.

Yaneff, A., Sigaut, L., Marquez, M., Alleva, K., Pietrasanta, L. I. and Amodeo, G. (2014) 'Heteromerization of PIP aquaporins affects their intrinsic permeability', *Proceedings of the National Academy of Sciences of the United States of America*, 111(1), pp. 231–236. doi: 10.1073/pnas.1316537111.

Yang, H., Menz, J., Haüssermann, I., Benz, M., Fujiwara, T. and Ludewig, U. (2015) 'High and Low Affinity Urea Root Uptake: Involvement of NIP5;1', *Plant and Cell Physiology*, 56(8), pp. 1588–1597. doi: 10.1093/pcp/pcv067.

Ye, Y., Shibata, Y., Yun, C., Ron, D. and Rapoport, T. A. (2004) 'A membrane protein complex mediates retro-translocation from the ER lumen into the cytosol', *Nature*, 429(6994), pp. 841–847. doi: 10.1038/nature02656.

Yoo, Y. J., Lee, H. K., Han, W., Kim, D. H., Lee, M. H., Jeon, J., Lee, D. W., Lee, J., Lee, Y., Lee, J., Kim, J. S., Cho, Y., Han, J. K. and Hwang, I. (2016) 'Interactions between Transmembrane Helices within Monomers of the Aquaporin AtPIP2;1 Play a Crucial Role in Tetramer Formation', *Molecular Plant*, 9(7), pp. 1004–1017. doi: 10.1016/j.molp.2016.04.012.

Zelazny, E., Borst, J. W., Muylaert, M., Batoko, H., Hemminga, M. A. and Chaumont, F. (2007) 'FRET imaging in living maize cells reveals that plasma membrane aquaporins interact to regulate their subcellular localization', *Proceedings of the National Academy of Sciences of the United States of America*, 104(30), pp. 12359–12364. doi: 10.1073/pnas.0701180104.

Zelazny, E., Miecielica, U., Borst, J. W., Hemminga, M. A. and Chaumont, F. (2009) 'An N-terminal diacidic motif is required for the trafficking of maize aquaporins ZmPIP2;4 and ZmPIP2;5 to the plasma membrane', *Plant Journal*, 57(2), pp. 346–355. doi: 10.1111/j.1365-313X.2008.03691.x.

Zhang, L., Zhang, H., Liu, P., Hao, H., Jin, J. B. and Lin, J. (2011) 'Arabidopsis R-SNARE proteins VAMP721 and VAMP722 are required for cell plate formation', *PLOS ONE*, 6(10). doi: 10.1371/journal.pone.0026129.

Zhao, J. (2013) 'Roles of PIP aquaporins in lateral root development and stress responses in Arabidopsis thaliana', *Thesis (LMU)*.

Zschauer, T., Kunze, K., Jakob, S., Haendeler, J. and Altschmied, J. (2011) 'Oxidative Stress – Induced Degradation of Thioredoxin-1 and Apoptosis Is Inhibited by Thioredoxin-1 – Actin Interaction in Endothelial Cells', *Arteriosclerosis, Thrombosis, and Vascular Biology*, 31(3), pp. 650–656. doi: 10.1161/ATVBAHA.110.218982.

Zwiazek, J. J., Xu, H., Tan, X., Navarro-Ródenas, A. and Morte, A. (2017) 'Significance of oxygen transport through aquaporins', *Scientific Reports*, 7, pp. 1–11. doi: 10.1038/srep40411.

8 Acknowledgements

First of all, I would like to thank my supervisor Dr. Anton Schäffner for all the support and advice he provided me with throughout my PhD study. I especially appreciate that he always had the time to discuss my project with me, to rise questions, help me interpret new results and give me his feedback on new ideas.

Moreover, I would also like to express my gratitude to the members of my thesis committee: PD Dr. Cordelia Bolle, PD Dr. Dietmar Martin and Prof. Dr. Jörg Durner. I appreciated the valuable advice and critical feedback regarding my result. This really helped to improve the quality of my work.

I would like to thank my colleagues, who immediately welcomed me into the group and always supported me with advice and assistance. I really enjoyed sharing the office and/or lab with Dr. Wei Zhang, Dr. Dörte Mayer, Dr. Felicitas Mengel, Dr. Eva König und Birgit Lange. Thank you for the good fellowship and the friendly atmosphere. Some of the best ideas regarding my project arose from our animated discussions.

Dr. Alexandra Ageeva Kieferle, Dr. Ming Jin, Dr. Jin Zhao, Dr. Rafal Maksym, Dr. Elisabeth Georgii and Birgit Geist were always ready to answer my questions and give advice. Please accept my thanks for always lending a helping hand, if I needed one.

In addition, I want to thank Dr. Chen Liu and Komal Jhala. Chen, for introducing me to my project and providing the data my thesis is based on and Komal for taking over the project after me and continuing with my ideas.

Moreover, I want to express my gratitude to Dr. Sibylle Bauer for keeping me up to date regarding the PIP project and my colleagues at the Helmholtz Centre during the time I waited for handing in my thesis and having my defense.

Last but not least, I want to thank my friends and family, who always were there for me to cheer me up when experiments failed or celebrate with me when I succeeded. Christoph Lehnert deserves a special thanks, since he not only put up with me all this time, but also accepted my marriage proposal and married me.